University of Stavanger

Faculty of Science and Technology

MASTER'S THESIS

Study program/Specialization: Petroleum Geosciences Engineering	Spring, 2016 Open
Writer: THANH PHUONG NGUYEN	(Writer's signature)
Faculty supervisor: ARILD BULAND External supervisor(s):	
Title of thesis: **Seismic Inversion for Fluid and Lithology Prediction of the Mikkel Field**	
Credits (ECTS): 30	
Keywords: Seismic inversion Lithology and Fluid prediction AVO modelling Seismic coloured inversion Extended elastic impedance Rock physics model	Pages: 90 Stavanger, 15th June, 2016

Seismic Inversion for Fluid and Lithology Prediction of The Mikkel Field

by

Thanh Nguyen, B.Sc

Thesis

Presented to the Faculty of Science and Technology

The University of Stavanger

The University of Stavanger

June 2016

Acknowledgements

This thesis report is submitted to fulfil the requirements for the Master of Science degree in Petroleum Geosciences Engineering. The data of this study was provided by Statoil AS and, mainly carried out at Cegal Office in Stavanger, Norway.

I would like to sincerely thank Professor Arild Buland for his guidance through this project, his encouragement and his patience to help me to improve my knowledge and my passion for seismic inversion.

I take this opportunity to express my gratitude to Cegal Company for providing facilities and software to perform this study. Especially I appreciate the Geoscientist Team for assisting me and giving the valuable technical recommendations in this study.

Finally, I am grateful to the South East Asia Petroleum Exploration Society (SEAPEX) for sponsoring me the scholarship to study in University of Stavanger for the last two years. Especially I thank Mr. Martin Bawden for his encouragement for my master study decision from day one and his technical support in my career path.

"You never know your limits until you push yourself to them"

Abstract

Seismic Inversion for Fluid and Lithology Prediction of the Mikkel Field

Thanh Phuong Nguyen, M.Sc.

The University of Stavanger, 2016

Supervisor: Arild Buland

The Mikkel Field is a gas condensate field located in the Norwegian Continental Shelf. The reservoirs are in the Garn Formation and the Ile Formation deposited in marine influenced environment in the Middle Jurrassic Fangst Group. The structural interpretation of the Garn reservoir is highly uncertain; especially in the eastern half-graben area where the seismic amplitude is weak in near angle stack and vary in far angle stack, dependent on the cap rock thickness. In addition to the ambiguous structural interpretation, the dynamic model indicates that the Garn Formation and the Ile Formation in this eastern half-graben have no contribution to the production of the field. An important question is whether this segment contains undrained hydrocarbons.

This study includes structural interpretation of main key horizons in the study area. AVO modelling, seismic colored inversion and extended elastic impedance are performed to support the structural interpretation and to produce an optimal fluid cube to highlight hydrocarbon presence. Prior to executing AVO analysis and inversion, the quality of the seismic data has been checked and the data are conditioned to ensure consistency between the different angle cubes. Finally, lithology and fluid probability (LFP) cubes are generated from a Bayesian inversion. The Pcube analysis increases the probability for gas sand in the Garn Formation and the Ile Formation of the Mikkel Field from 0.4 to about 0.6-0.7 in the drilled high structure and reduces the probability to about 0.3 in the un-drilled eastern half graben. Due to the complex fault pattern and limited time of this study, it is recommended to perform a detail structural fault interpretation and its influence on erosion and sediment variation in each fault block in the Mikkel Field to improve the rock physics model and a further Pcube testing on the refine models for the future.

Table of Contents

List of Figures

List of Tables

1. Introduction

Seismic data is a main source for finding and risking prospects in oil and gas industry. The seismic reflection method is a useful tool to delineate structure of prospect and define its possible trap system, however, the structure alone is not sufficient for detection of hydrocarbons. The technique of amplitude variations with offset (AVO) explains the seismic reflectivity variation by the P-wave, S-wave and density contrasts over the interface. The changes in lithology and fluid can lead to vary the AVO response (Russell *et al*, 2006). Although AVO has proved its great benefit, it is still considered as single contrast, negligence of multi-layered interference limiting its applicability. Seismic coloured inversion (SCI) has been introduced as a simple, fast and cost efficient way to invert seismic reflectivity to layer based relative acoustic impedance (Lancaster *et al*., 2000). By using SCI, we can produce acoustic impedance (AI) and gradient impedance (GI) combined into extended elastic impedance (EEI). The projection of AI and GI together with different rotation angles Chi (χ) can highlight different features. Therefore, finding an optimum rotation angle Chi (χ) is essential to allow interpreter to project the lithology and fluid changes.

The AVO, SCI and EEI techniques are qualitative workflows that mainly support structural interpretation and highlight hydrocarbon effect. The quantitative objective of seismic inversion is prediction of lithology and fluid (LFP). Though, the lithology/fluid prediction uncertainty by inversion is often high, and mainly derives from two reasons: (1) different lithology occupies overlapping ranges of elastic properties (Houck, 2012), and (2) relationship between elastic parameter and seismic data (Buland and Omre, 2003a). Seismic inversion transforms seismic reflection to elastic properties correlated to facies and rock properties from rock physics model in order to discriminate the lithology, and fluid component in reservoir. However, inverse problems are usually large, and multidimensional, and the Bayesian framework is a natural choice (Duijndamn, 1998a, b; Tarantola, 1987; Ulrych *et al*., 2001; Scales and Tenorio, 2001; Buland and Omre., 2003a, b, c; Gunning and Glinsky, 2004). Bayesian lithology and fluid prediction from prestack seismic data is a recent technique joining results of inversion and stochastic rock physics model. A fast Bayesian seismic simultaneous inversion includes prior knowledge, and uncertainty measurement; and it can provide optimal solutions, associated uncertainty, and simulated solutions completely defined by the posterior distribution (Buland and Omre, 2003a). The rock physics model defines the link from rock properties for each facies to effective elastic properties (Avseth *et al*., 2005). The rock physics model can be generated from well-log data or from a stochastic rock model.

A stochastic rock model combines deterministic relationships with varying rock parameters and natural variation not explained by the rock model. Lithology/fluid prediction is usually done location-wise; thus it is fast and computer efficient. However, hydrocarbon accumulation may not appear as continuous pocket in terms of geology. The final result of LFP is a set of probabilities of lithology and fluid classes such as oil sand, gas sand, brine sand and shale.

In this study, AVO, seismic coloured inversion and extended elastic impedance will firstly perform on angle stack seismic to support conventional structural mapping and highlight fluid effect in the study area. Those methods are quick, time efficient and in addition to complement knowledge about reservoir characteristic in the study area so that it helps to explain the result from LFP. The main objective is to predict lithology and fluid classes from prestack seismic data.

This study is an application of a Bayesian lithology and fluid prediction methodology (Buland *et al*., 2008) on a real data set provided from the Mikkel Field. The Mikkel Field has been in production since 2001. An eastern half-graben has shown no contribution into production of the field, hence the area is suspected whether it is still un-drained and hydrocarbons remain in its reservoirs to be potential in future development plan. The area is structural complex and the interpretation is challenging that Statoil could not achieve in previous studies. The LFP is executed to predict the probabilities of fluid and lithology classes (LFC) in this area to reduce risk for up-coming in-filled well. The additional amplitude versus offset, seismic coloured inversion and extended elastic impedance were applied to support structural interpretation and complement reservoir characteristic to explain the results from LFP. The study included eight chapters and the main part of the study is from chapter 3 to chapter 6. Finally, the study gives a discussion on the Mikkel Field and a conclusion of application methodologies.

2. Geological background

2.1 Introduction

The study area in this project is Mikkel field located in block 6407/5 and 6407/6, 120 km west of the Norwegian coast (Figure 2.1). The Mikkel field is located in a North-South trending horst structure in the transition between Bremstein Fault Complex (BFC) in the West and Halten Terrace in the East (Figure 2.2). The water depth ranges between 210m to 260m. The reservoir is structurally complex and highly faulted, separated by main bounding faults. The major reservoir levels are the Garn Formation and the Ile Formation within the Middle Jurassic Fangst Group. The hydrocarbon present was mainly gas and condensate. The reservoir quality varies from good to excellent. In total, six wells were drilled in the field: three exploration wells (6407/6-3, 6407/6-4, 6407/6-5) and three production wells (6407/6-A-1H, 6407/6-A-3H, 6407/5-B-3H). The field has been in production since 2001.

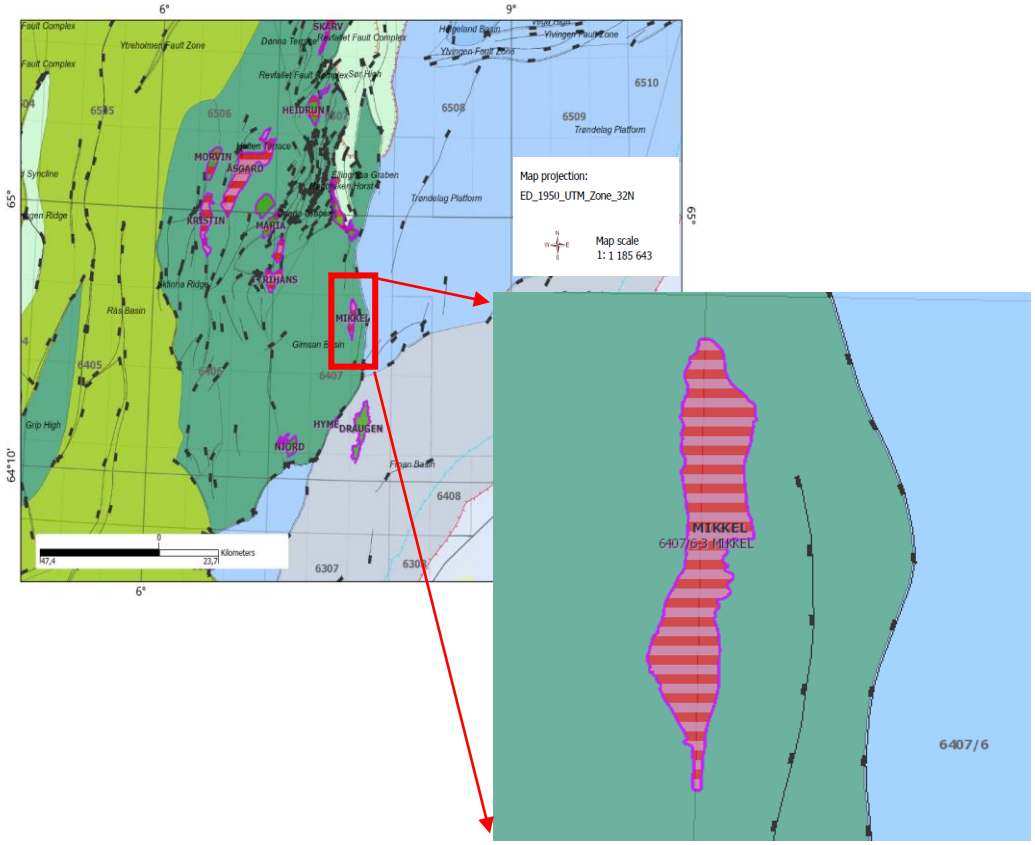

Figure 2.1 Location map of the Mikkel Field in the Norwegian Continental Shelf (NPD, 2016)

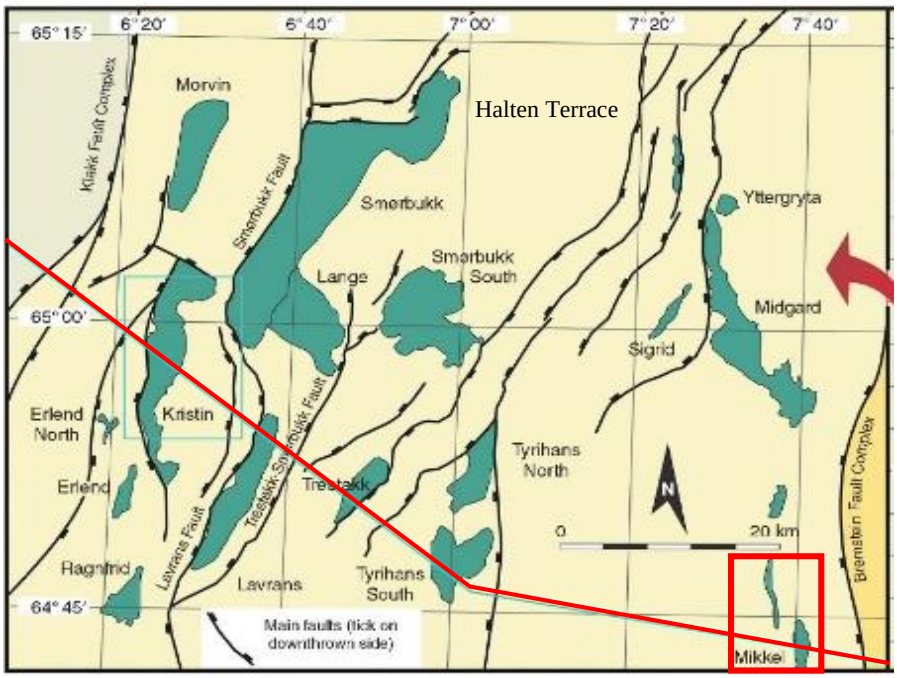

Figure 2.2 The Mikkel Field location map between Bremstein Fault complex and the Halten Terrace

(Messina *et al*., 2014)

2.2 Regional Tectonic

The Halten Terrace structure is a stepwise series of tilted fault blocks striking SW-NE and down-thrown towards the NW (Figure 2.3). The Halten terrace is the most prolific hydrocarbon province in Norwegian continental shelf, containing many fields with gas, condensate and light to medium oil within Lower to Middle Jurassic siliciclastic reservoirs (Spencer *et al*., 1993; Koch & Heum, 1995). The main reservoirs are tidal and deltaic deposits of the Early Jurassic Båt Group and the Middle Jurassic Fangst Group (Gjelberg *et al*., 1987; Dalland *et al*., 1988). The tectonic structure of the Norwegian Continental Shelf has experienced four main rifting phases, which are Permo-Triassic, Late Jurassic, Middle Cretaceous and Palaeocene (Bukovics *et al*., 1984; Dore, 1992; Dore *et al*., 1999; Brekke *et al*., 2001). Among these four phases, the Cretaceous phase had the greatest magnitude of extension (Pascoe *et al*., 1999; Corfield *et al*., 2001). The last Palaeocene phase finally separated the Fennoscandian and Greenland cratons and opened the North Atlantic. Hydrocarbons began to generate and migrate into reservoirs in the Halten Terrace until the early Pliocene (Skar *et al*., 1999).

The presence of Triassic salt complicated the extensional pattern, resulting in listric detachment faults and deep planar faults at the continental margin (Jackson & Hastings, 1986;

Withjack *et al*., 1989; Pascoe *et al*., 1999; Corfield & Sharp, 2000; Marsh *et al*., 2010*)*. The base of Jurassic syn-rift deposits in the Halten Terrace is usually placed between the shallow-marine sandstones of the Middle Jurassic Fangst Group and the neritic mudstones of the Viking Group (Dalland *et al*., 1988; Ehrenberg *et al*., 1992; Koch & Heum, 1995). However, a recent study from Messina *et al*. (2014) suggested that the rifting phase could have commenced earlier and extended into the earliest Cretaceous (Figure 2.3)

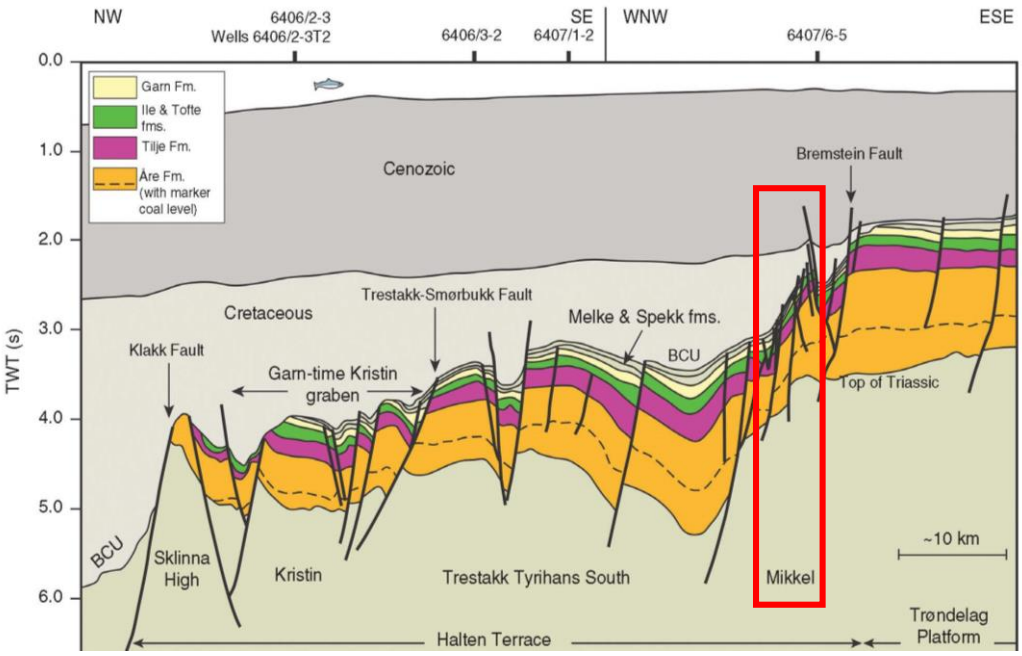

Figure 2.3 Geo-seismic cross-section through the Halten Terrace along the traverse line shown in Figure 2.2 with the BCU symbol denoting the Base-Cretaceous regional unconformity

(Messina *et al*., 2014)

2.3 Jurassic stratigraphy and depositional environments in Halten Terrace

The Jurassic latitude of the Halten Terrace was between 49° N and 53° N (Smith *et al*., 1994) and the regional climate was warm and probably seasonal (Hallam *et al*., 1994).

The Mesozoic succession of the Halten Terrace is marine influenced in origin as summarized in stratigraphic column (Figure 2.4). Firstly, the early Jurassic (Båt Group) including Åre, Tilje, Tofte and Ror. The Åre Formation (Hetangian to Sinemurian) overlies the Triassic salt-bearing terrestrial deposits and composes of alluvial and tidal coal layers**.** The Tilje Formation (Pliensbachian) overlies the Åre Formation and consists of heterolithic deposits representing tide-dominated coastal plains, deltas and bays or estuaries. The following transgressive succession culminates in the Ror Formation (latest Pliensbachian to Toarcian) interpreted as neritic offshore mudstones interbedded with the westerly deltaic sandstone wedges of the Tofte Formation.

Following the middle Jurassic (Fangst Group) is a sand-dominated and largely regressive sequence consisting of the Ile, Not, Garn and Melke Formations, and the group is regarded as largely equivalent to the Brent Group of the northern North Sea (Helland-Hansen *et al*., 1992). The Ile Formation (late Toarcian to Aalenian) conformably overlies the Ror Formation on the Halten Terrace, and it shares many of the characteristics of the Tilje Formation. It comprises of heterolithic deposits of tide-dominated deltas. The Not Formation (Aalenian to earliest Bajocian) places on top the Ile Formation and is consisted of bioturbated offshore mudstones, which is another transgressive succession and transitions into sand-rich heterolithic tidal deposits near the top of the formation. The overlain Garn Formation is separated from the Not Formation by a very sharp unconformity surface. The contact between Not and Garn is normally sharp, erosive and represents an uncomfortable event associated with a slight dip change (Corfield et al., 2001). Thus, the contact is considered as a regionally significant regressive erosion surface of intra-early Bajocian age. However, it is necessary to emphasise that it was an exceptional case that the contact between Not and Garn was more gradational, associated with an apparently related to progradational association of facies from offshore/shelf to upper shoreface/shelf in wells 6406/2-3, 6406/3-2, 6407/4-1 and 6407/6-3 (Corfielld *et al*., 2001). In general, the Garn Formation is a deltaic sandstone in the Halten Terrace and its thickness is varying as typically characteristic of a syn-rift tectonic (Gjelberg *et al*., 1987).

The late Jurassic includes Melke and Spekk Formations. The Melke Formation (Bajocian to early Oxfordian) consists of heterolithic sublittoral deposits and bioturbated neritic mudstone

and is covered by the rich source rocks of the Spekk Formation. The transgression that caused deposition of the Melke and Spekk formations can be related to large scale regional extension that began in Late Bathonian and continued through the Early Cretaceous.

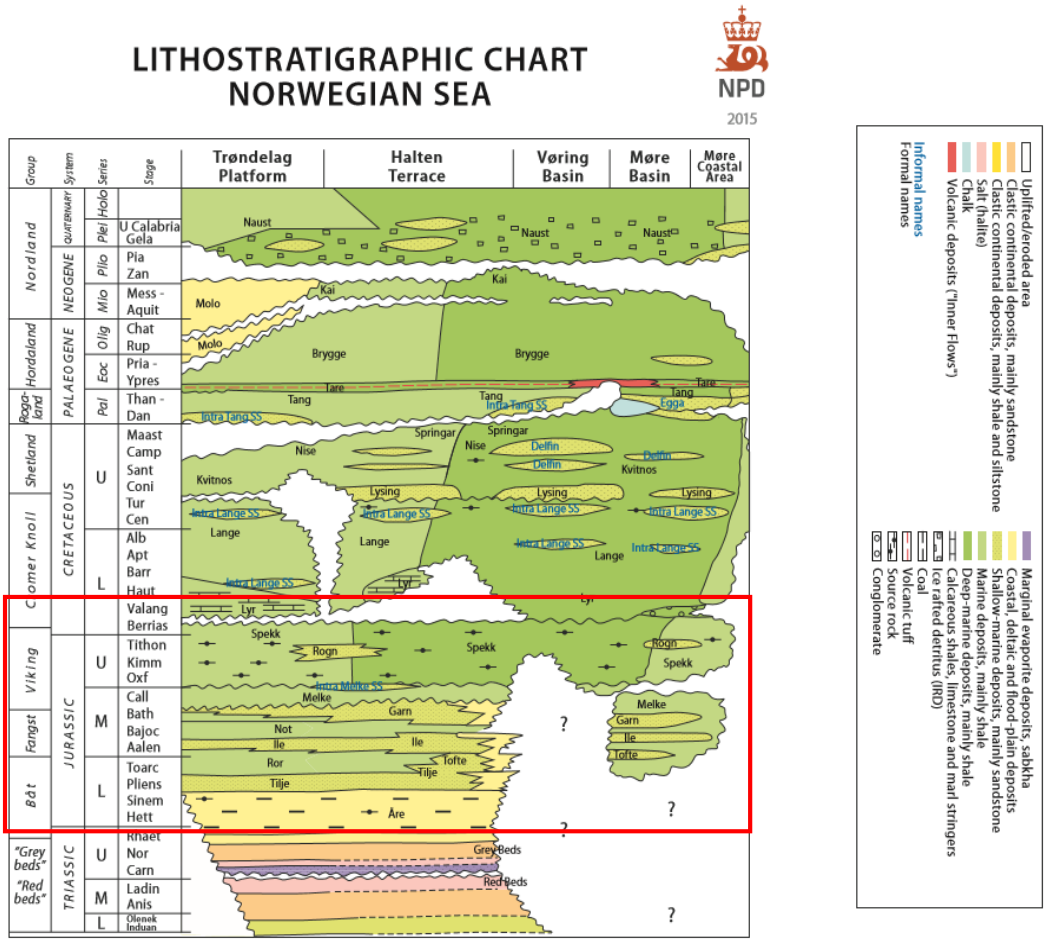

Figure 2.4 The Upper Triassic to the Middle Jurassic stratigraphy of the Halten Terrace and interest interval (red rectangle)

(NPD, 2016)

2.4 Geological conceptual model and fault seal model for the Mikkel Field

The Mikkel Field is a gas/condensate field and has been in production since 2001. The field has seven segments divided by main bounding faults. In total three exploration wells and three horizontal production wells were drilled in this field (Figure 2.5). They are 6407/6-3, 6407/6-4, 6407/6-5, 6407/6-A-1H, 6407/6-A-3H and 6407/5-B-3H. Following the regional trend in Halten Terrace, the middle Jurassic (Fangst Group) in the Mikkel Field has marine influence. Since the Halten Terrace is a quite large area, the geological structure inside it varies and each field has its own unique characteristics.

Based on the previous study from Statoil AS, the geological conceptual model for the Garn Formation is a fluvial influenced deltaic environment and divided into Lower Garn 1 and Upper Garn 2 (Figure 2.6). The second Ile reservoir is a tidal influenced delta and a tide flooded system has a large impact on reservoir quality. The detail of reservoir in Ile Formation is described as lower Ile 3, middle Ile 2 and upper Ile 3 as shown in conceptual model (Figure 2.7).

Based on the depositional conceptual model for the Garn and the Ile reservoir, the Garn reservoir properties are better than the Ile reservoir in terms of porosity however, the Garn reservoir is eroded in some locations. In the Mikkel Field, the erosion of the Garn reservoir was recorded in production well 6407/5-B-3H, in the south of structure (Figure 2.8) where the whole reservoir was completely absent while the neighbour well 6407/65-5 penetrated a thick gas column. Thus, structural interpretation of the Garn Formation needs to be taken care. The Ile formation has calcite cementation occurring as thin beds which is the main factor reducing permeability in its reservoir. The attempt to define the trend of the Ile reservoir calcite-cemented sand is one of the objectives of inversion in the later part of this study. However, those calcites cemented sands are quite thin between 0.5 m to 2.5 meter, which is under seismic vertical resolution. Hence, traditional techniques have faced large obstacles to define them.

Among the three exploration wells, 6407/6-4 was drilled on the flank of the Mikkel Field to test the lowest spill point and resulted as a brine well. Nevertheless, reservoir quality of this well was good to excellent and its location in the south confirmed the continuity of reservoirs. The crossover of gas bearing observation in well 6407/6-3 suggested that the gas/light oil water contact (GWC) was at 2555 TVDSS. However, RFT pressure measurements, DST results and geochemical analyses indicated a gas/light oil contact at ca. 2570 - 2575 TVDSS

(NPD web page). The difference between two GWCs would raise the uncertainty in defining actual contact for reservoirs and the transition height above it (Figure 2.8).

There was a fault seal evaluation in the Mikkel Field under Statoil in 2010. It is necessary to introduce a fault seal model to provide the background and motivation to perform seismic inversion study in the northern part of the Mikkel Field, particularly in segment 7, is the eastward area. As the fault seal study suggested that main bounding fault dividing the Mikkel Field into east and west is sealing in the Ile interval and open in the Garn interval (Figure 2.9). However, dynamic modelling from reservoir team suggested that segment 7 has not contributed production in Mikkel Field. Hence, the attempt to perform seismic inversion in this area is to define lithology and probability of fluid presence in it.

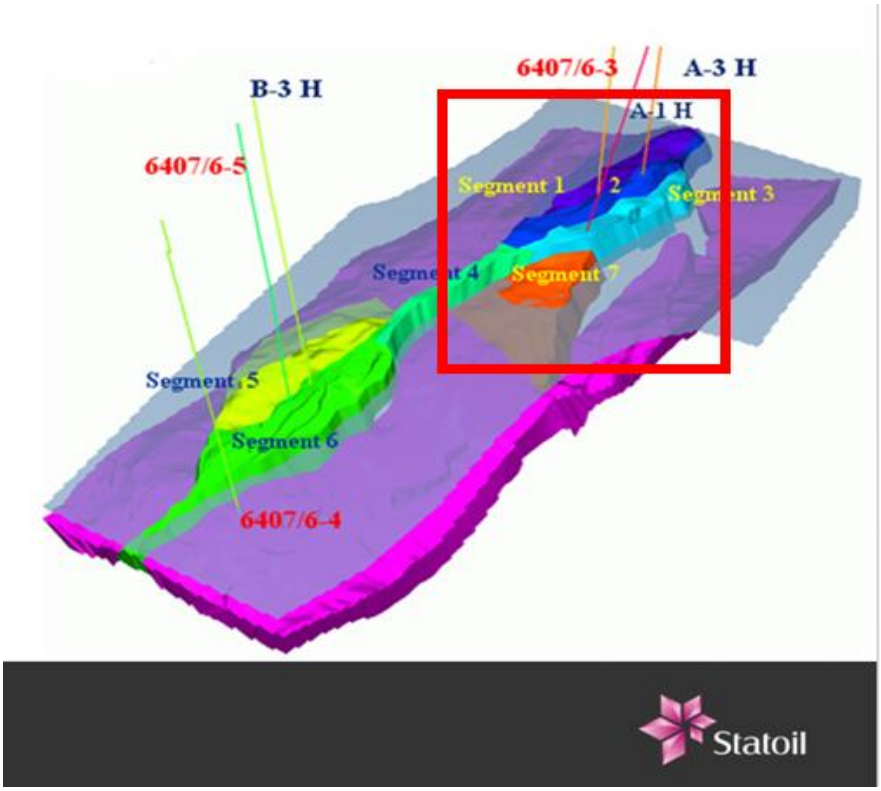

Figure 2.5 Schematic structural model of the Mikkel Field (red rectangle highlight study area)

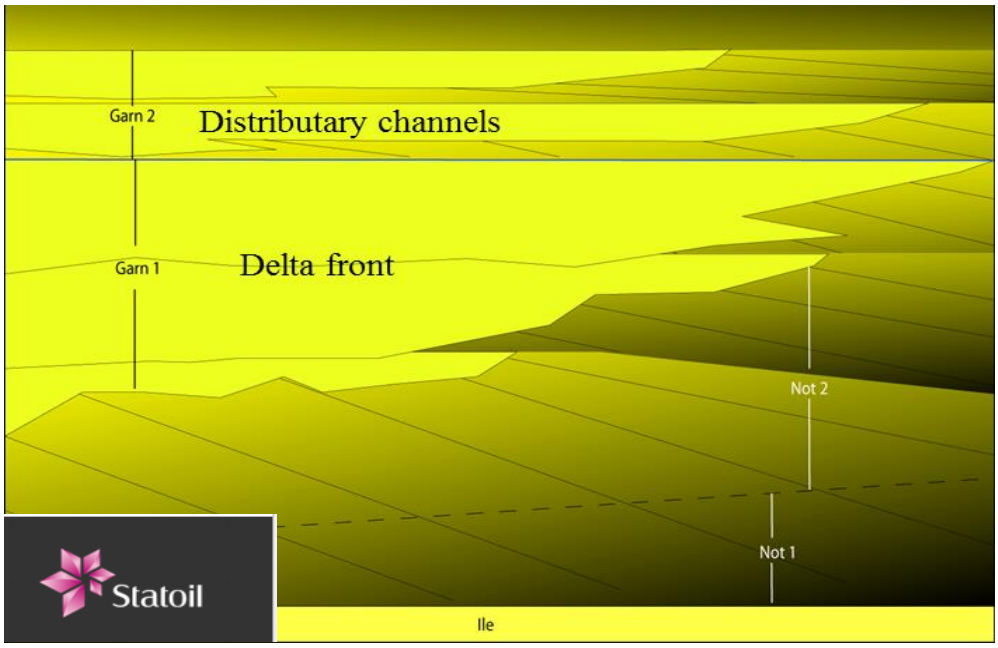

Figure 2.6 Geological conceptual model for the Garn Formation (Courtesy of Statoil)

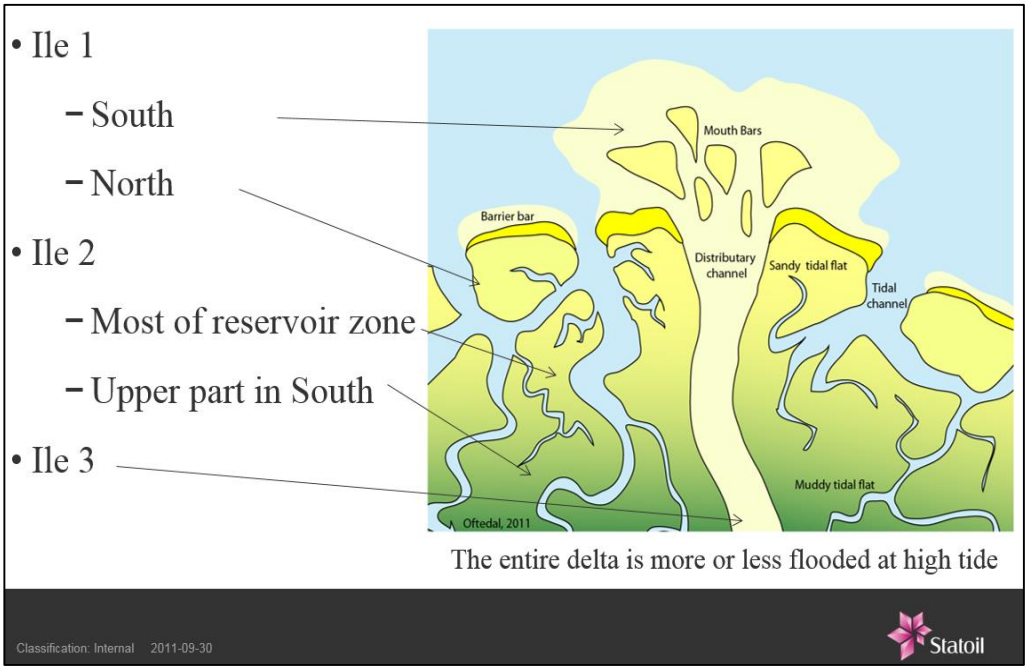

Figure 2.7 Geological conceptual model for the Ile Formation (Courtesy of Statoil)

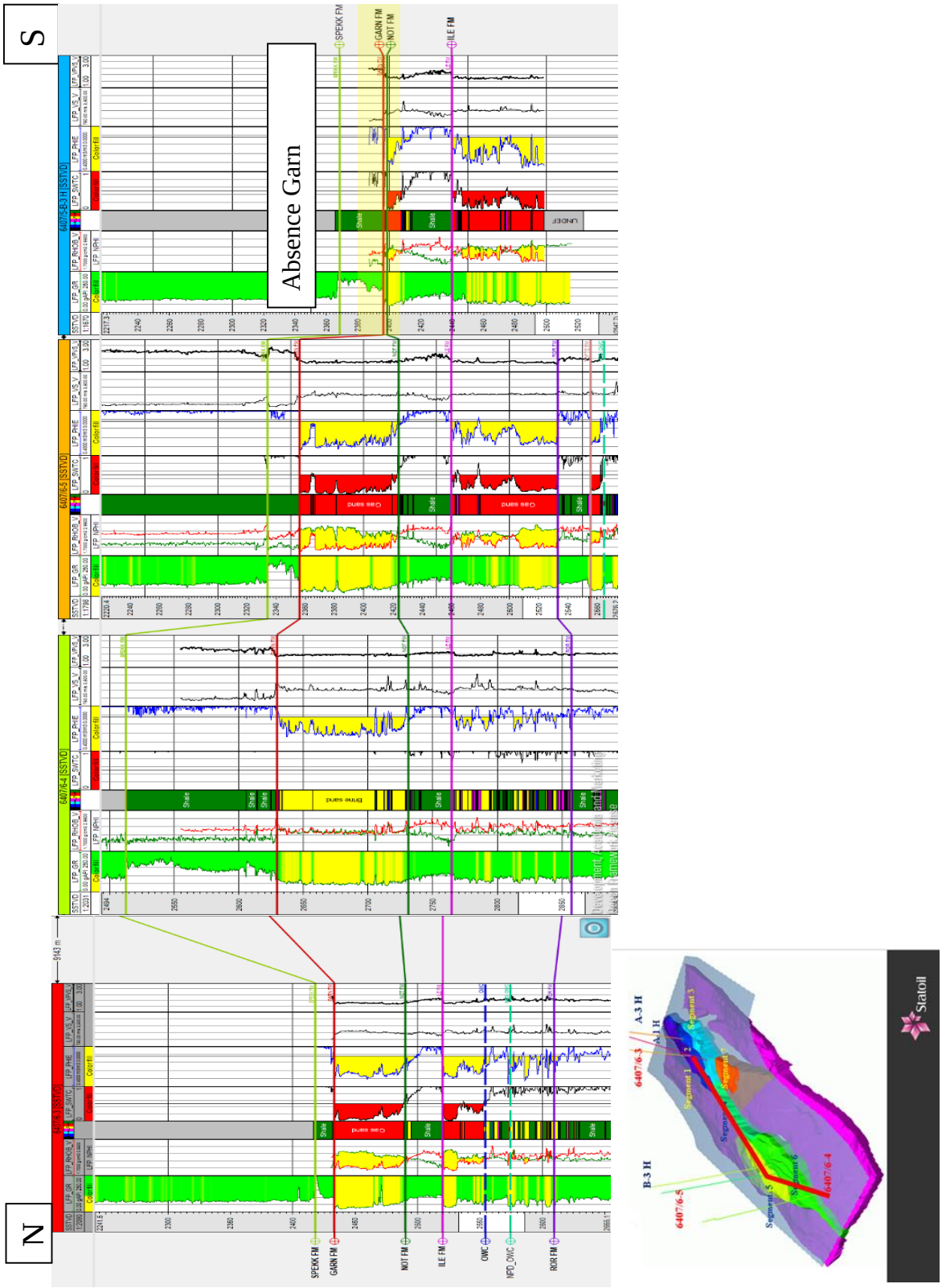

Figure 2.8 Well correlation from North to South in the Mikkel Field (Courtesy of Statoil)

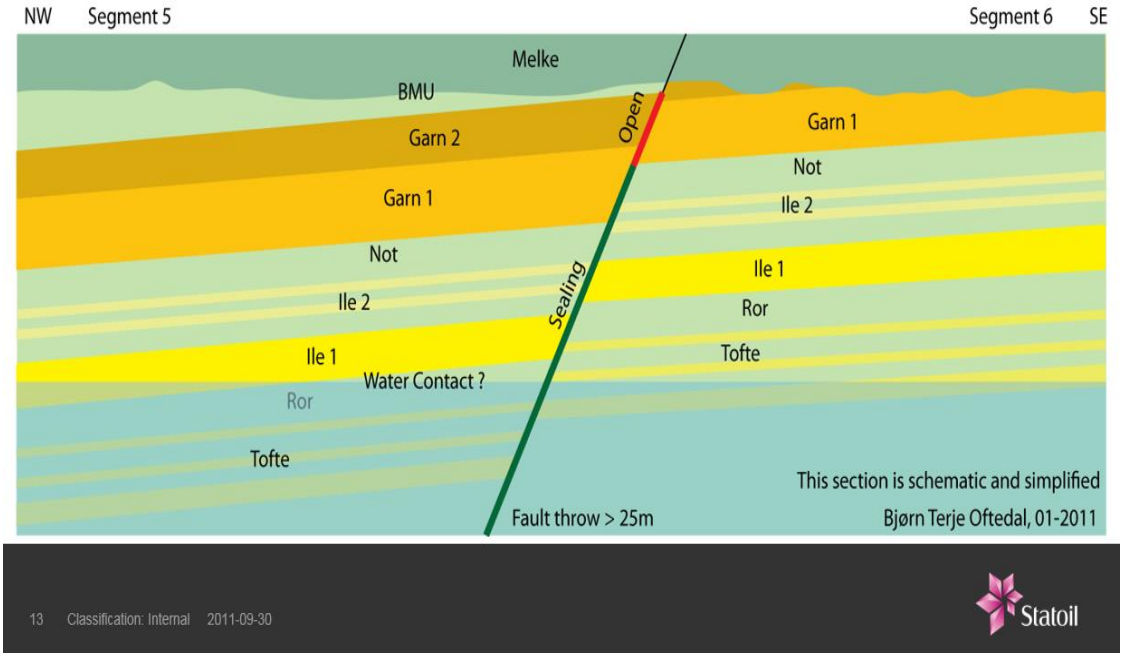

Figure 2.9 Fault seal conceptual model for the Mikkel Field

(Courtesy of Statoil)

3. Database and data conditioning

From this chapter onward, all figures and tables were produced by the author

3.1 Database

3.1.1 Seismic data

The study area is 9 km^2 3D and covered by angle stack seismic data. The provided seismic is in the northern part of the original 3D data covering total North-South trending of the Mikkel Field. This seismic is acquired in 2014 and processed in 2015. The acquisition sampling rate was 2ms and the processing was at 4ms sampling. Furthermore, three seismic arbitrary lines crossing north to south of the Mikkel Field from the original 3D seismic were provided to help understanding the structure and use for well tie. (Figure 3.1)

The available angle stacks consist of the four following groups: (1) a near angle stack 12-20 degree; (2) a mid-angle stack 20-28 degree; (3) a far angle stack 28-36 degree, and (4) ultra-far angle stack 36-44 degree. Generally, the seismic data is close to zero phase amplitude and in good condition to be able to interpret structures. However, some areas have reduced signal to noise ratio due to fault shadow effects. This is an unavoidable issue of seismic data in a complex fault pattern like the Mikkel Field.

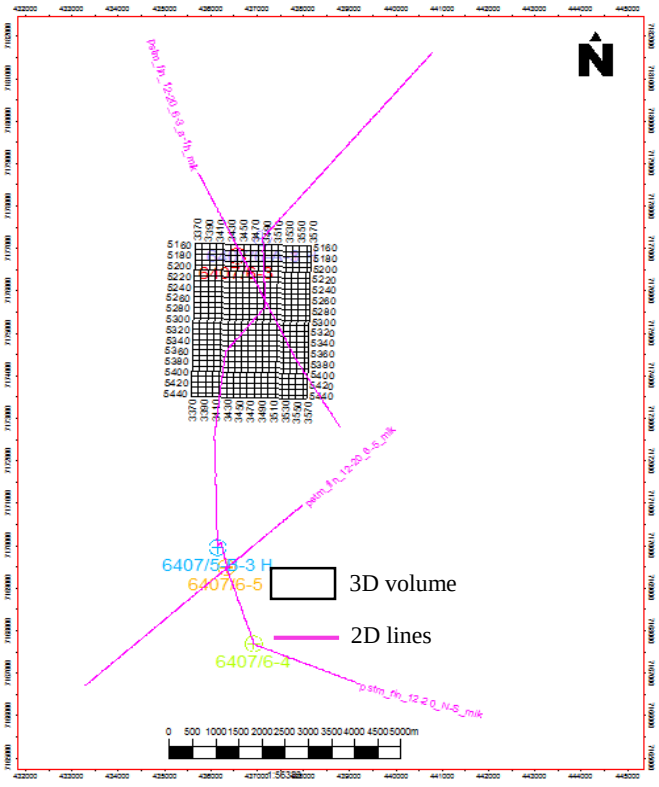

Figure 3.1 Map view of available seismic data in the Mikkel Field

3.1.2 Well database

The Mikkel Field has three exploration wells and three horizontal production wells. They are 6407/6-3, 6407/6-4, 6407/6-5, 6407/6-A-1H, 6407/6-A-3H and 6407/5-B-3H. The three production wells were deviated and unfortunately, their well paths were not available. Therefore, they were excluded in well tie and amplitude versus offset (AVO).

All of the wells have wireline logs and petrophysical interpretation curves such as volume of shale, porosity, saturation, volume of coal, and volume of calcite. All of exploration wells have checkshot data that help to calibrate the sonic data in the well- tie process. Most of the provided wells have measured sonic velocity (Vp) and shear velocity (Vs) that are key for calibration of a rock physics model. There are two exploration wells 6407/6-3 and 6407/6-4 without shear sonic, however an estimated shear sonic data was used for those two. The empirical estimation was calculated by Statoil. In this study, the petrophysical logs are assumed to be depth shift edited and borehole correction by Statoil. The list of provided well data is as shown in table 3.1.

Well	Check shots	VSP	Walk away	OB	Relevant logs						
		Corridor stacks			Sonic	Shear Sonic	Density	Res Horizontal	Res Vertical	Neutron	Gamma Ray
6407/6-A-3 H	Yes	30Hz, 50Hz, 70Hz	No		Yes	Yes	Yes	No	No	Yes	Yes
6407/6-3	Yes	No	Yes? Data?		Yes	No	Yes	No	No	Yes	Yes
6407/6-A-1 H	No	No	No		Yes	Yes	Yes	No	No	Yes	Yes
6407/5-B-3 H	No	No	No		Yes	Yes	Yes	No	No	Yes	Yes
6407/6-5	Yes	30Hz - [10Hz] - 100Hz	No	Yes	Yes	Yes	Yes	No	No	Yes	Yes
6407/6-4	Yes	ZOVSP??	No	Yes	Yes	No	Yes	No	No	Yes	Yes

Table 3.1 Summary of available wireline and checkshot in the Mikkel Field

3.2 Data conditioning

Data conditioning is an important step before performing AVO analysis and inversion. Phase and amplitude spectra difference between angle stacks will lead to the false AVO analysis. Data from routine seismic processing may not be prepared for quantitative seismic analysis. In order to achieve a set of good angle stacks to perform any further study, a conditioning data workflow is recommended including four steps:

1. Phase matching;
2. Amplitude bandwidth matching;
3. Time alignment and,
4. Amplitude offset scaling.

Four angle stacks were loaded into AVOCADO software to perform data conditioning. The chosen interval was set at 2,000 ms to 3,000 ms that covered the complete interest zone from Top Spekk to the base Ile reservoir.

3.2.1 Phase matching

The phase check is essential before executing AVO modelling and inversion. The difference phase between angle stacks would lead to a false AVO modelling. Especially, inversion is always based on an assumption of original seismic input is symmetrical and zero phase. The absolute phase of seismic data is usually defined from well-tie analysis. Hence, this phase analysis without well data will inspect the symmetry of seismic data in the study interval. The phase analysis was set at 2000 ms and near angle stack was used as the master among fours. The composites including a cross-correlation, an envelope cross-correlation, an instantaneous cross-correlation, a quad- envelope cross-correlation and a rotation cross-correlation between each angle stack with the master stack were executed in Figure 3.2. As shown in Figure 3.2, the phase of each angle stack is symmetrical and consistent along the study level. Therefore, no phase rotation was applied to angle stacks as seen in the final rotation cross-correlation in Figure 3.2. The phase analysis has confirmed that seismic data phase is symmetrical and consistent between angle stacks to perform AVO modelling and inversion.

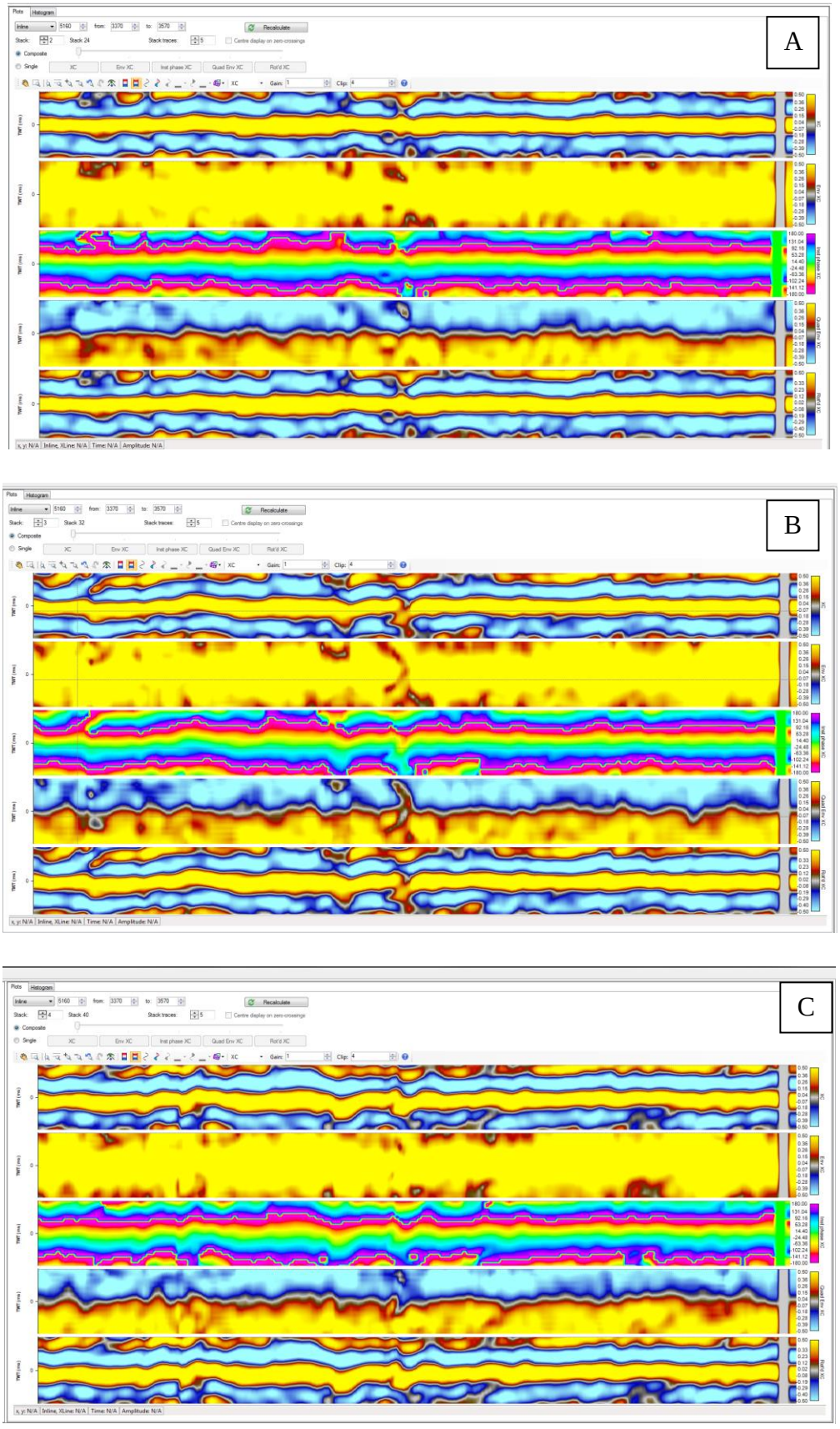

Figure 3.2 The composite of phase analysis between angle stacks and master stack: (A) angle stack 24 with master stack, (B) angle stack 32 with master stack and (C) angle stack 40 with master stack

3.2.2 Amplitude bandwidth matching

The aim of amplitude matching is to match frequency spectrum from each angle stack into a design operator without introducing any noise. Based on the frequency spectrum study in Figure 3.3, the operator filter is designed at frequency 4-6-25-70 Hz (four red dots). The target wavelet after shaping into the operator filter was produced as shown in figure 3.4.

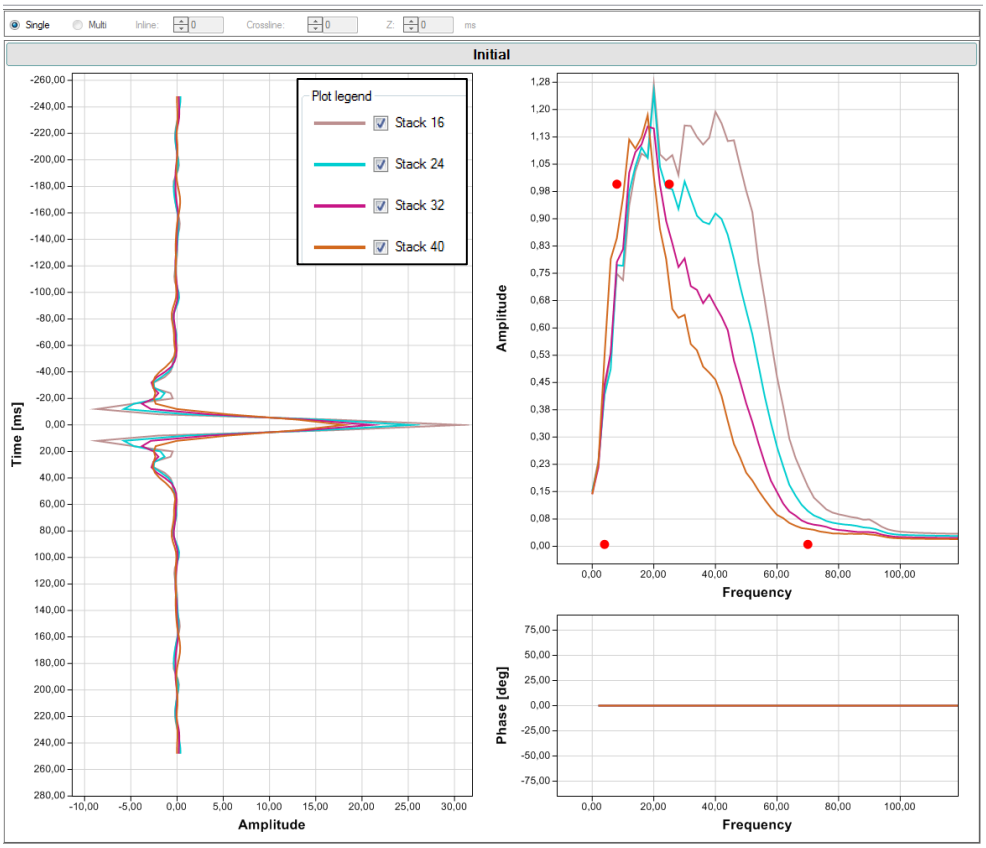

Figure 3.3 Frequency spectrum of the four angle stack and operator filter at 4-8-25-70 Hz (presented by four red dots)

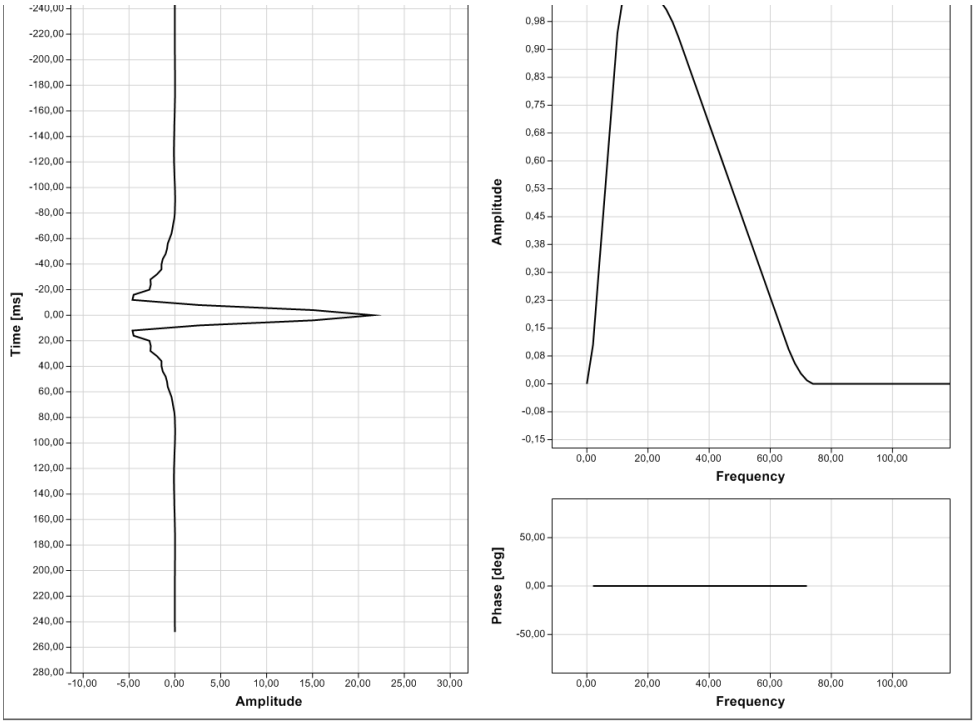

Figure 3.4 Final target wavelet after bandwidth matching the four angle stacks

3.2.3 Time alignment

The purpose of performing time alignment is to correct the residual normal move out (RNMO) between angle stacks. The near angle stack was set as master stack. Maximum threshold time shift was set at 20ms and cross correlation cut off was 0.01. Figure 3.5 shows the comparison of before (A) and after (B) time alignment of XL 3427. Time shift is not significantly different between two gathers. From the gathers, we are able to observe that Top Spekk has amplitude reducing with offset. In the opposite, Top Garn has amplitude increasing with offset and interfered with the response of Top Spekk in the far/ultra-far angle stack. Top Not and Top Ile are two strong events with high amplitude and their amplitudes are stronger in the far/ultra-far angle stack. The time alignment was performed to generate a good set of angle stacks to input to further study. In general, seismic data is good quality and the time shift is not significant in this study area. Figure 3.6 shows the final time shift in far angle stack and ultra-far angle stack at XL 3370. The maximum time shift is around 8ms in this area.

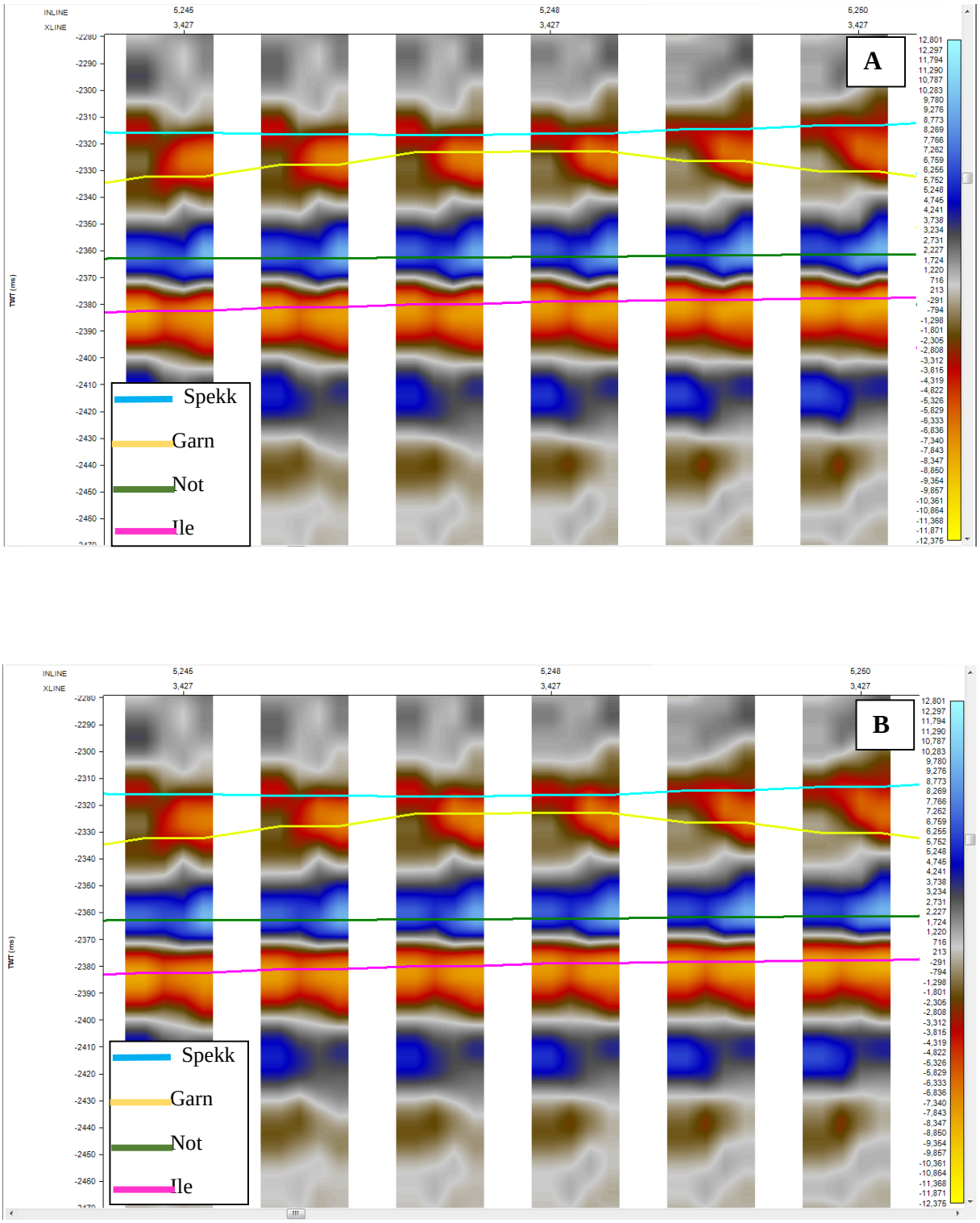

Figure 3.5 Comparison between two gathers (A) before and (B) after time alignment in XL 3427

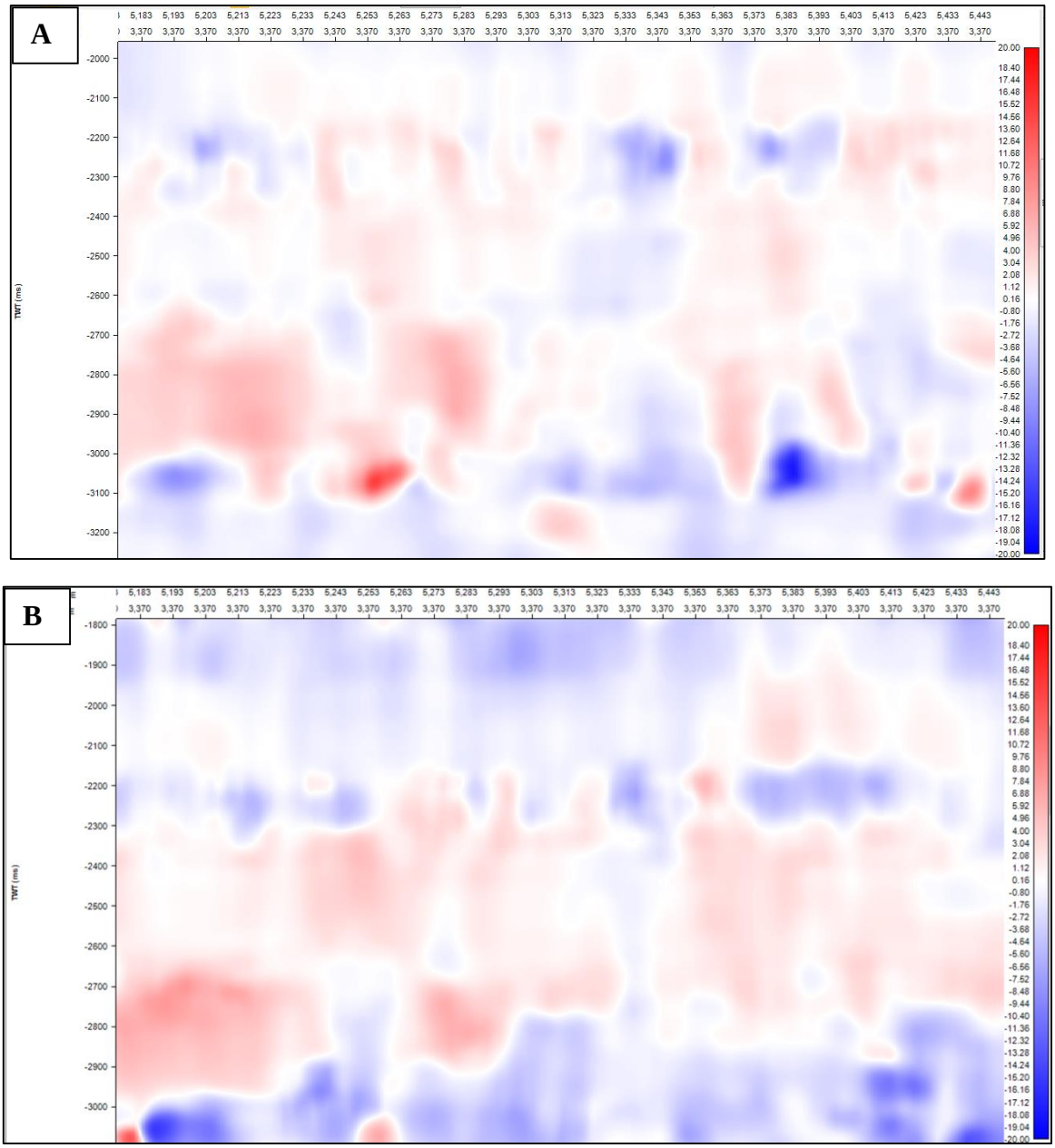

Figure 3.6 Final actual time shift map of far angle stack (A) and ultra-far angle stack (B) at XL 3370

3.2.4 Amplitude offset scaling

Amplitude offset scaling is crucial when studying AVO and inversion. In forward modelling, the reflection coefficient is convolved with a seismic wavelet to produce the synthetic traces. In order to match the synthetic traces with the real seismic data, the scale factor is applied to the process. This scale factor is important in AVO modelling and inversion. In inversion, a high wavelet scale factor will lead to a weak reflection coefficient (RC) or less detail in the result. In contrast, a low scale factor will result in an unrealistic RC model. Thus, finding a right scale factor to model synthetic amplitude as close to the real seismic is essential in the synthetic well tie. The best way to decide a good scale factor is comparison synthetic traces with the real seismic which is going to discuss in detail in section 4.1. The recommended scale factor is around 2,000 in this study. This scale factor is applied to the target wavelet defined from bandwidth matching of four angle stacks to produce the final wavelet that will be used in the AVO modelling and inversion study (Figure 3.7).

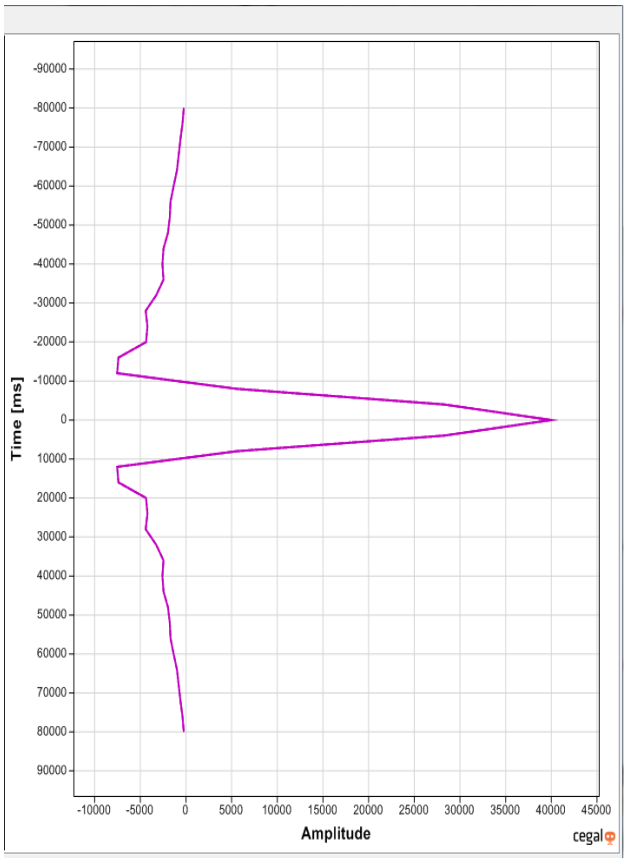

Figure 3.7 Final wavelet using scale factor value at 2,000

4. Seismic interpretation

4.1 Synthetic well-tie

The well data is in depth domain and a calibration from time to depth is necessary before performing tie to the seismic data. There are several objectives with well tie. However, there are four most important objectives (Rob Simm and Mike Bacon, 2014):

1. To check if seismic data is zero phase so that it can be adjusted if necessary;
2. To generate the time-depth relationship between well and seismic gather;
3. To perform wavelet extraction for seismic inversion or modelling and;
4. To check the offset scaling to define whether seismic data has true amplitude processed to have the correct AVO behavior and adjust amplitudes if necessary.

The well calibration process included log editing, wavelet estimation, wavelet scaling, synthetic seismograms generation and establishing correlation between the synthetic seismograms of seismic data with geological key surfaces. The first important step in the procedure was calibration of the checkshot to sonic log. The new calibrated sonic log was later used into synthetic seismogram to perform the well tie. Total "check shot point fit" method was applied in sonic calibration workflow.

In order to define the absolute phase of the seismic data, the deterministic wavelets were extracted at well 6407/6-3, 6407/6-4 and 6407/6-5 as shown in Figure 4.1. All extracted wavelets from wells data have phase around -12 degree which is approximately close to zero phase. In the previous section 3.2, the angle stacks were conditioned and defined a target wavelet representing their frequency spectrums with zero phase assumption. Since the absolute phase of seismic data is close to zero phase, it is acceptable to use the target wavelet defined in the data conditioning in section 3.2 to perform in the synthetic well tie and in the forward modelling. The last objectives performing synthetic seismogram is defining wavelet scale factor (SF). The importance of scale factor was explained in the section 3.2.4. The scale factor value at 2000 defined in section 3.2 was fine-tuned by comparison synthetic traces with the real seismic. Results of synthetic well tie are shown well by well in Figure 4.2 to Figure 4.4. In general, well-ties show good fit in all three wells. The amplitude of the synthetic seismogram shows a good match with the real seismic data. Thus, it confirmed a scale factor of 2000 is a good value to use in further AVO modelling and inversion. The maximum correlation between synthetic seismogram and seismic data occurs in the Spekk, Not and Ile

Formation. Those three horizons have strong responses in seismic and can be mapped with more confidence compared to the Garn reservoir.

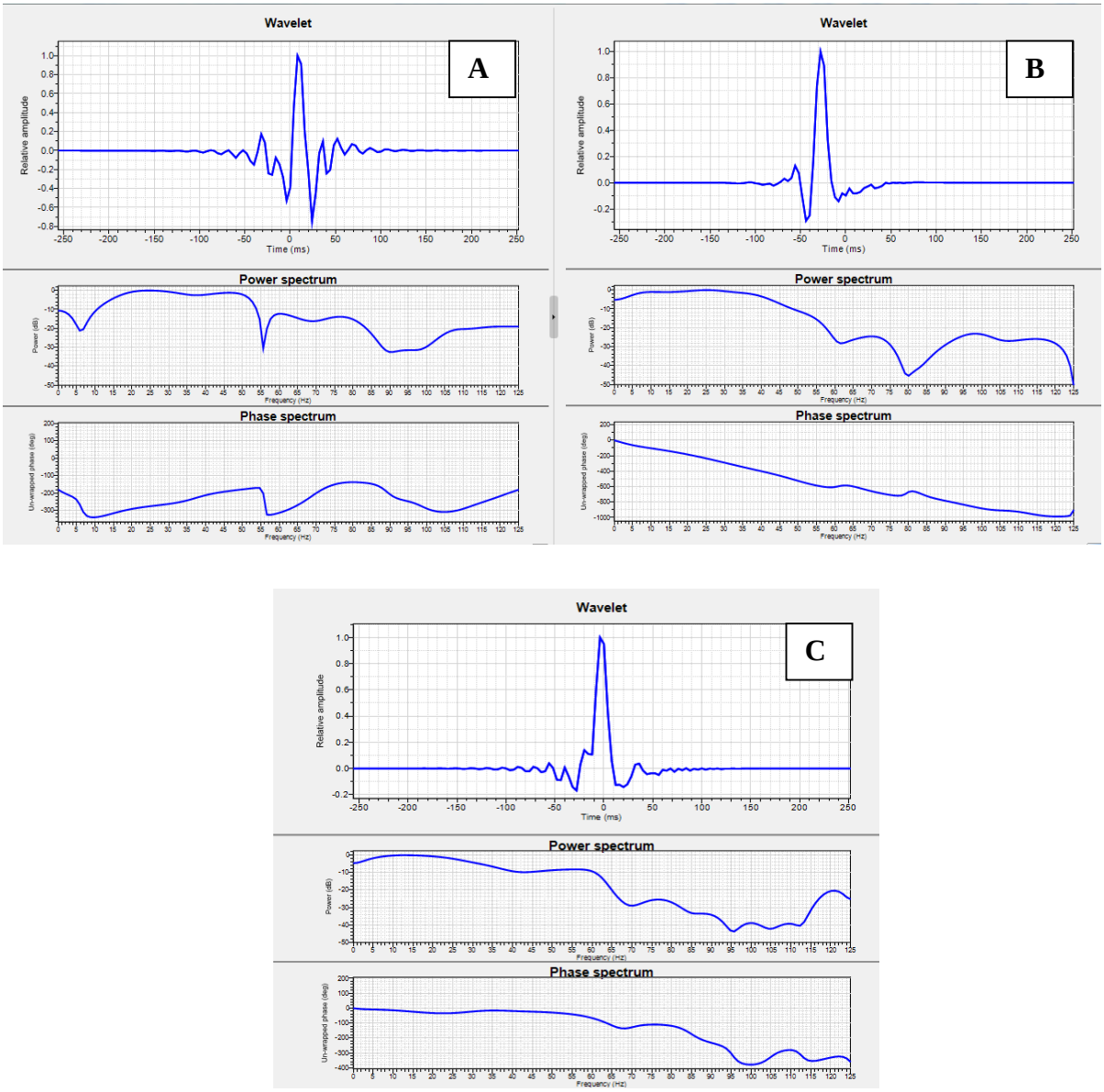

Figure 4.1 Comparison of extracted wavelet at well 6407/6-3 (A), extracted wavelet at well 6407/6-4 (B) and extracted wavelet at well 6407/6-5 (C)

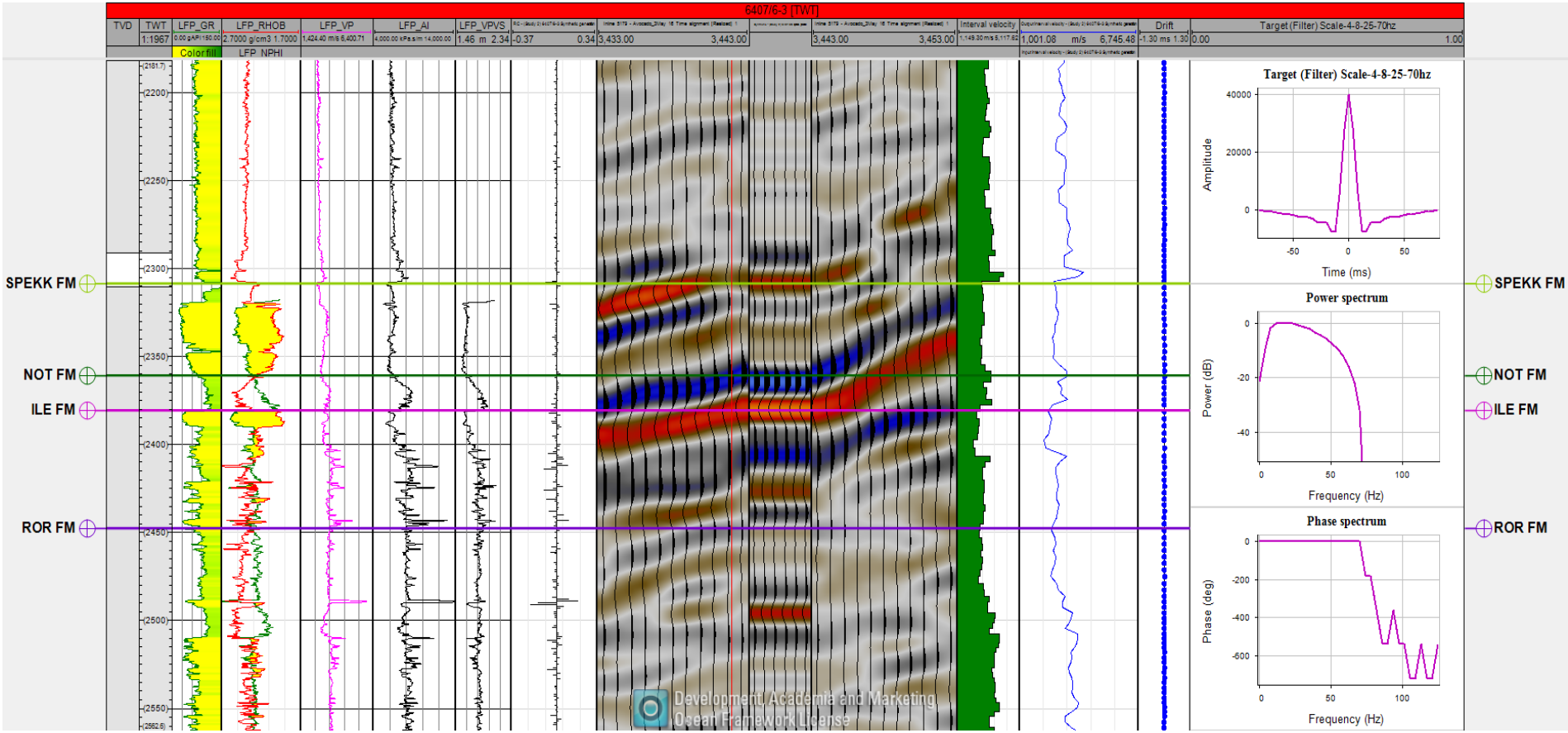

Figure 4.2 Well tie of near angle stack at well 6407/6-3

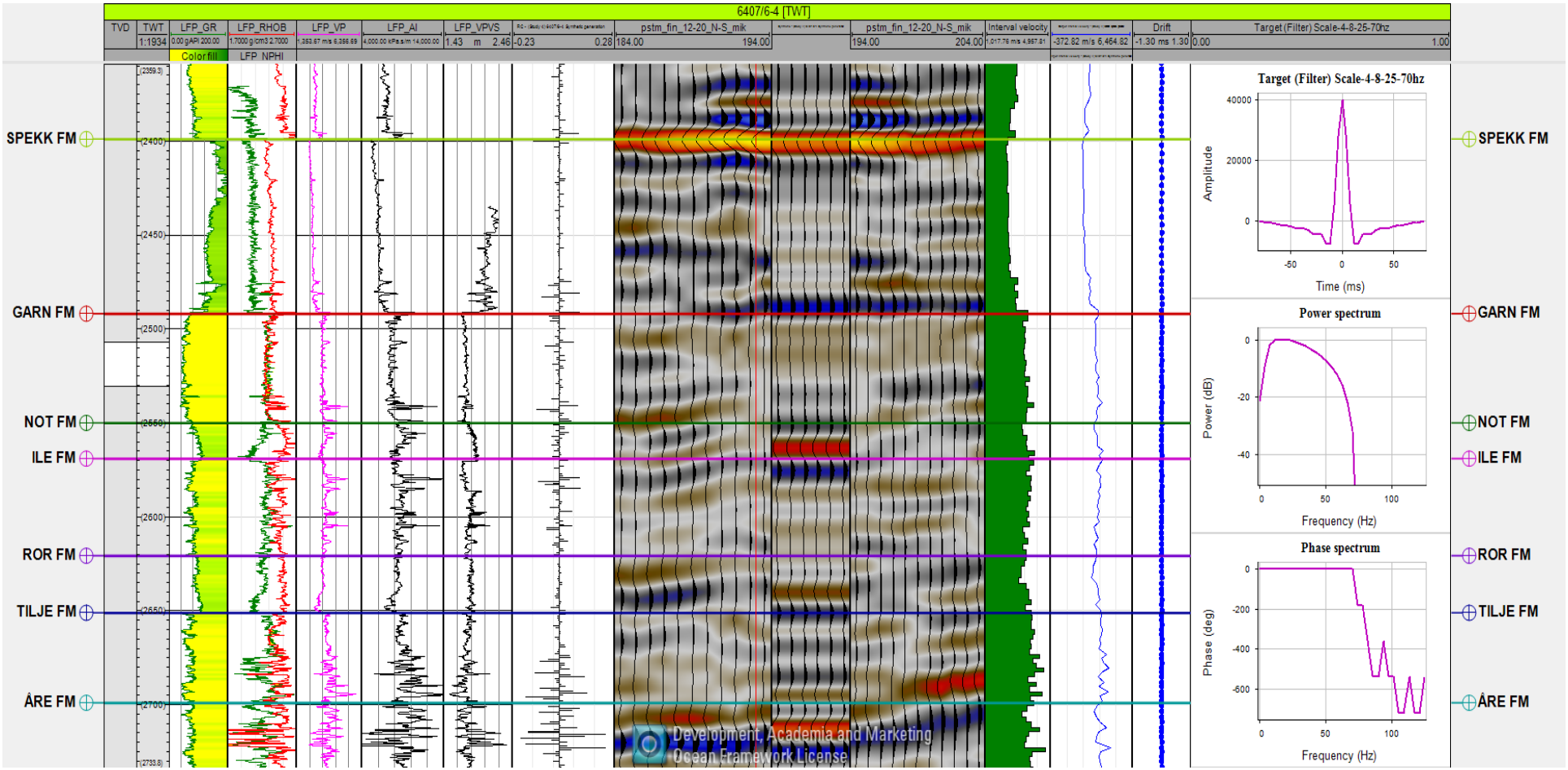

Figure 4.3 Well tie of near angle stack at well 6407/6-4

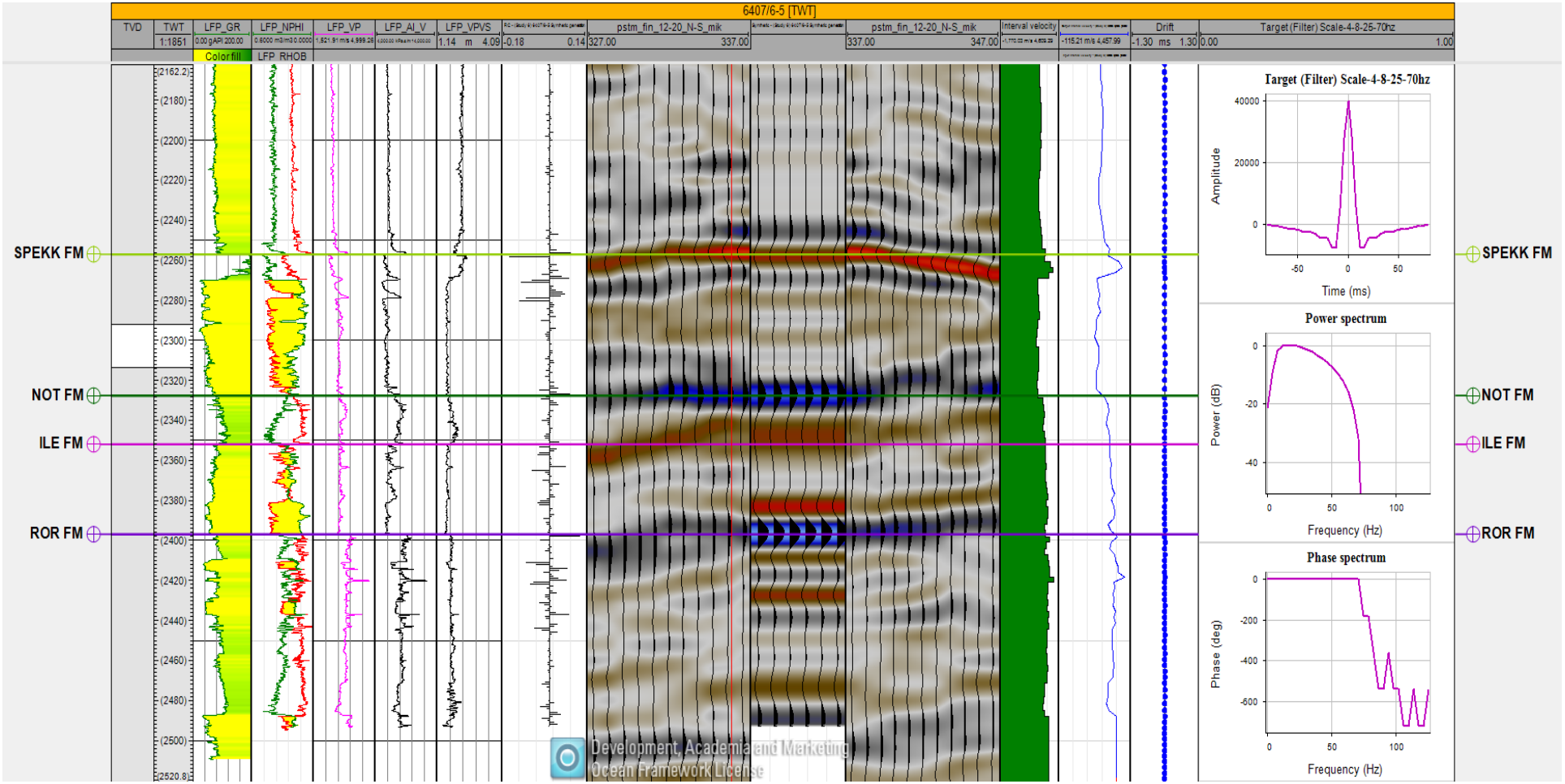

Figure 4.4 Well tie of near angle stack at well 6407/6-5

4.2 AVO modelling

AVO analysis is an effective technique in reservoir characterization. Since AVO modelling is able to link rock properties and offset-dependent amplitude response, it is a useful tool in assisting interpretation and studying fluid effect in seismic data. The required input to the modelling are the elastic parameters Vp, Vs and Density from well log. The target wavelet and the wavelet scale factor from previous study are used to build AVO model.

Among three exploration wells, well 6407/6-5 has a full measured Vs from Top Spekk to total depth (TD). Figure 4.5 shows the AVO model of well 6407/6-5, using convolution modelling with reflection coefficient computed by the Zoeppritz equation. As shown in Figure 4.5, the amplitude at Top Spekk reduces with offset. In the opposite, the amplitude of Top Garn slightly increases with offset. If the amplitude response of Top Garn is very weak in near angle stack, it has changed into a soft kick in far/ultra-far angle. Top Not and Top Ile always come in pair with hard kick and soft kick respectively. Their amplitude has gained strongly in far/ultra- far angle stack. A cross-plot of amplitude versus angle was also generated in well 6407/6-5 as shown in Figure 4.6. Four top horizons was plot to describe their AVO classes. For an example, Top Spekk starts with high negative amplitude in near stack and reduces with offset. It indicates a typical class IV in AVO classification. Therefore, Top Spekk should be mapped as a soft kick in near angle stack. Following, Top Garn has close to zero intercept and negative gradient. This leads it to be class II or IIp. As AVO class II/IIp character, Top Garn is not easy to map as its amplitude is always too low or even could be reverse polarity in far/ultra-far stack and increase with offset. In general, Top Garn is recommended to be interpreted below Top Spekk and its horizon placed where the weak amplitude of near stack changing to the strong negative in far/ulta-far stack is observed. Top Ile is a typical AVO class III that its amplitude is always negative in all angle stacks and increases with offset significantly. Top Not is a base of AVO class III of the Ile Formation. Top Not is a strong hard kick in all of angle stacks and its amplitude increases with offset. Those two horizons were confidently recognized in far cube, which their AVO classes work most.

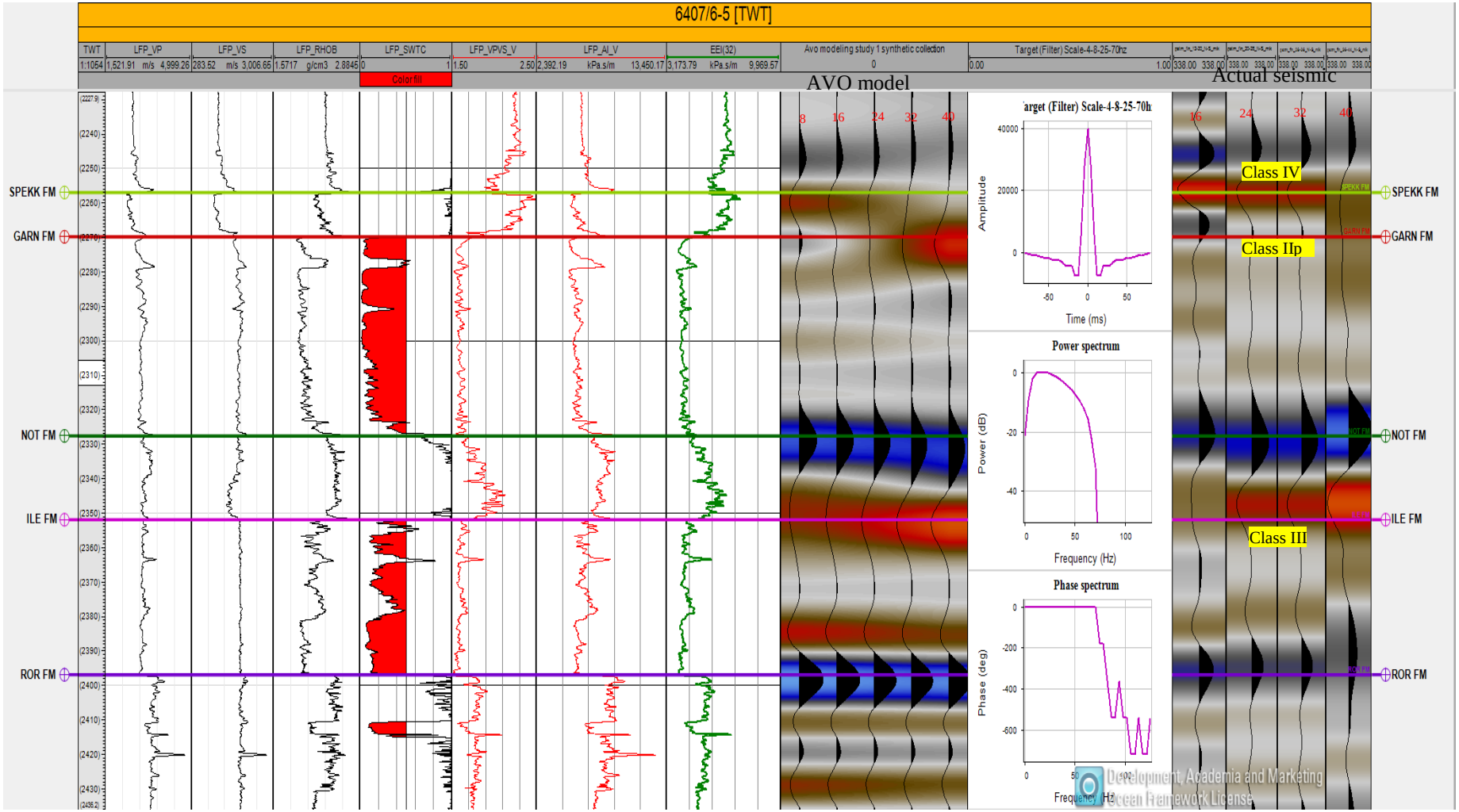
6407/6-5 [TWT]
TWT
LFP_VP
LFP_VS
LFP_RHOB
LFP_SWTC
LFP_VPVS_V
LFP_AI_V
EEI(32)
Avo modeling study 1 synthetic collection
Target (Filter) Scale-4-8-25-70hz
AVO model
Actual seismic
SPEKK FM
GARN FM
NOT FM
ILE FM
ROR FM
Class IV
Class IIp
Class III
Amplitude
Time (ms)
Power spectrum
Power (dB)
Frequency (Hz)
Phase spectrum
Phase (deg)
Development, Academia and Marketing
Ocean Framework License

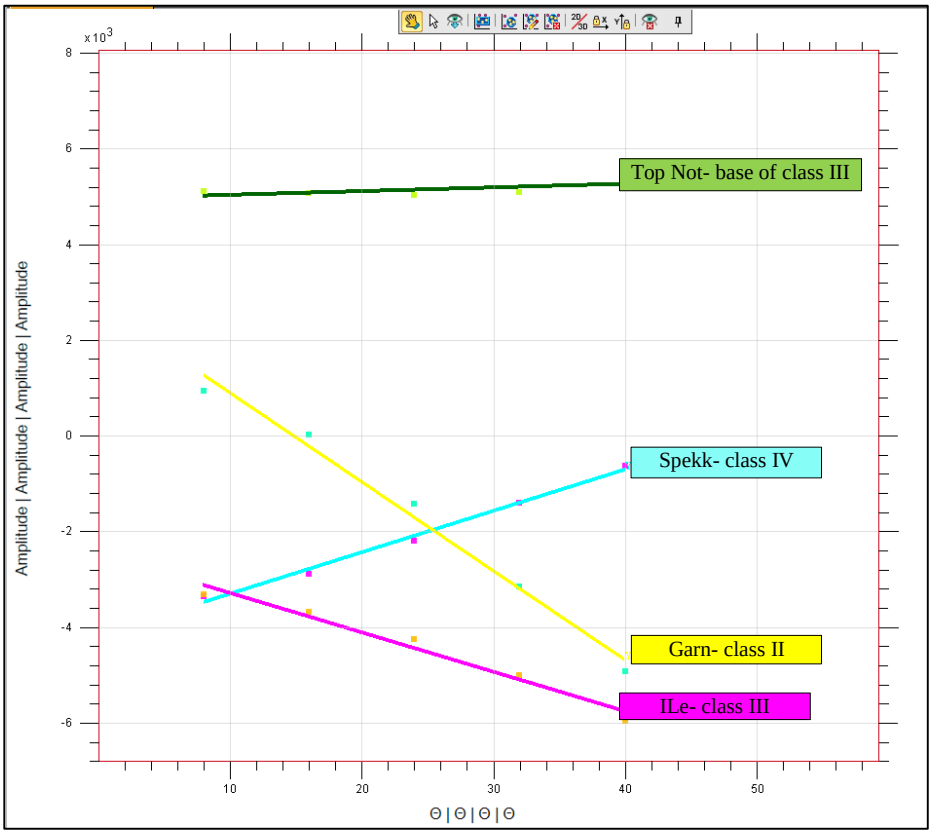

Figure 4.6 Cross-plot of amplitude versus angle in well 6407/6-5

Well 6407/6-3 didn't have measured Vs data; but estimated curve was calculated to test AVO response. Figure 4.7 shows the AVO modelling in well 6407/6-3. In general, the AVO response in Top Spekk, Top Garn, Top Not and Top Ile follows similar pattern as seen in AVO model of 6407/6-5.

The last AVO modelling was tested in 6407/6-4 which was a wet well at the down flank of the structure. Both the Garn Formation and the Ile Formation showed good quality of sand and their continuities in the southern part. The AVO modelling is shown in Figure 4.8. AVO behavior at Top Garn is still class II, however the presence of thick cap rock of soft organic shale of the Spekk Formation in deep basin affected amplitude response at Top Garn as a clear hard kick in the near stack. In the far stack, the amplitude remained low positive. Hence, mapping Top Garn in the deep basin without well control is highly sensitive and uncertain.

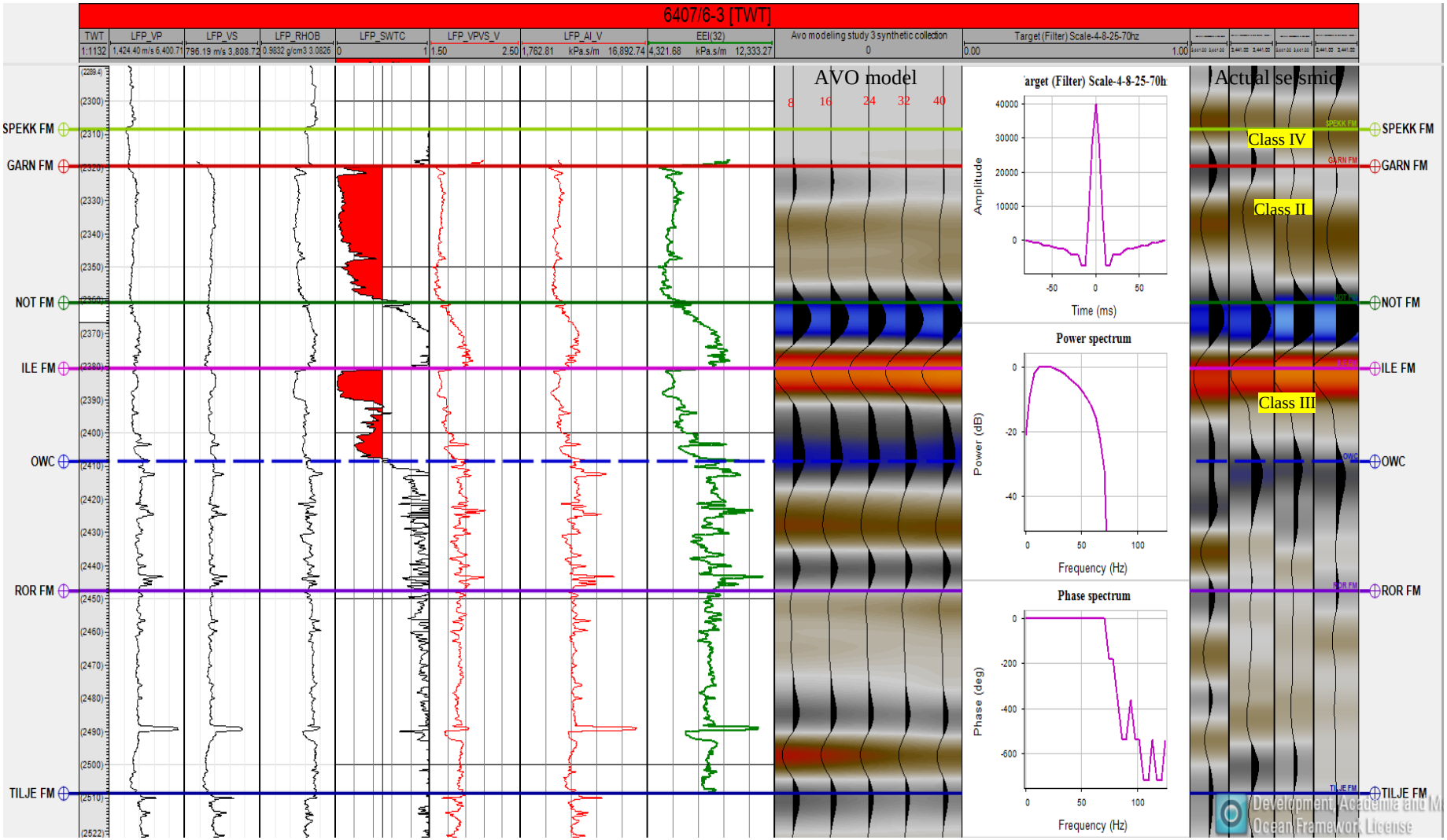
6407/6-3 [TWT]
TWT
LFP_VP
LFP_VS
LFP_RHOB
LFP_SWTC
LFP_VPVS_V
LFP_AI_V
EEI(32)
Avo modeling study 3 synthetic collection
Target (Filter) Scale-4-8-25-70hz
AVO model
Actual seismic
8 16 24 32 40
Target (Filter) Scale-4-8-25-70h
Amplitude
Time (ms)
Power spectrum
Power (dB)
Frequency (Hz)
Phase spectrum
Phase (deg)
Frequency (Hz)
Class IV
Class II
Class III
SPEKK FM
GARN FM
NOT FM
ILE FM
OWC
ROR FM
TILJE FM
16 24 32 40

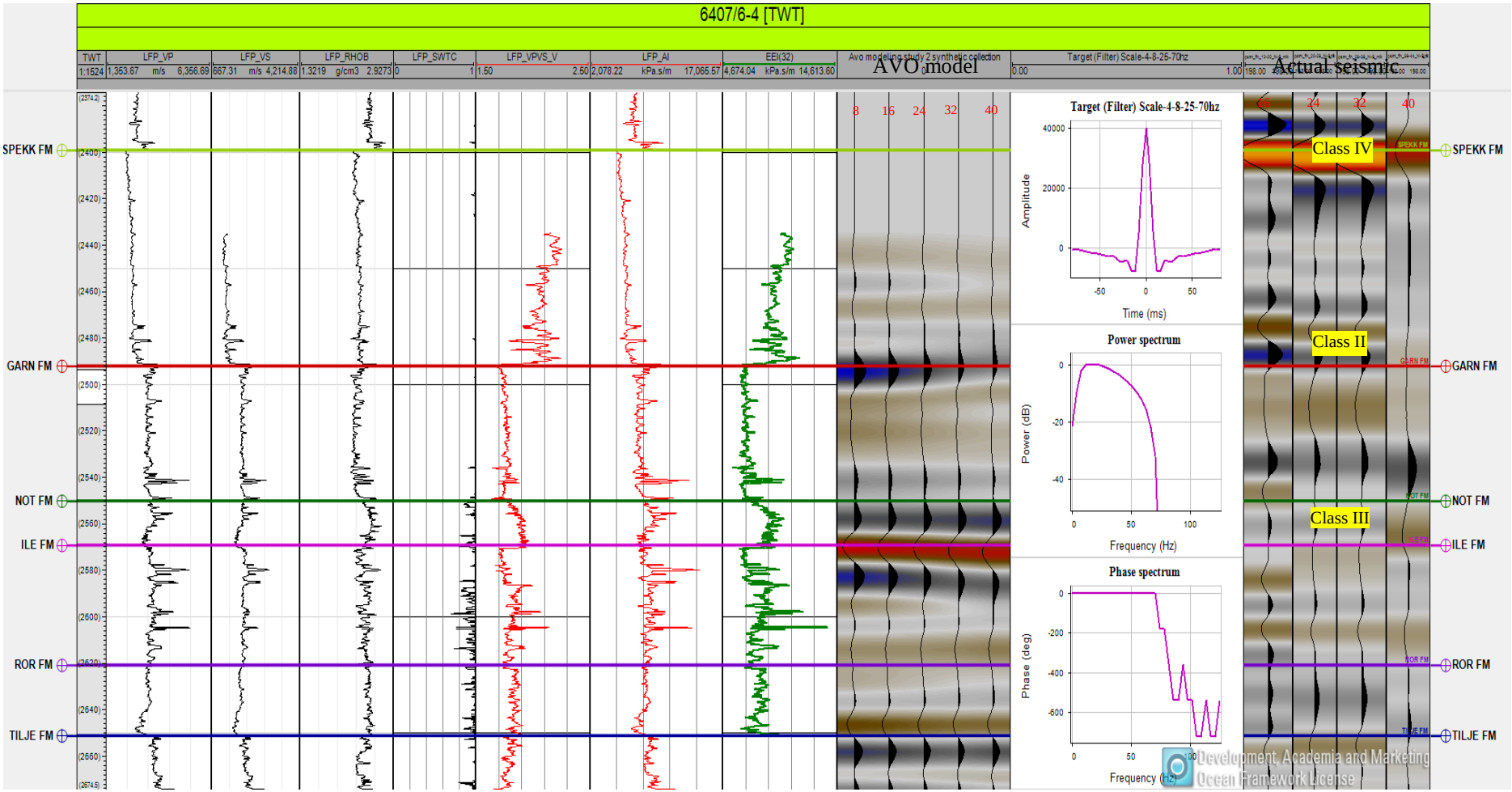

Figure 4.8 AVO model of well 6407/6-4

AVO modelling was performed in three exploration wells to understand the seismic response in both case of gas sand and brine sand. For a complicated area like the Mikkel Field, AVO model helps to reduce an uncertainty during mapping. Summary of AVO observation and its response for each horizon is as shown in table 4.1

Horizons	AVO class	High structure		Down flank	
		Geology	Seismic pick	Geology	Seismic pick
Top Spekk	IV	Could be eroded	- Trough response in all angle stacks. - Strongest trough on the near stack.	Thick package.	- Trough response in all angle stacks. - Strongest trough on the near stack.
Top Garn	II/ IIp	Gas sand	- Low trough in near and amplitude increase on the Far/Ultra far stack. - Possible polarity flip from weak peak in near to a trough in far/ultra-far	Possible brine.	- Amplitude response dependent on the Spekk Formation thickness. - Possible a weak peak on the near stack. - Mostly dimming in far/ultra-far stack.
Top Not	Base of class III	Mostly shale	- Strong peak in all angle stacks. - Strongest peak in Far/ultra-far stack.	Mostly shale	- Strong peak from near. - Amplitude increases with offset.
Top Ile	III	Gas sand	- Trough in all stacks. - Strongest trough in Far/ultra-far stack.	Possible brine	- Trough in all stacks. - Strongest trough in Far/ultra-far stack.

Table 4.1 Summary AVO model observation in the Mikkel Feld

4.3 Structural interpretation

The goal of interpretation is to define stratigraphic horizons and delineate reservoirs. There are two interpretation performed: (1) horizons interpretation and (2) fault interpretation

4.3.1 Horizon interpretation

Total four mains horizons were selected to delineate the reservoirs: (1) Base Cretaceous Unconformity (BCU); (2) Top Garn reservoir; (3) Top Not; (4) Top Ile reservoir.

Base Cretaceous Unconformity (BCU) or Top Spekk

BCU or Top Spekk is represented for a change in tectonic environment in the Halten Terrace. It is a regional unconformity between the syn-rift Jurassic Formation and the post-rift Cretaceous Formation. The transition from higher velocity of overlain Cretaceous Formation into lower velocity of the Spekk shale creates a decrease in acoustic impedance representing a strong trough (in normal polarity) in the seismic data. Since Top Spekk is a typical class IV as shown in the previous AVO study in section 4.2, the amplitude response of Top Spekk reduces with offset. Thus, Top Spekk is ideally mapped on the near angle stack.

The BCU response is strong and expected all over the field. However, there is possible erosion happening in the high structure as amplitude is extremely brighten up because of tuning effect. In the deep basin, the thickness of the organic shale significantly increases and the Top BCU amplitude is brightening up. The BCU was interpreted every 5^{th} line to capture the details of its structure. The structural time map of Top Spekk is as shown in Figure 4.9.

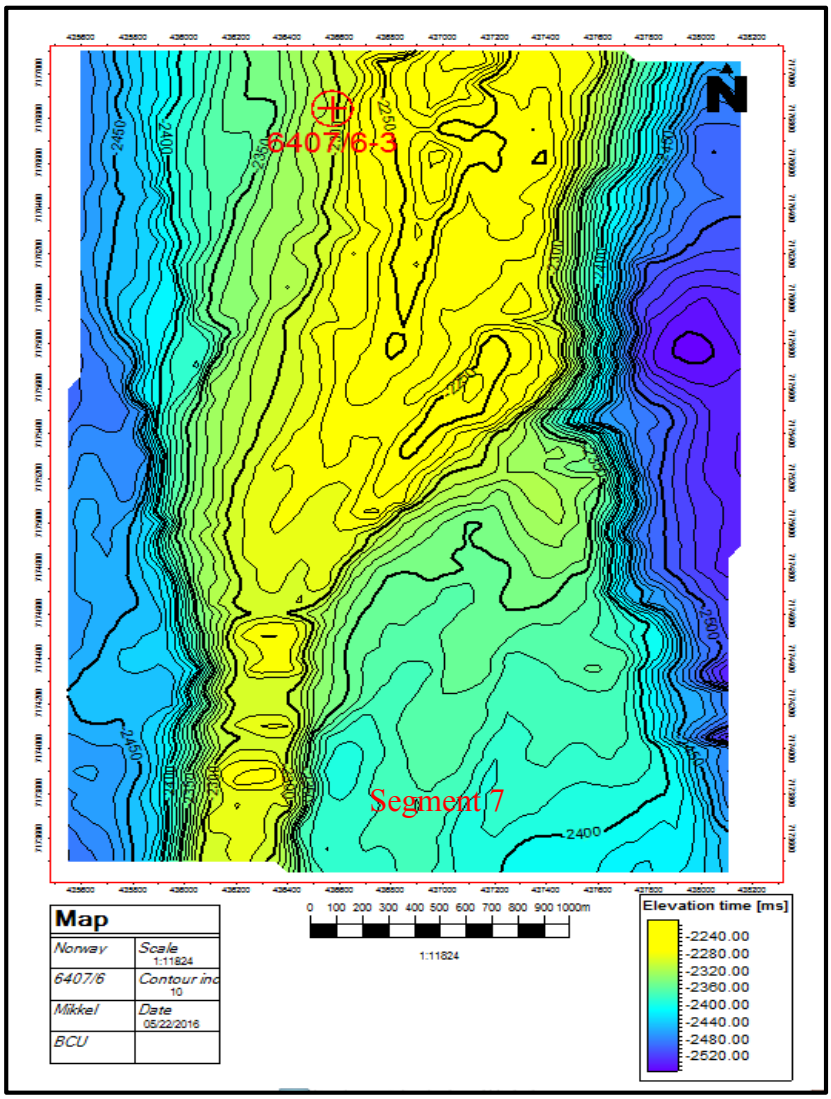

Figure 4.9 Structural time map of Top Spekk

Top Garn reservoir

Top Garn is complicated to map in the Mikkel area. Firstly, the Garn Formation was deposited in the syn-rift phase. Thus, the thickness and deposited sediments of the Garn Formation could be varying in each fault block that leads to strata response on seismic image is inconsistent and unpredictable. Secondly, Top Garn is an AVO class II/IIp as explained in section 4.2, with a low amplitude response in near angle stack. This means Top Garn is weak and hard to be recognized. In far and ultra-far, amplitude response of Top Garn increases, however it still depends on the thickness of cap rock of the Spekk

Formation to increase negative amplitude (section 4.2). Though Top Garn is bright up on the far/ ultra-far angle stack, the effect of low frequency of the far/ultra-far angle stack causes Top Garn and Top Spekk interfered as seen in Figure 3.5. Moreover, the presence of the complex fault pattern causes signal to noise ratio reduce significantly, which lead to top Garn extremely dimming in the eastern part (segment 7) of the Mikkel area. The best strategy to map Top Garn is by placing its horizon below Top Spekk, where the negative amplitude clearly increases from the near stack to the far/ultra-far stack. The geology of the Garn Formation is complicated. In the Mikkel Field, it is likely that erosion occured which was recorded in well 6407/5-B-H-3. The Garn reservoir in the well 6407/-B-H-3 was totally absent. The uncertainty in mapping Top Garn is higher than the others horizons. Thus, the area without well control is highly uncertain in interpretation. Top Garn was map every 5th line to capture the details of its structure. The structural time map of Top Garn is shown in Figure 4.10.

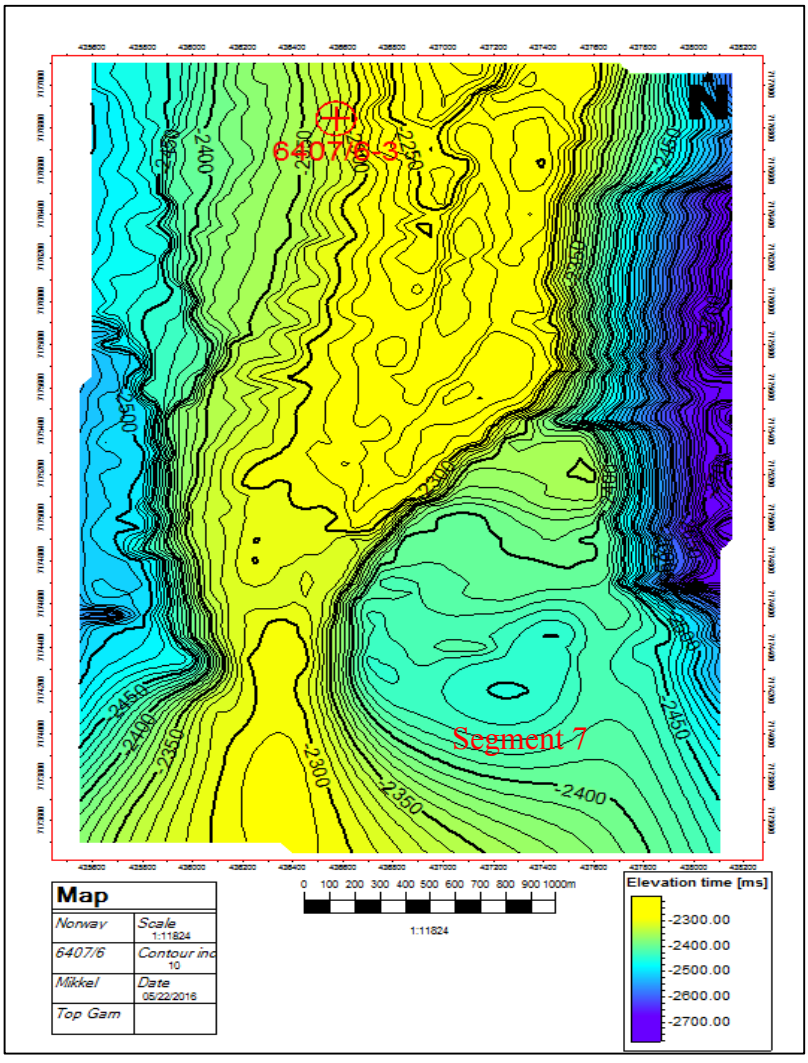

Figure 4.10 Structural time map of Top Garn

Top Not

The Not Formation consists of the upper laminated sand and lower thick shale package. Because of limited seismic resolution, the horizon couldn't separate the difference between the sand in the Garn Formation and the upper laminated sand of the Not Formation. Thus, the final mapping of Top Not has been interpreted as an Intra Not horizon, which placed at top of hard shale package.

The transition from the soft gas sands in the Garn Formation to the shaley Not Formation creates a strong peak amplitude. The presence of below soft gas sand in the Ile Formation increases the strength of amplitude response of Top Not in all angle stacks. The Not Formation and the Ile Formation always come in pair as peak and trough respectively. Their amplitudes are strongest in far/ultra-far stack. Top Not was interpreted every 5th and its structural time map is shown in Figure 4.11.

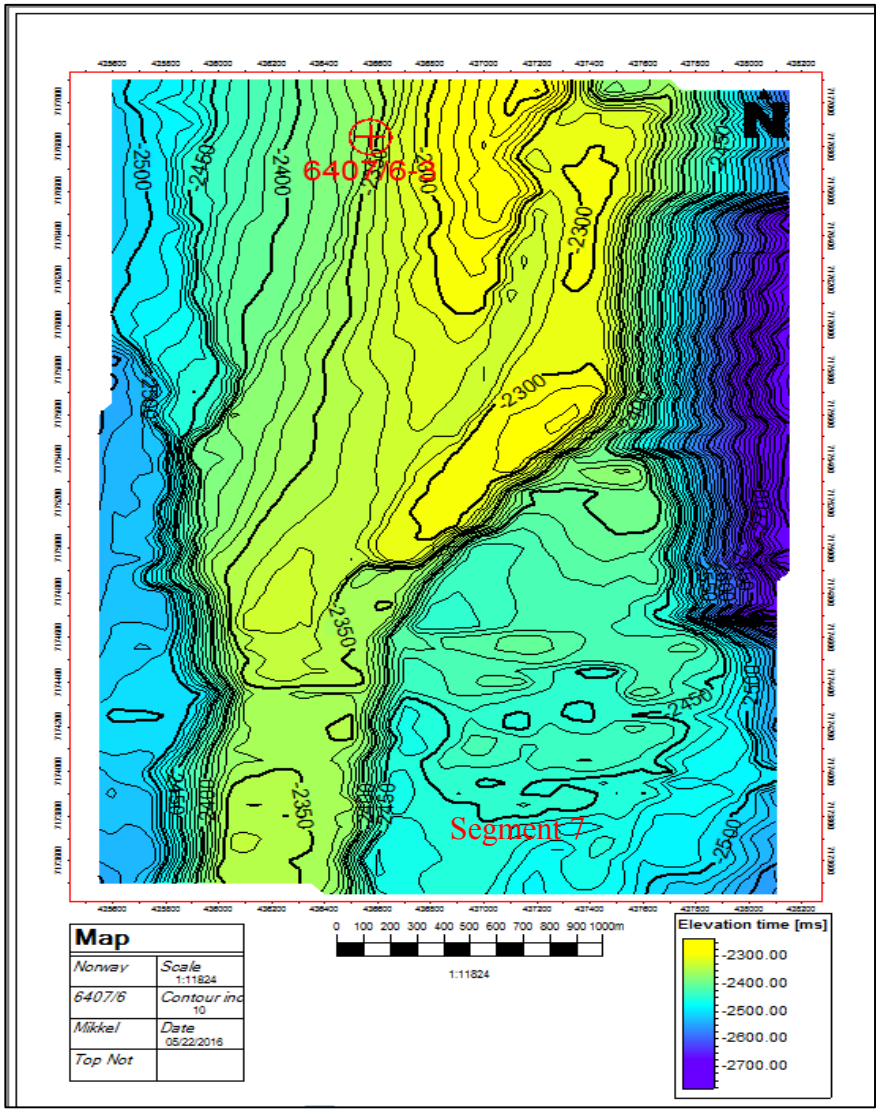

Figure 4.11 Structural time map of Top Not

Top Ile

The Ile Formation is a gas reservoir in the Mikkel Field. In geological modelling, Ile was separated into Ile 1, Ile 2 and Ile 3 according to its depositional environment. However, seismic resolution is not able to distinguish them separately. Therefore, only Top Ile was mapped as a trough transition from the Not shale to the soft gas Ile sand.

As the AVO modelling in section 4.2, Top Ile is a typical AVO class III. Thus, Top Ile was strongest response in far/ultra-far. In general, Top Ile is easy to be recognized and its thickness is quite consistent as a typical character of pre-rift tectonic. Top Ile was mapped on every 5th lines. Its structural time map is shown in Figure 4.12

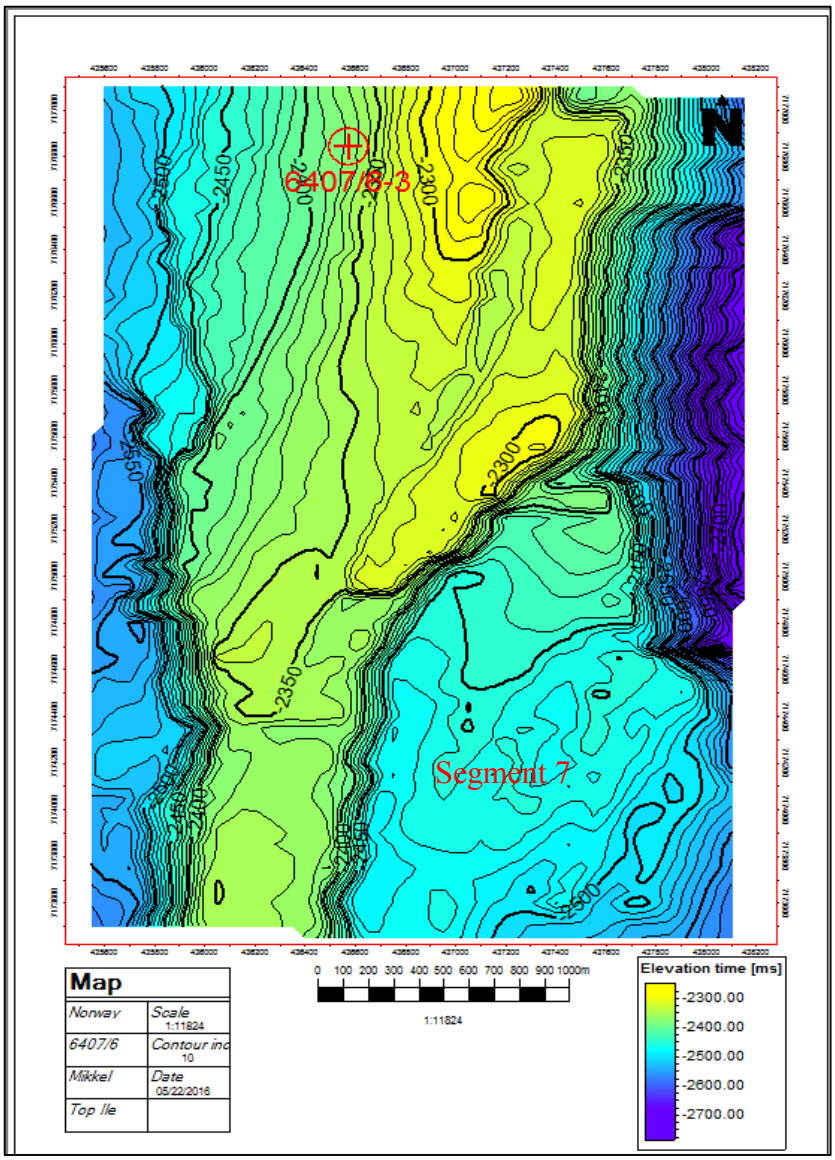

Figure 4.12 Structural time map of Top Ile

4.3.2 Fault interpretation

Fault interpretation was not originally on the plan for this study, however, it is required to divide the study area into separated segments so that each fault block character can be analyzed. Most of the main faults have been interpreted to stop as the BCU.

Beside a conventional fault interpretation, variance attribute was generated to guide fault location. The variance attribute can be explained as the variance of the reflection strength normalized by the average reflection strength. Since fault has a discontinuous character between its fault plane, the variance attribute can help to place fault location. Generally, area with high variance will have high probability of fault presence. Total five main faults were mapped in this area and its variance with fault interpretation is as shown in Figure 4.13.

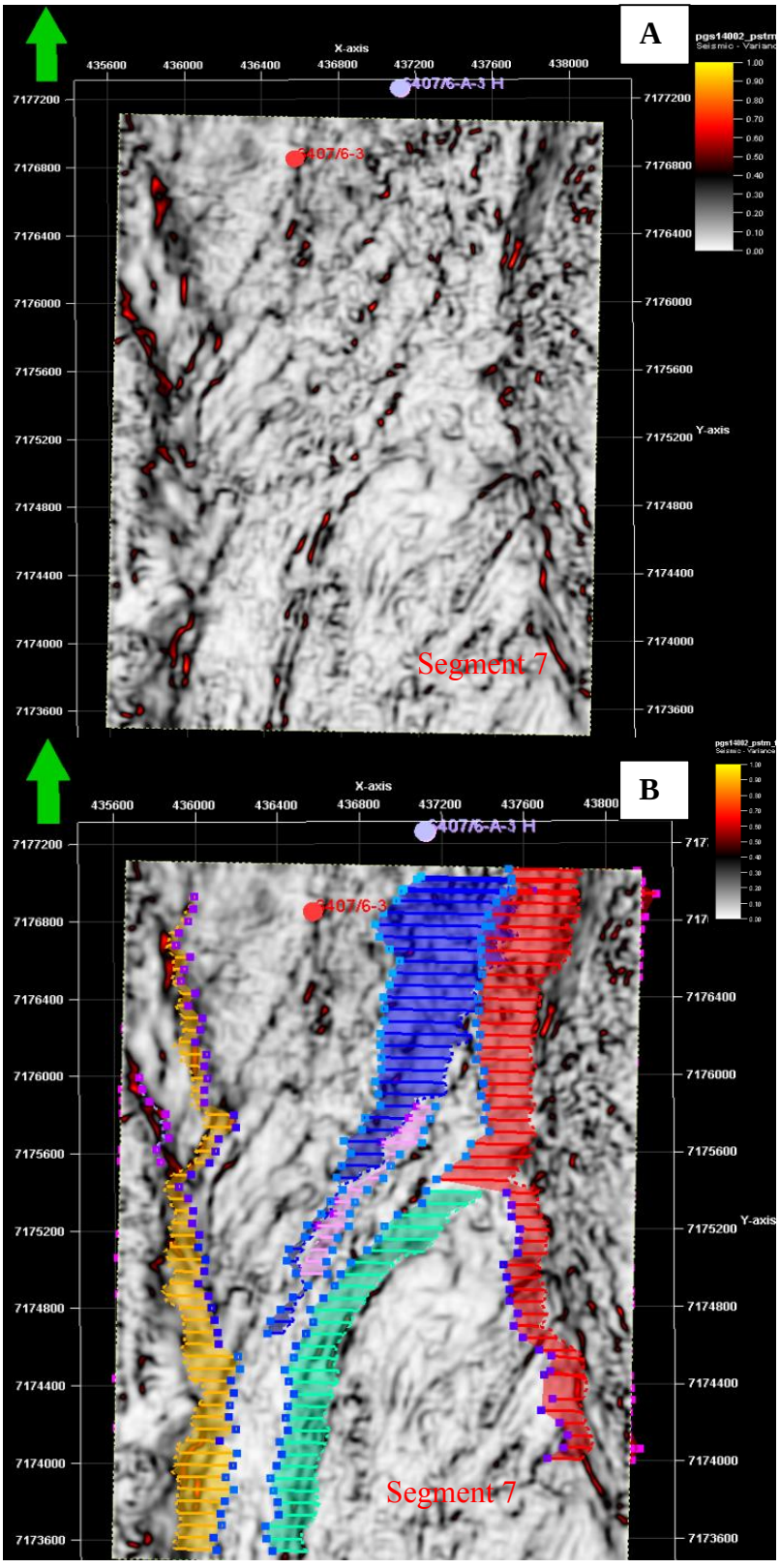

Figure 4.13 Variance attribute at time slice -2428 ms.

(A) Variance attribute map without fault interpretation

(B) Variance attribute map including 5 interpreted faults

4.3.3 Discussion

The Mikkel Field is a gas field which gives a first impression that seismic response should be easy to recognize as a typical AVO class III. Unfortunately, the presence of the overlying soft organic shale in the Spekk Formation significantly reduces the gas effect in seismic response and turns the gas reservoir Garn into a class II/IIp. Moreover, extensive fault patterns have lowered signal to noise ratio causing many areas in down flank being dimmed and hard to separate reflections. In the high structure, erosion occurred into the Not Formation that causes tuning effect in the seismic data.

In the northern part of the seismic data where well 6407/6-3 is located, the interpretation has a high level of confidence. Figure 4.14 shows a comparison between near stack and far stack at IL 5179. Both the Garn Formation and the Ile Formation have brightened up as their AVO classes suggested. This confirms gas presence in northern part of structure. Going to the southern part of the structure, seismic response in segment 7 significantly reduces. As shown in Figure 4.15, the Not Formation and the Ile Formation are still strong reflections in ultra-far stack. In contrast, Top Garn reflection can't be recognized and interpreted. Nevertheless, strata are still planar to sub-planar with each other. Further down to southern part at IL 5414, seismic response is very dim and chaotic as shown in Figure 4.16. Strata has changed from planar/sub planar to dipping surfaces. The Not Formation and the Ile Formation are being wavy surfaces and their seismic facies are different to what has been observed in the northern part. It is very difficult to interpret Top Garn in the south of structure. Traditional mapping cannot resolve this problem. Therefore, Top Garn is not interpreted in segment 7. Further seismic inversion will be generated to optimize the fluid effect in reservoir and predict their facies. Figure 4.17, 4.18, 4.19 and 4.20 are cross-line and north-south arbitrary seismic lines of near and ultra-far angle stack to show profile structure.

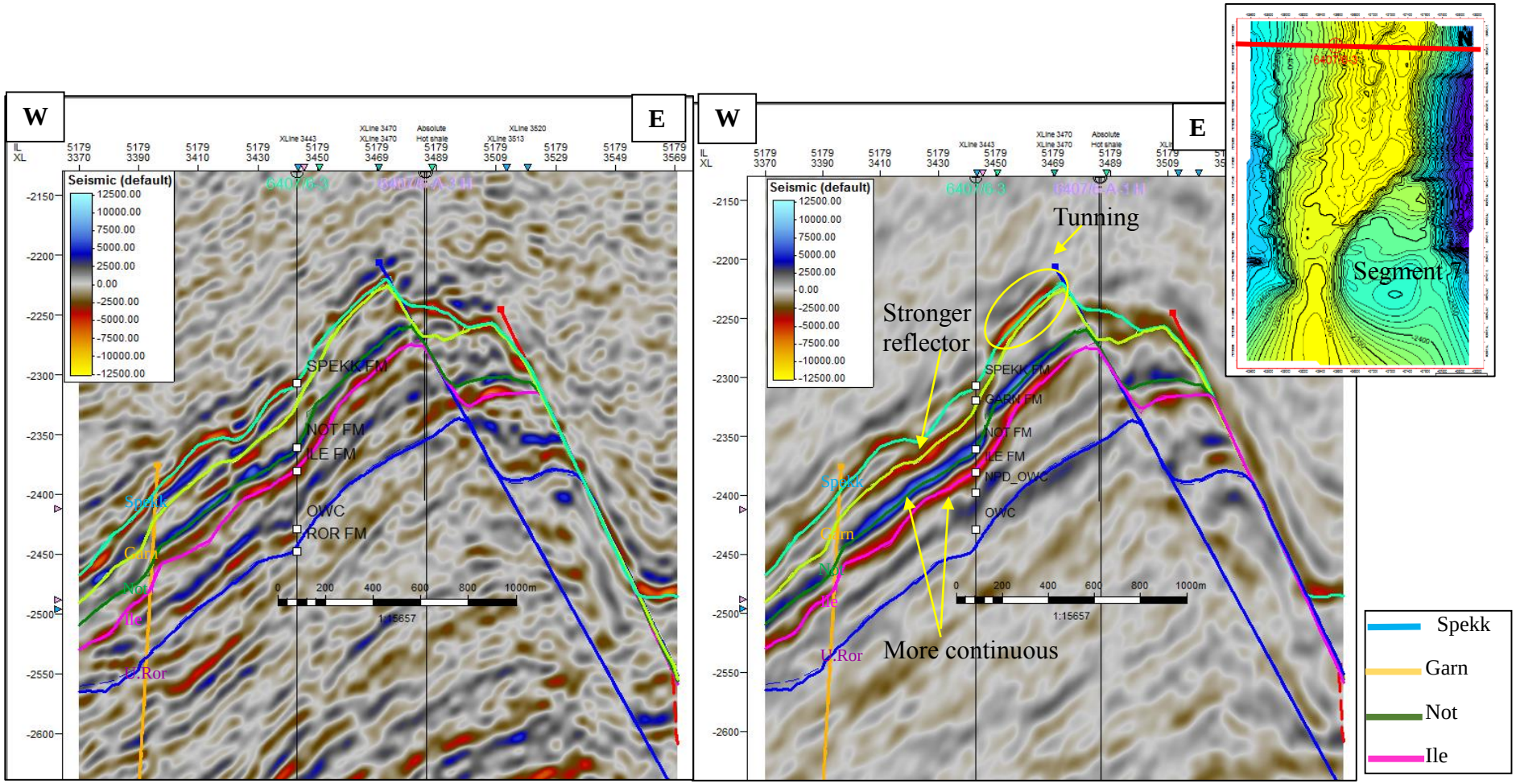

Figure 4.14 Comparison amplitude respond between near angle stack (left) and ultra-far angle stack (right) at IL 5179

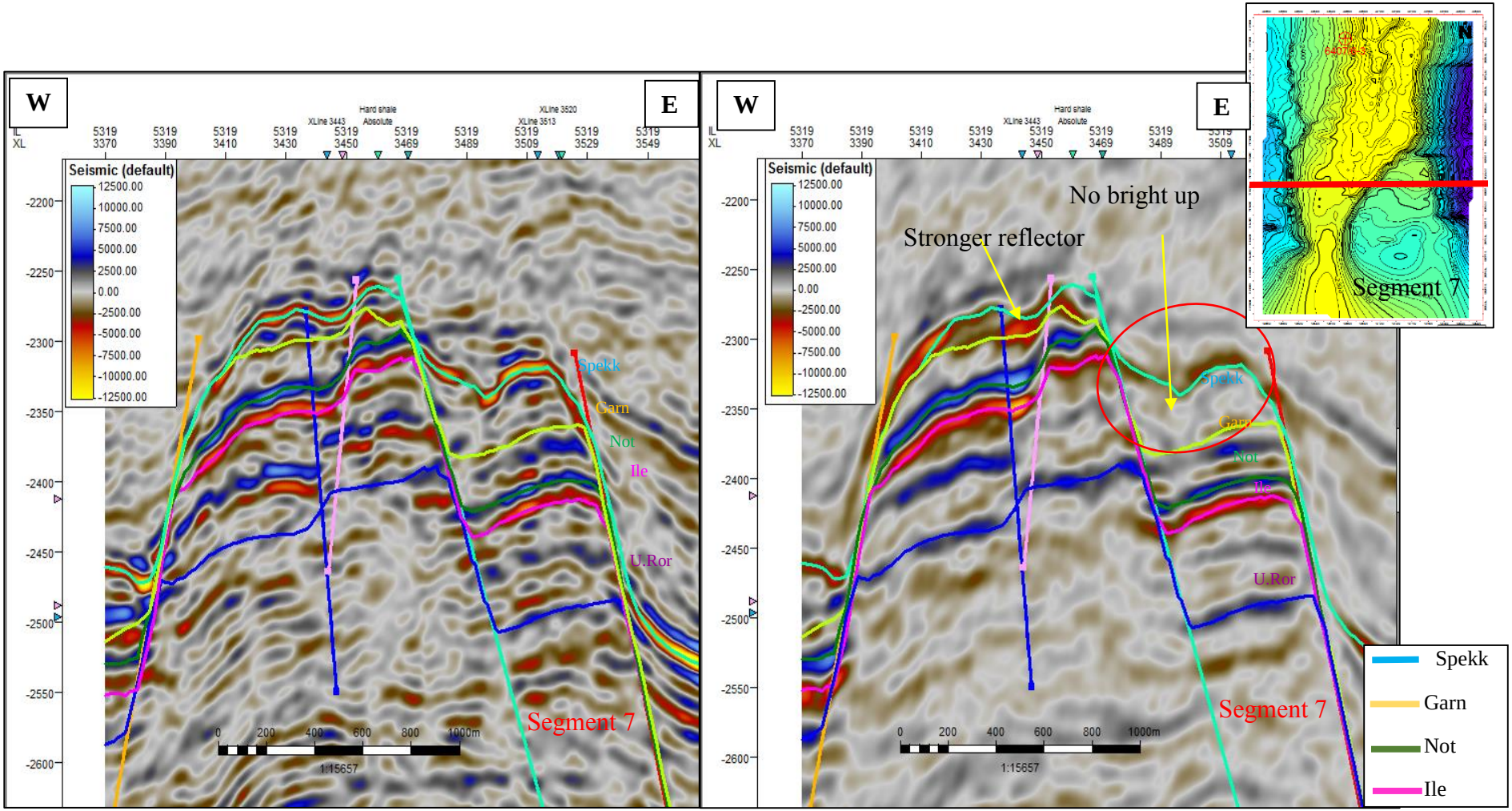

Figure 4.15 Comparison amplitude respond between near angle stack (left) and ultra-far angle stack (right) at IL 5319

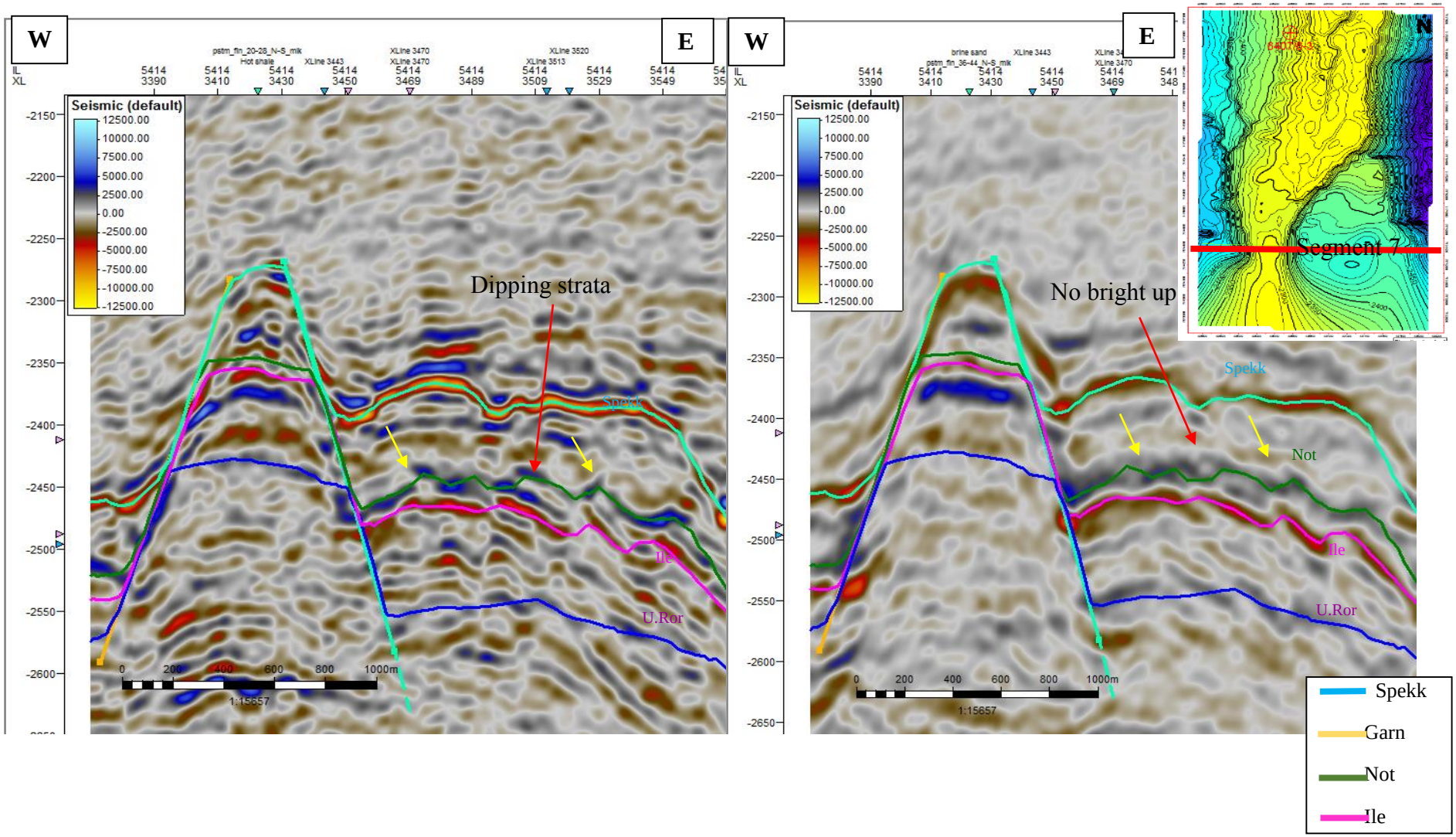

Figure 4.16 Comparison amplitude respond between near angle stack (left) and ultra-far angle stack (right) at IL 5414

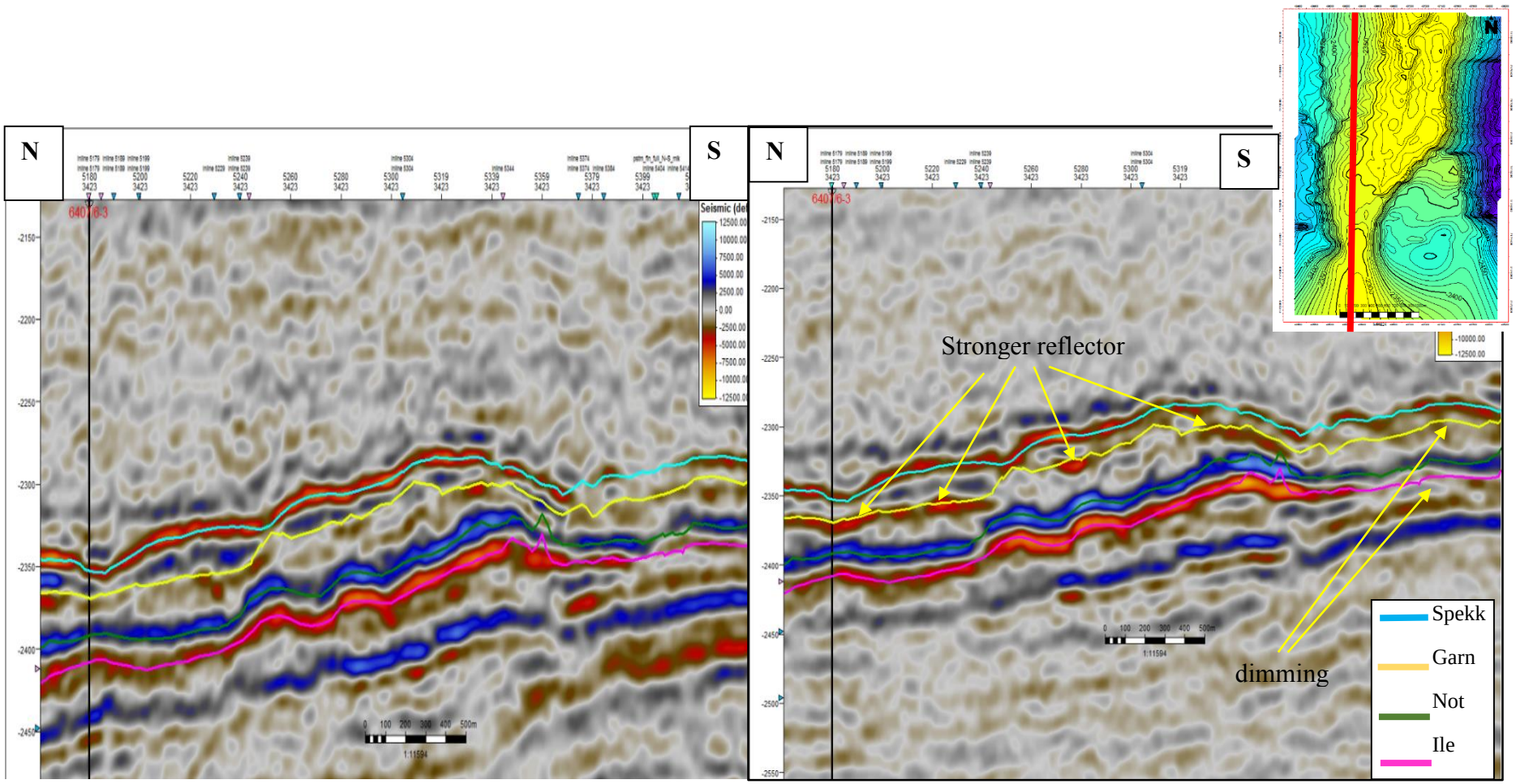

Figure 4.17 Comparison amplitude response between near angle stack (left) and ultra-far angle stack (right) at XL 3423

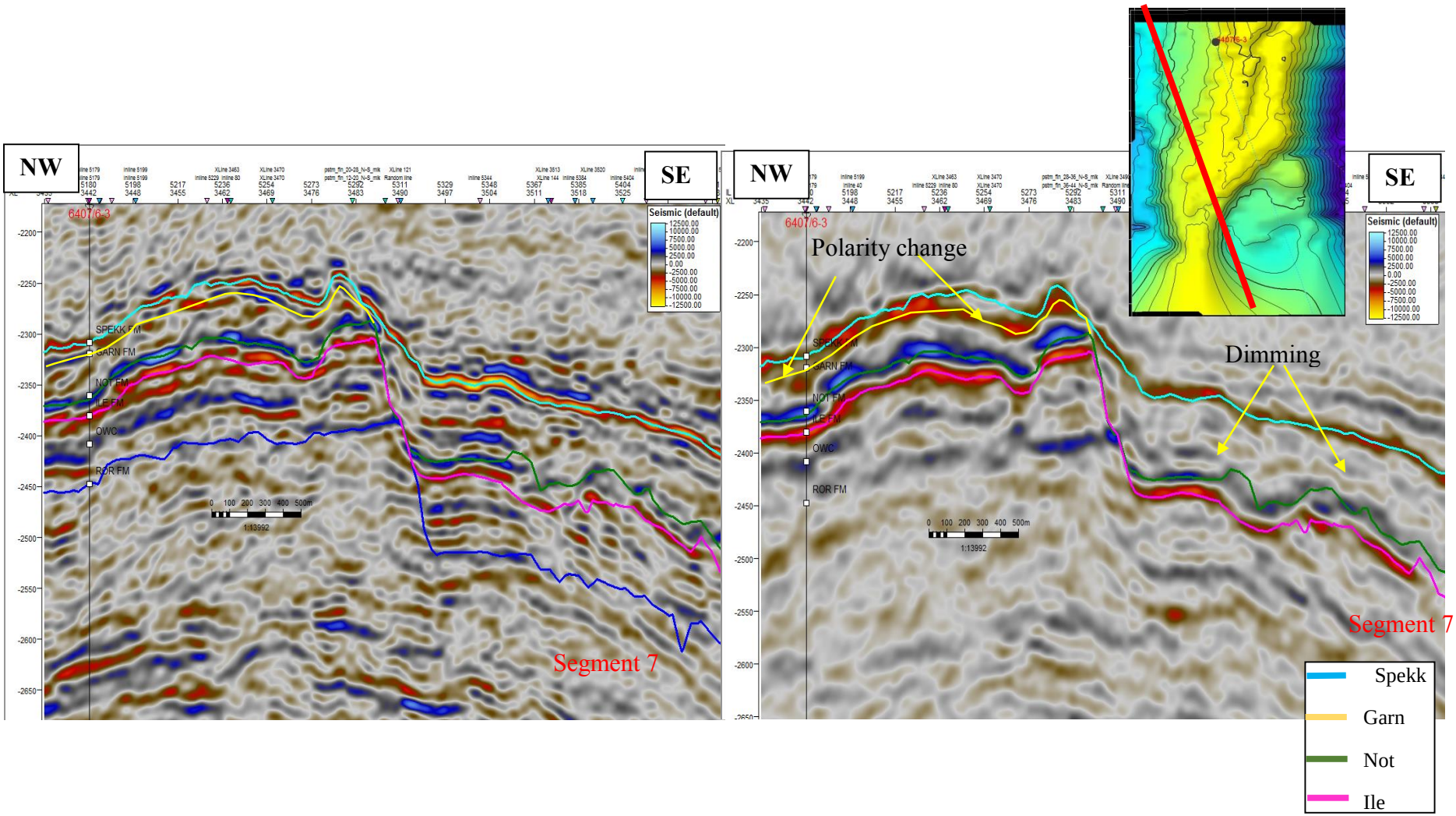

Figure 4.18 Comparison amplitude response between near angle stack (left) and ultra-far angle stack (right) of a random line

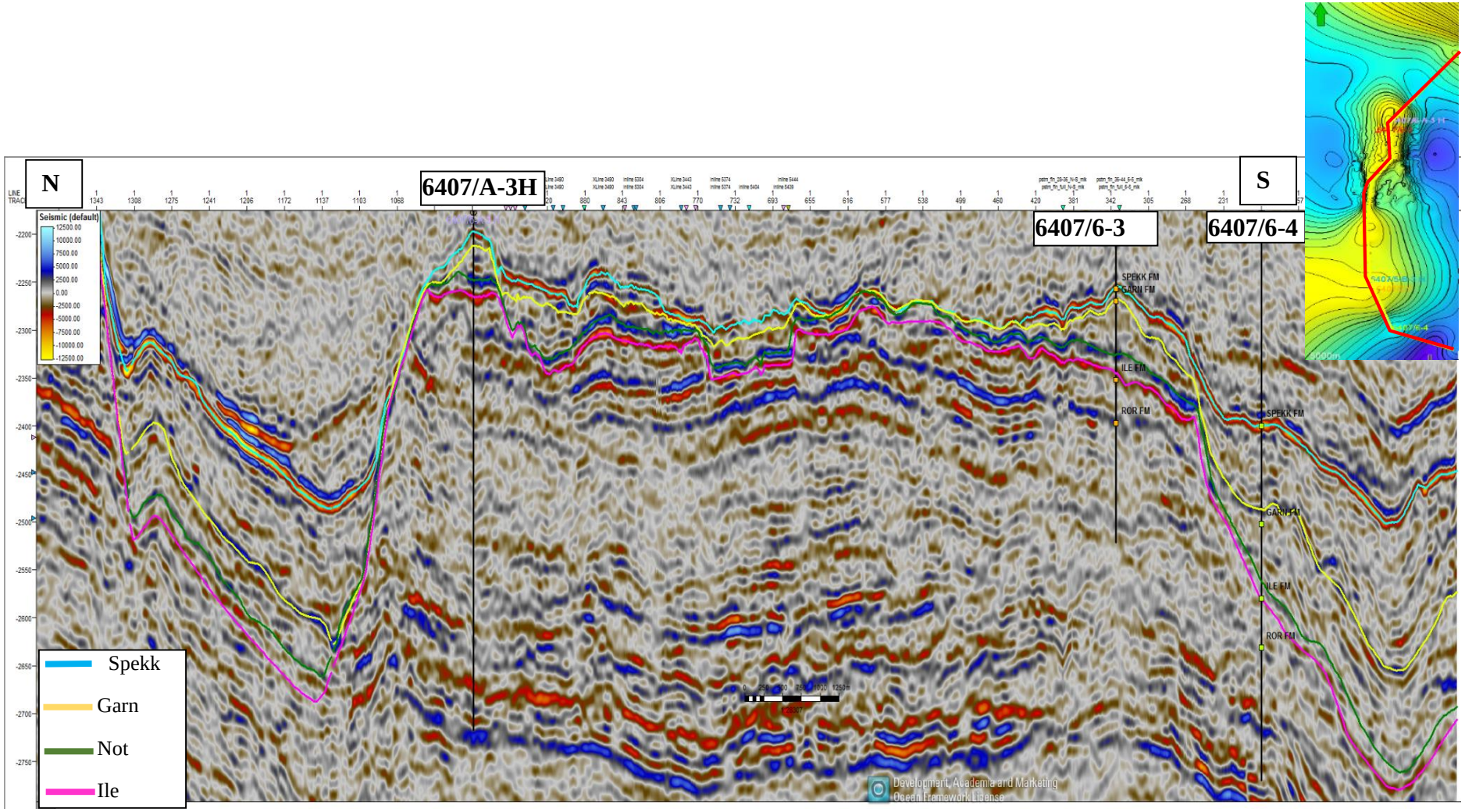

Figure 4.19 North – South arbitrary seismic line of near angle stack

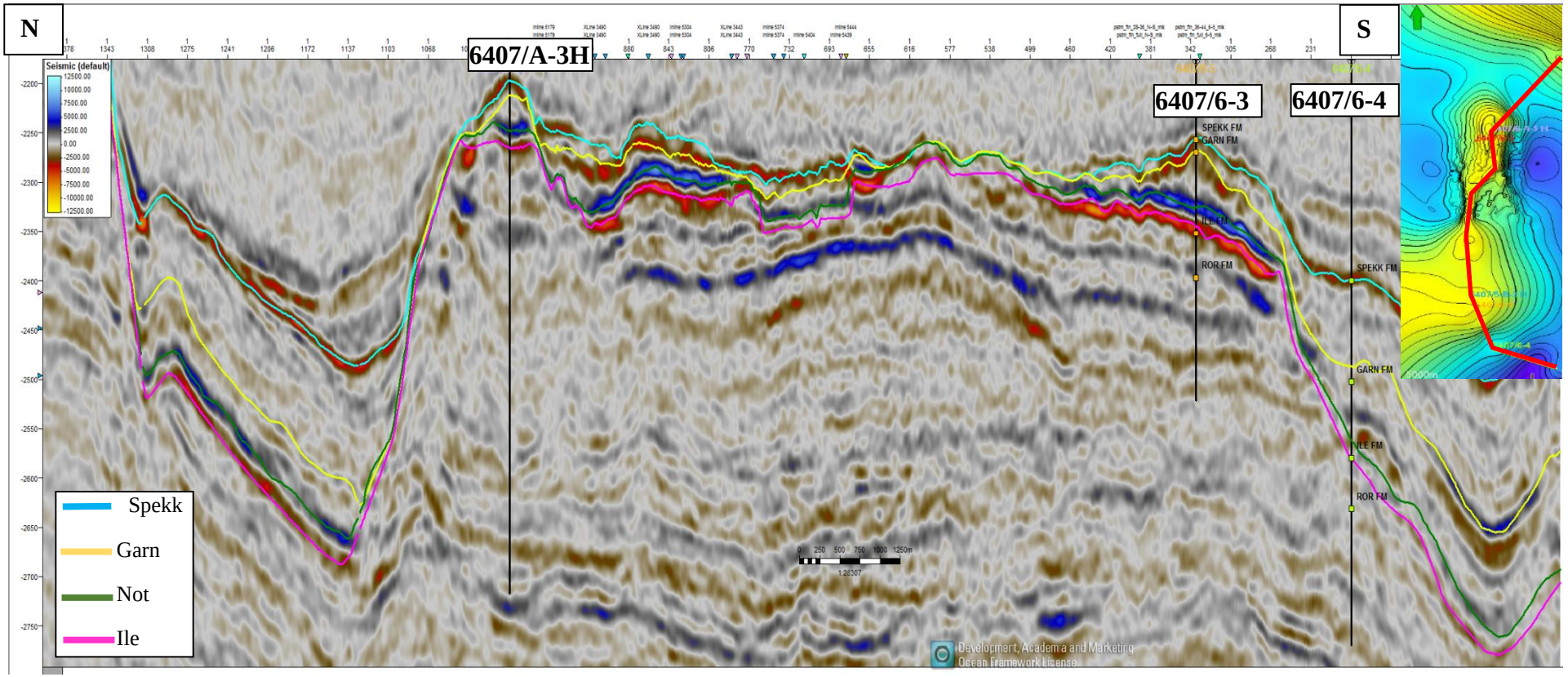

Figure 4.20 North – South arbitrary seismic line of ultra-far angle stack

5. Extended elastic impedance Analysis

5.1 Methodology

Seismic Coloured Inversion (SCI) is a simple, fast and cost effective way of inverting seismic reflection data from an interface attribute to a layer-based attribute. The process creates a volume that its phase rotates -90 degrees with respect to the reflection data and its amplitude spectrum matches to that of well log impedance, with an assumption that input seismic data is zero phase. At first, using the amplitude spectrum of the impedance logs is plotted against frequency on a log-log scale, the average impedance spectrum of the wells is selected by fitting a curve to the impedance logs spectrum.

$$AI(f) = c * f^{a} \quad (1)$$

where AI is impedance spectrum; c is intercept; f is frequency and α is the gradient (Lancaster *et al*., 2000)

This process is designed to shape the mean seismic spectrum towards the well log impedance spectrum. The actual coloured inversion is conducted by performing band-pass filter the amplitude spectrum of real impedance to the seismic band-width. Hence, the result of coloured inversion is a band-limited version of the impedance of the earth. Finally, the SCI is convolved with each seismic trace to create a relative acoustic impedance volume.

The extended elastic impedance (EEI) was introduced by Whitcombe *et al*. (2001). The general background of the method comes from the replacement of $\sin^2\theta$ by $\tan(\chi)$ in two term of AVO equation, and then scaling this equation by $\cos(\chi)$, such as

$$R(\chi) = A\cos(\chi) + B\sin(\chi) \quad (2)$$

where A is intercept and B is gradient in reflectivity domain

The extended elastic impedance corresponding to expression:

$$EEI(X) = \alpha_0\beta_0\left[\left(\frac{\alpha}{\alpha_0}\right)^{p}\left(\frac{\beta}{\beta_0}\right)^{q}\left(\frac{\rho}{\rho_0}\right)^{r}\right] \quad (3)$$

where $p = \cos(\chi) + \sin(\chi)$ (4)

$$q = -8k^2\sin(\chi)$$

$$r = \cos(\chi) - 4k^2\sin(\chi)$$

Compressional wave velocity, shear wave velocity and density are denoted as α, β, ρ respectively while $\alpha_0, \beta_0, \rho_0$ are reference constant.

The relative acoustic-impedance (AI) and gradient impedance (GI) computed from SCI are input into the elastic impedance (EEI) process to define the rotation angle Chi (χ) that allows the interpreter to project the lithology and fluid changes. In another view, EEI considers as a rotation in the impedance domain similar to rotation of intercept and gradient in the reflectivity domain. The EEI rotation can be defined as:

$$EEI(X) = AI_0 \left[\left(\frac{AI}{AI_0} \right)^{\cos(\chi)} \left(\frac{GI}{AI_0} \right)^{\sin(\chi)} \right] \quad (5)$$

From equation (5), the different χ corresponds to different EEI represented for varying rock properties (Figure 5.1). The objective of the EEI method is to generate an optimal fluid and lithology cubes by turning the Chi angle that represent lithology and fluid change in reservoir.

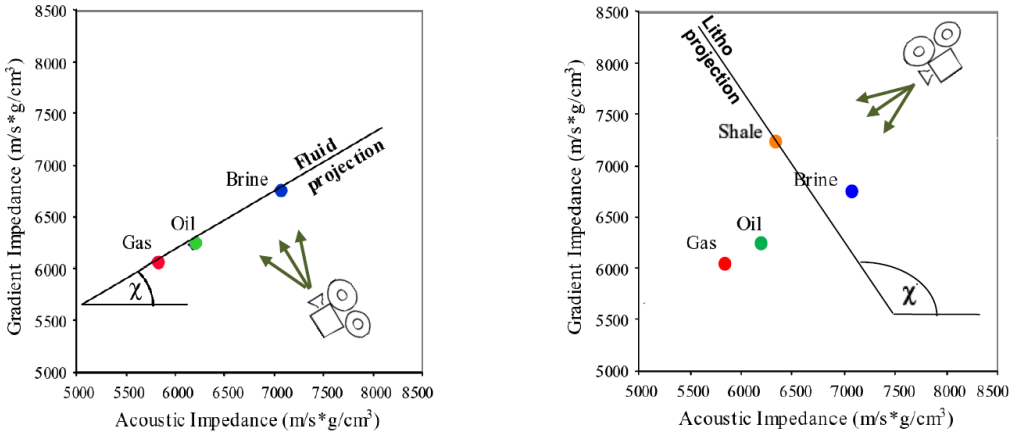

Figure 5.1 The fluid and lithology factor are defined as rotation of χ in intercept (AI or A) and gradient (GI or B) domain

(Kemper.M & Huntbatch.N, 2012)

5.2 Inversion result and interpretation

The first step in the coloured inversion process is using the available well logs from the area of interest and determining the correct α value. Three exploration wells were used and α value was defined at -0,7 (Figure 5.2). After having derived the α number, we now have a target spectrum that can be used to shape the mean seismic spectrum. Since the nature of the seismic response is band limited, care must be taken when selecting the correct upper and lower limits of seismic spectrum. The objective is to only shape the seismic spectrum where sufficient energy is encompassed, paying particular attention to the low frequency end of the spectrum. In this data set, the desired seismic spectrum was designed at lowest 3 Hz and at highest 60 Hz. Figure 5.3 shows the process of designing the transfer function. The lower blue curve shows the band limited well log response (target spectrum), the center red curve is the band limited seismic response, with the lower green curve depicting the transfer function required to shape the mean seismic response to that of the target spectrum. The final operator is then generated after designing process.

The final step in the inversion process is to use the final operator by convolving with the reflection seismic data to generate relative acoustic impedance. After convolution, near and far angle stacks change from zero phase to -90 phase or from reflective interface to layer base which is more closely to geological thickness. Figure 5.4 to 5.6 are seismic sections of relative acoustic impedance of near and far angle stack. They have shown a layer-based characteristic which is easier to observe in terms of geology.

In this workflow, intercept and gradient were also computed. Then, they were convolved with final operator from coloured inversion to produce AI and GI to later input EEI study. Figure 5.7 and 5.8 are two examples of AI and GI generated after SCI.

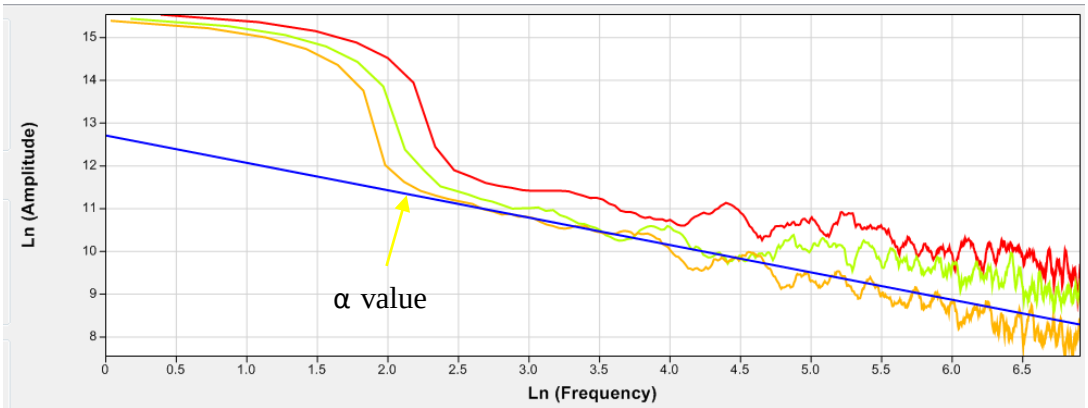

Figure 5.2 Average well spectrum to define α value (blue line slope presented for α value)

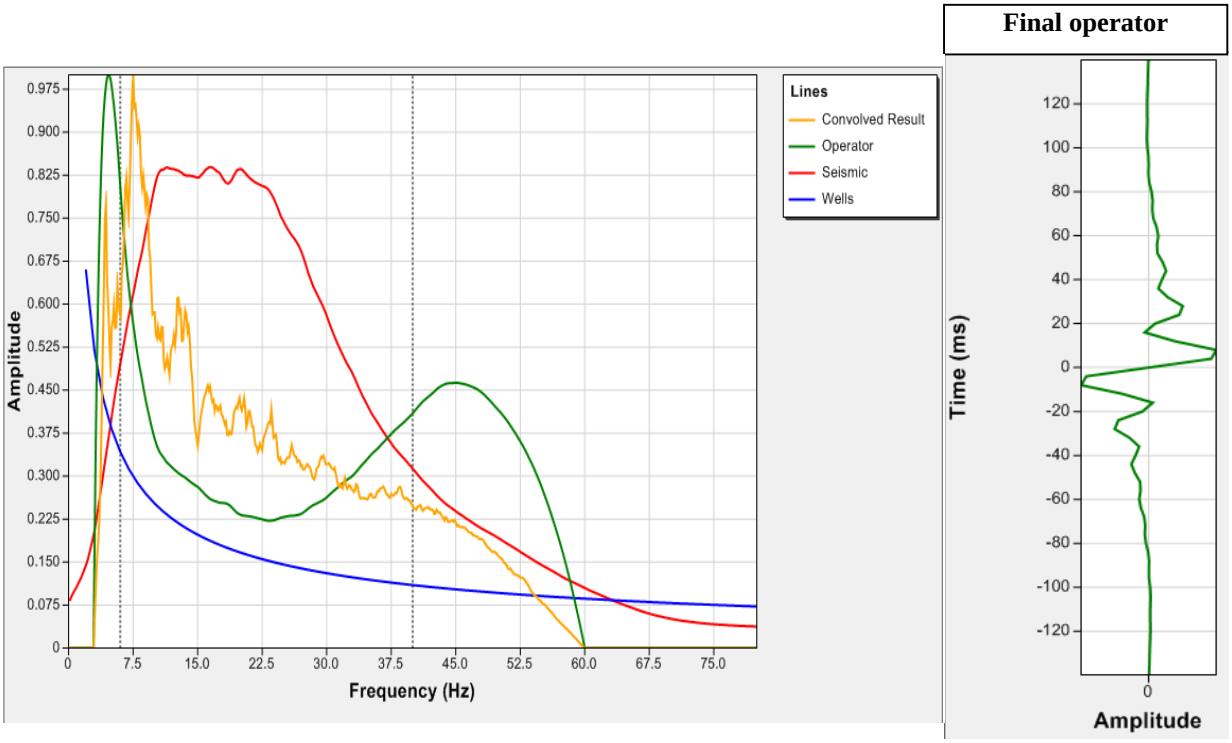

Figure 5.3 Operator design process and final operator

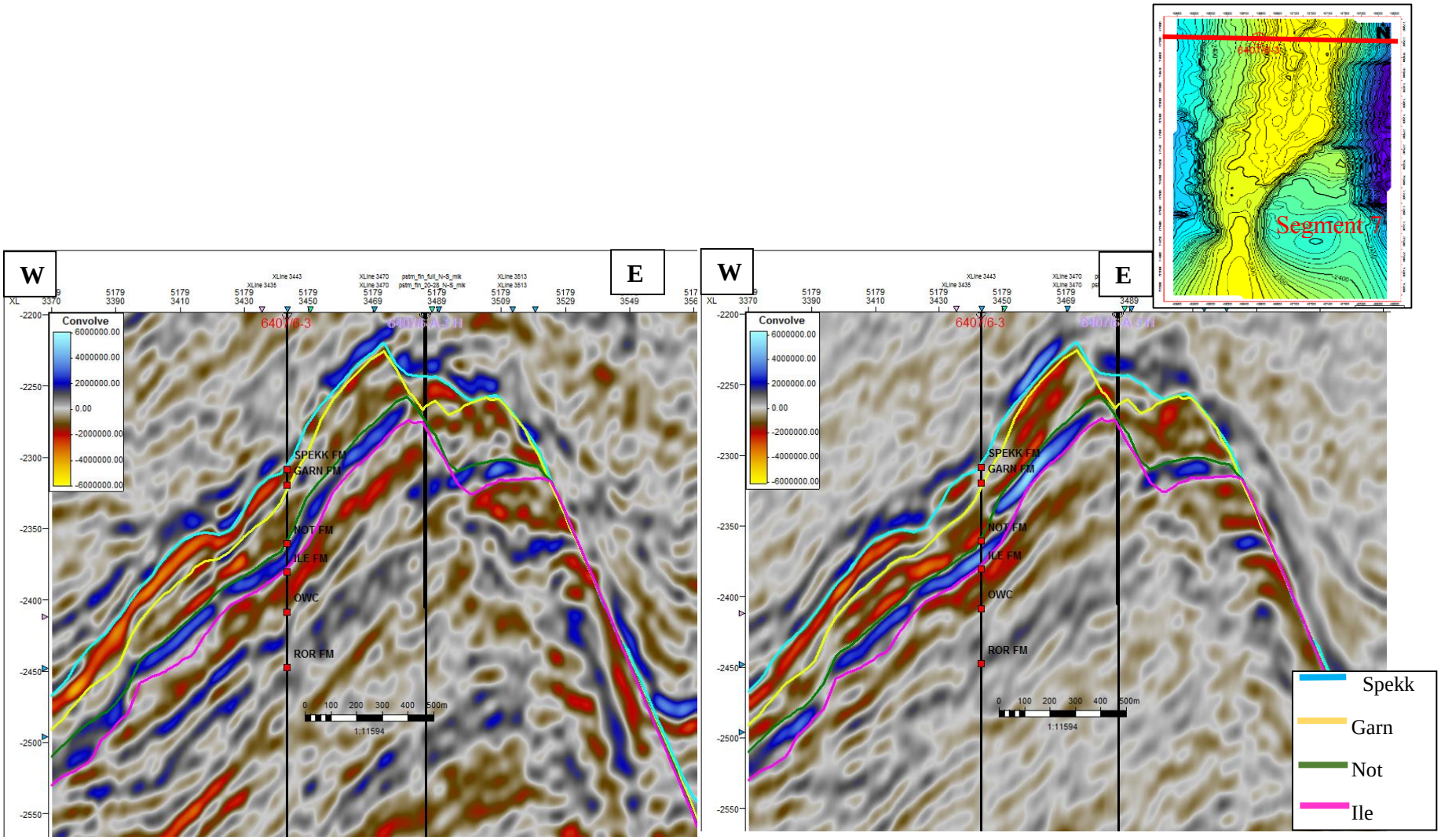

Figure 5.4 Comparison relative acoustic impedance between near angle stack (left) and far angle stack (right) at IL 5179

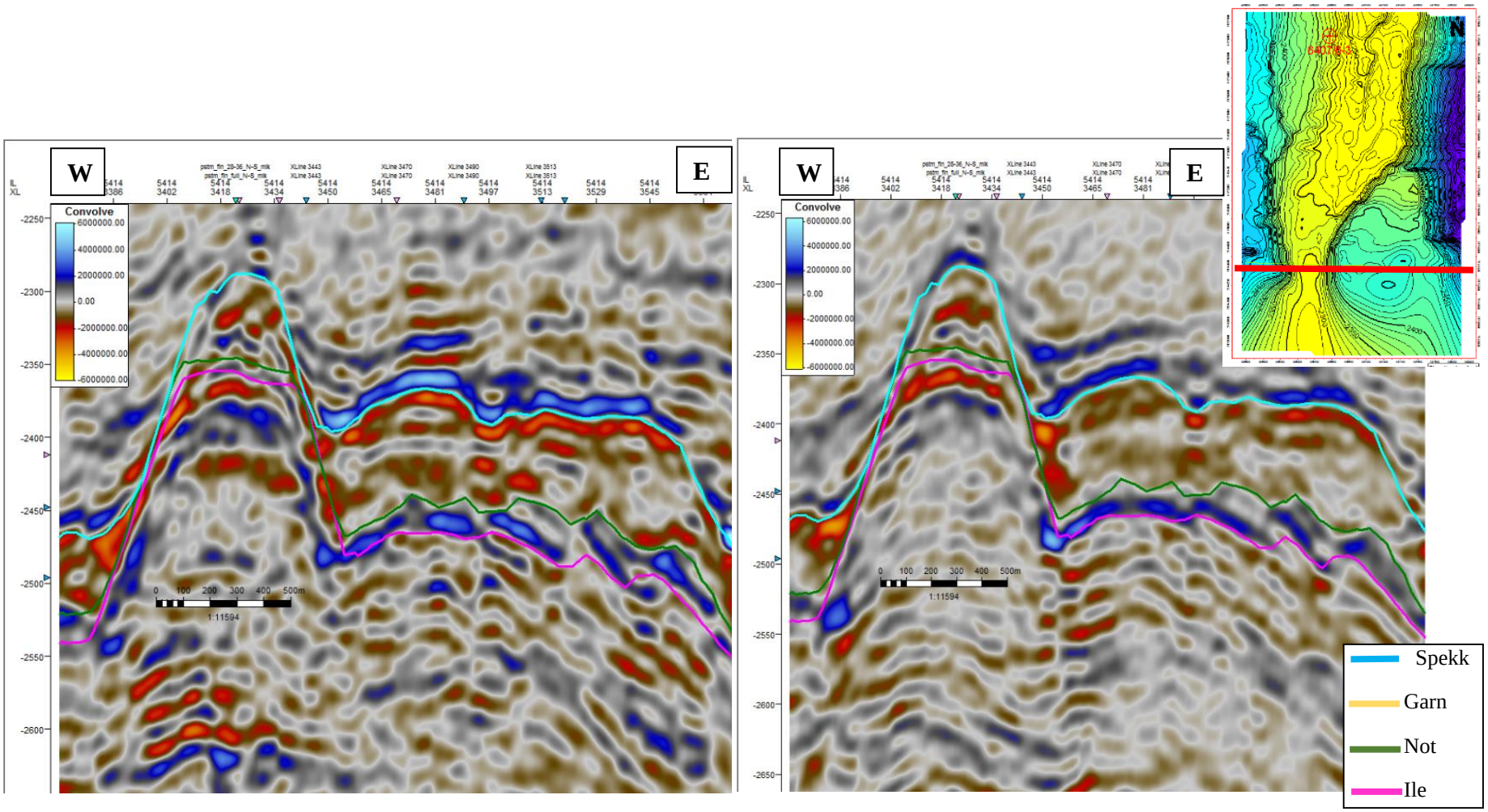

Figure 5.5 Comparison relative acoustic impedance between near angle stack (left) and far angle stack (right) at IL 5414

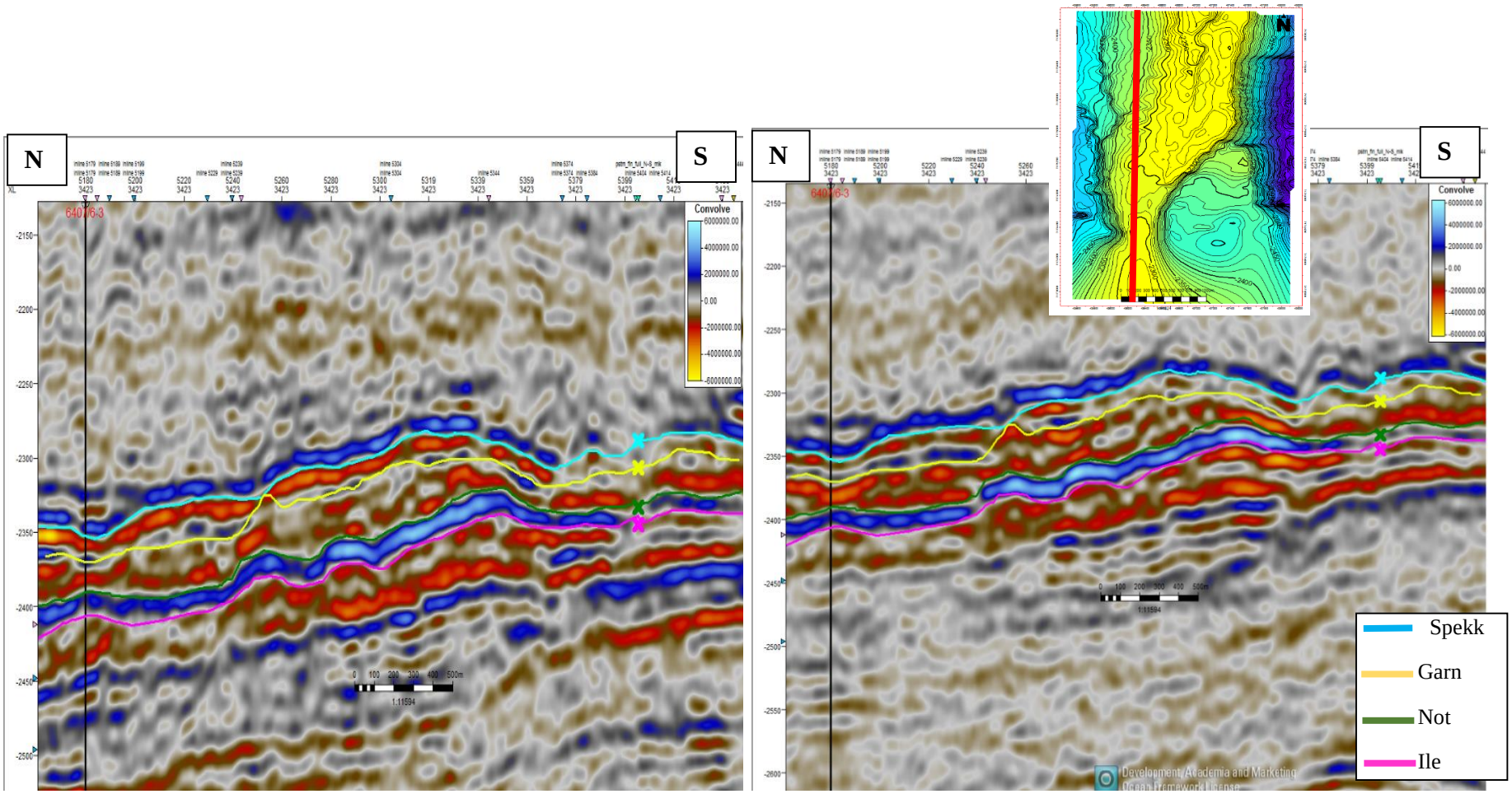

Figure 5.6 Comparison relative acoustic impedance between near angle stack (left) and far angle stack (right) at XL 3423

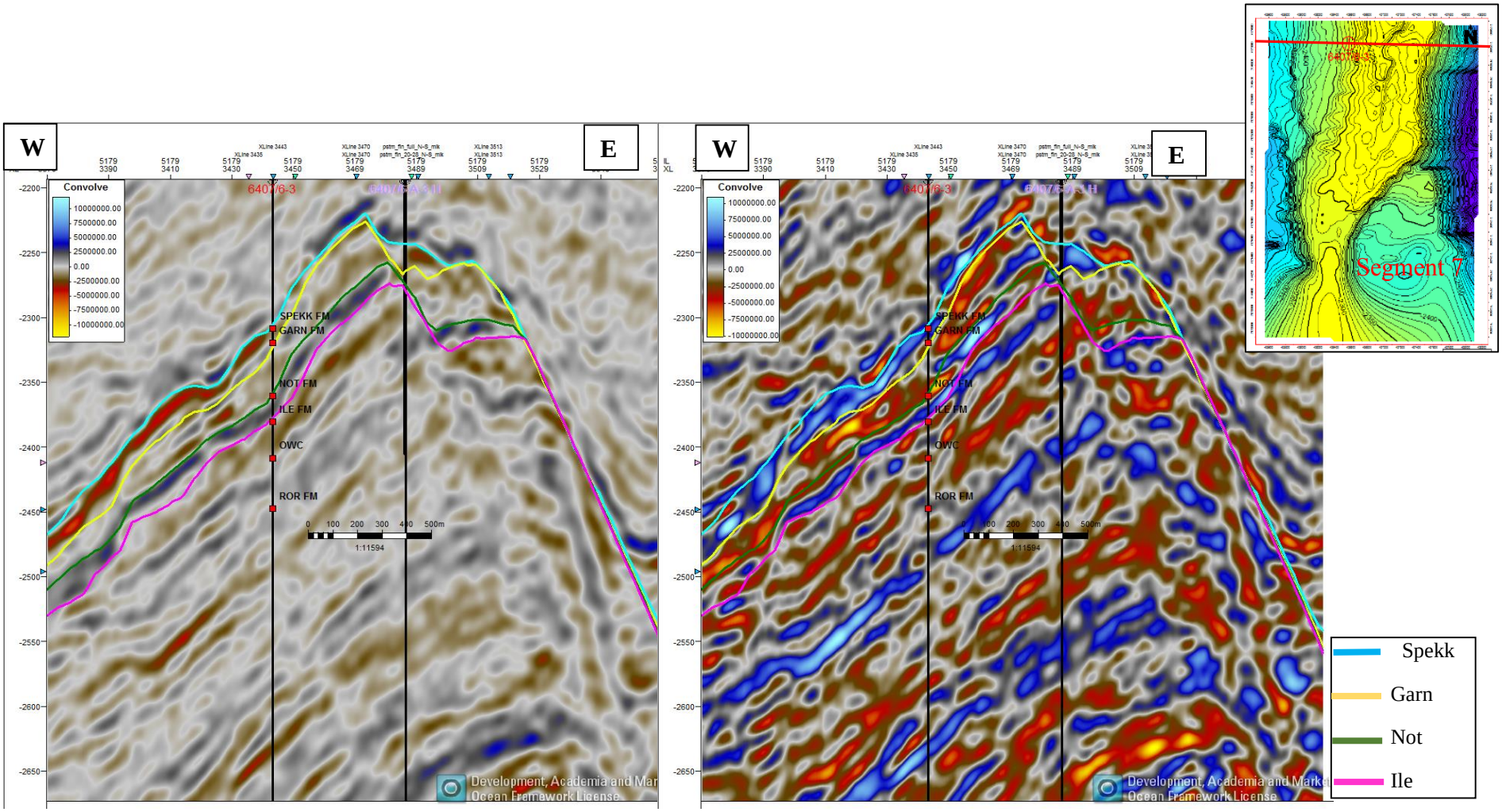

Figure 5.7 Comparison AI (left) and GI (right) at IL 5179

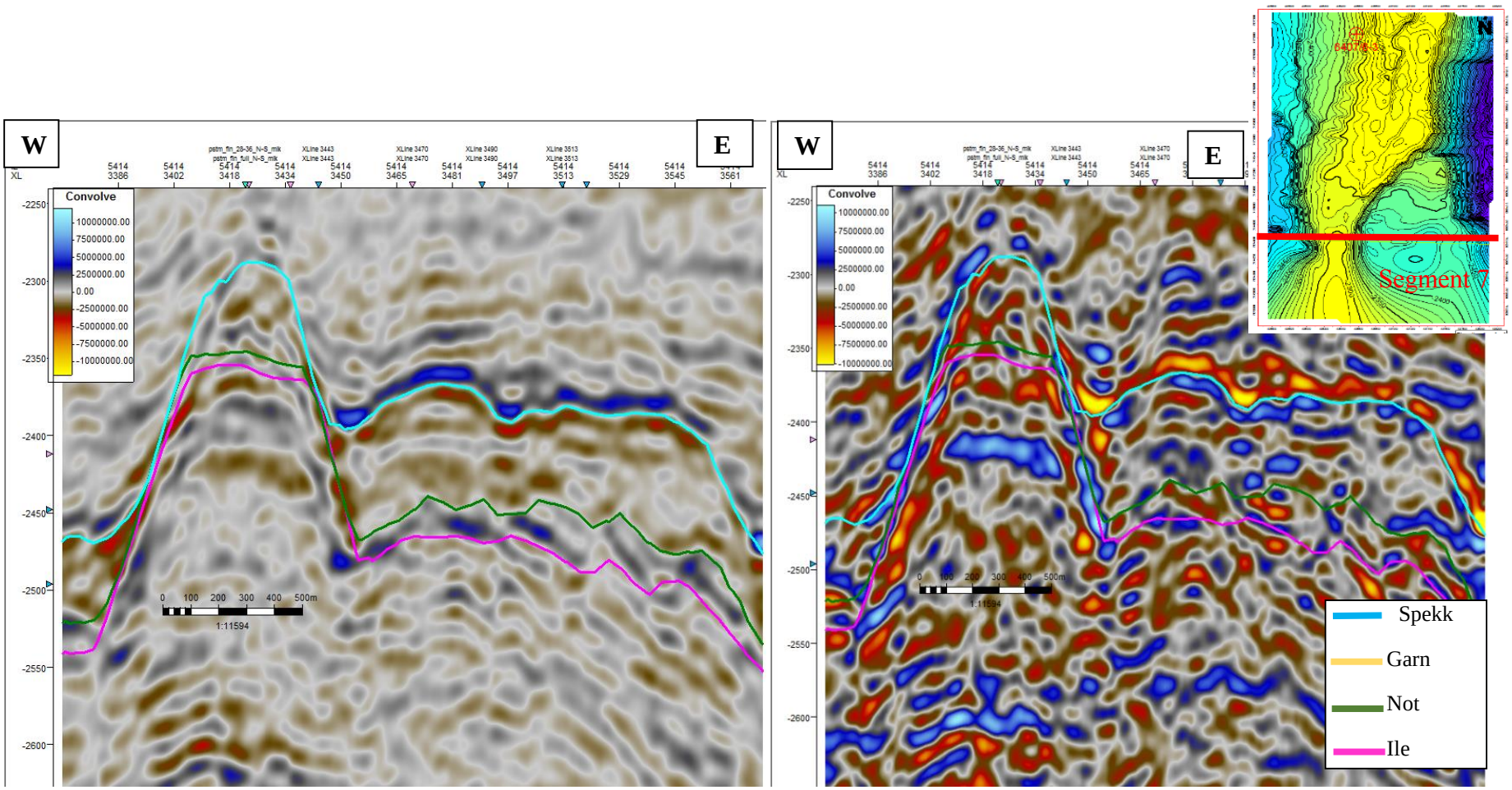

Figure 5.8 Comparison AI (left) and GI (right) at IL 5414

Following, AI and GI from previous coloured inversion were used in the EEI study. An important step of the EEI analysis is finding a rotation angle χ which can deviate hydrocarbon reservoir from background trend.

Firstly, elastic log such as Vp, Vs and density from three exploration wells was used to compute AI and GI from the well data. Those two parameters were plotted against each other in logarithm unit and colored by water saturation ratio. As seen in Figure 5.9 (right), hydrocarbon presence effect leads those points deviated from background trend and helped to define the angles χ. Moreover, angles χ can also be calculated by correlating EEI estimation curve with Vp/Vs curve. As shown in Figure 5.9 (left), maximum correlation between Vp/Vs curve and estimated EEI was found at angle of 24 degrees. Thus, angle χ was decided at 24 degrees to optimize the fluid cube in the Mikkel Field.

Secondly, AI and GI generated from seismic coloured inversion were plot again each other and applied angle χ at 24 degrees which was decided from well estimation (Figure 5.10). Finally, EEI of 24 degrees was generated and visualized to observe fluid effect in study area. Figure 5.11 to Figure 5.13 are the comparisons between the relative acoustic impedance of far angle stack with the EEI of 24 degrees. In common, they both show layer-based character in seismic section. In Figure 5.11, EEI (24) shows a stronger and more continuous layer in the Garn reservoir compared to relative AI of far angle stack. EEI of fluid angle helped to highlight gas presence in reservoir. In contrast, Figure 5.12 has an opposite character that EEI (24) has no bright up event comparing to relative AI of far angle stack. It seems to be that the fluid effect does not present in southern area of the Mikkel Field. Also, a cross line from north to south in Figure 5.13 has a clear observation that gas effect has reduced in the southern area. Though AVO and EEI show a consistent analysis that gas presence seems not occur in segment 7 and less effect in the southern part of the Mikkel Field, it is still uncertain if the fault shadow effect has disrupted signal to noise ratio of the seismic data.

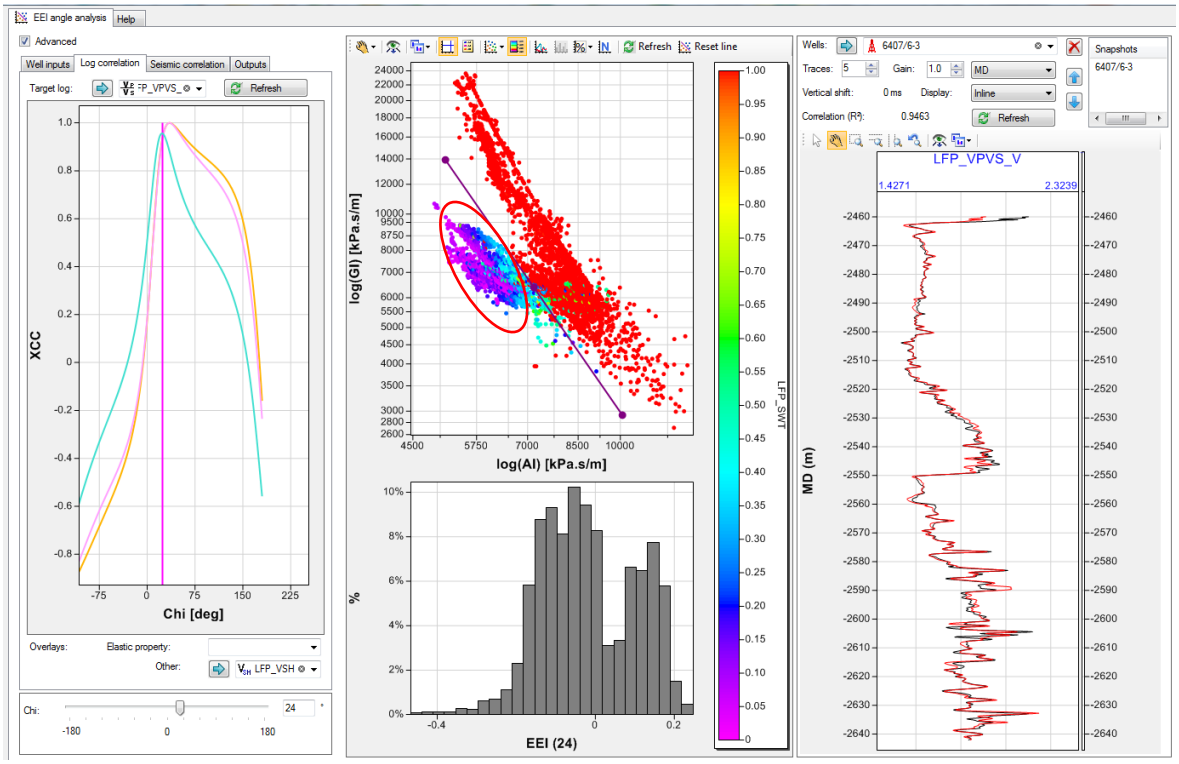

Figure 5.9 Defining angles χ process at well location: (left) estimated EEI correlates with Vp/Vs curve, (middle) Cross plot of AI-GI, (right) Vp/Vs from estimated Chi angle (red) vs orginal Vp/Vs curve (black)

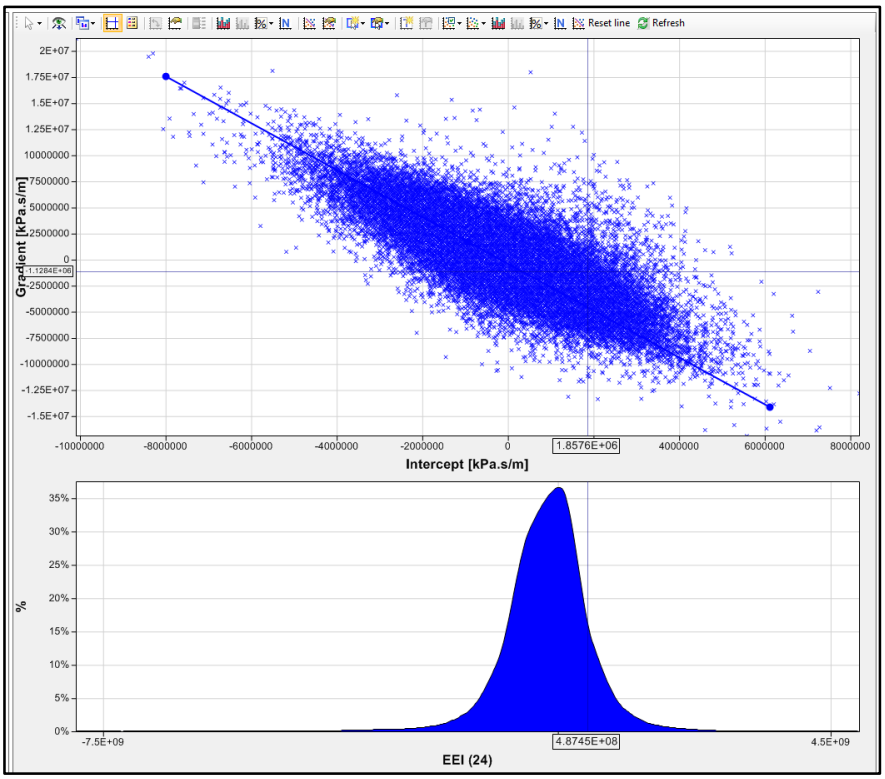

Figure 5.10 Defining angles χ process from seismic data

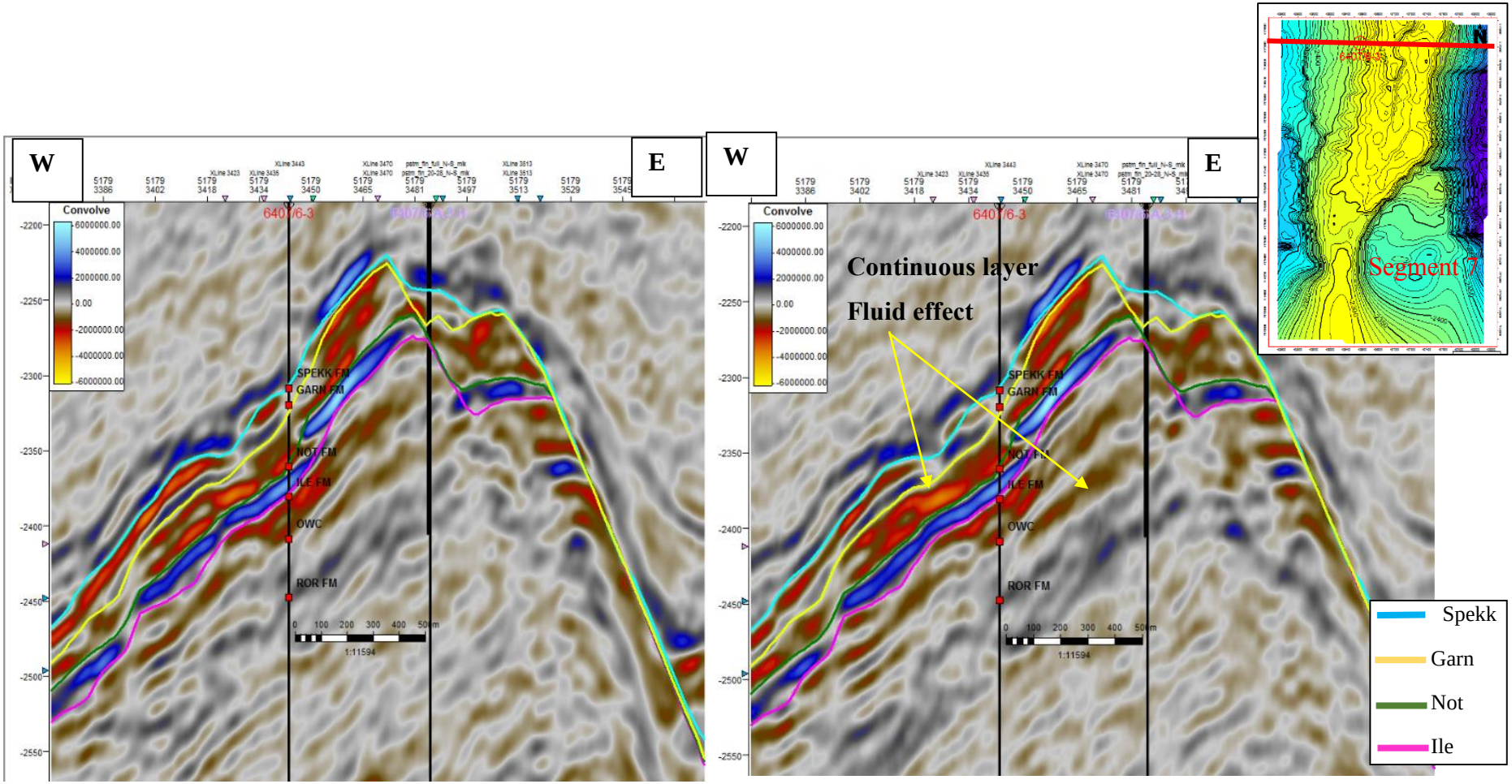

Figure 5.11 Comparison relative AI of far angle (left) and EEI of fluid angle 24 (right) at IL 5179

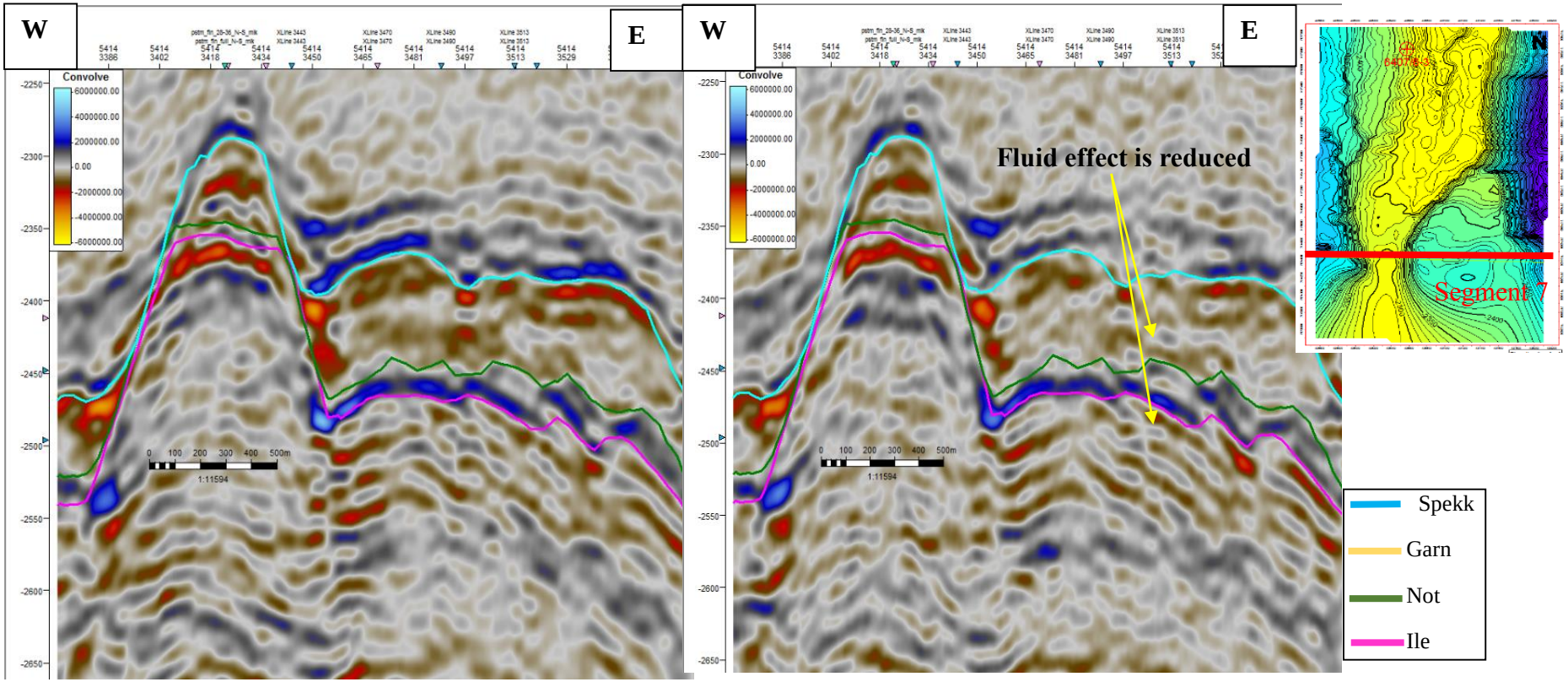

Figure 5.12 Comparison relative AI of far angle (left) and EEI of fluid angle 24 (right) at IL 5414

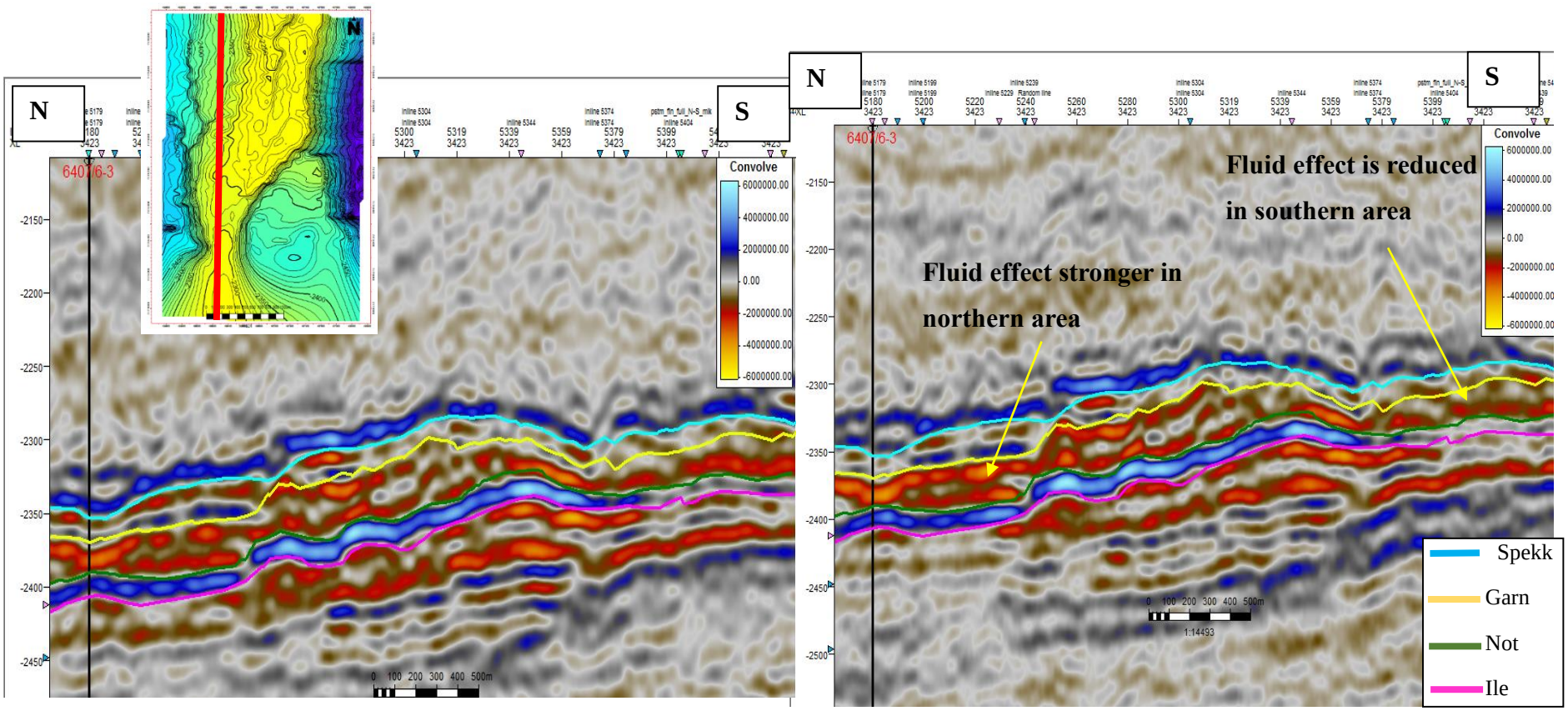

Figure 5.13 Comparison relative AI of far angle (left) and EEI of fluid angle 24 (right) at XL 3423

6. Bayesian lithology and fluid prediction from angle stacks

6.1 Methodology

Pcube is a Bayesian lithology and fluid prediction (LFP) from angle stacks developed by Statoil (Buland *et al*., 2008). It combines stochastic rock physics relations between the elastic parameters and the different facies classes with the results from a fast Bayesian seismic simultaneous inversion from seismic data to elastic parameters. A summary of the LFP methodology is illustrated in Figure 6.1. LFP includes prior knowledge which could derive from either drilled wells or regional geology of concerned area. The result of FLP provides optimal solutions, associated uncertainty and simulates a complete solution by posterior distribution. The posterior distribution provides probability of different facies classes which present in a study area. However, LFP is often highly uncertainty and this uncertainty is rarely assessed.

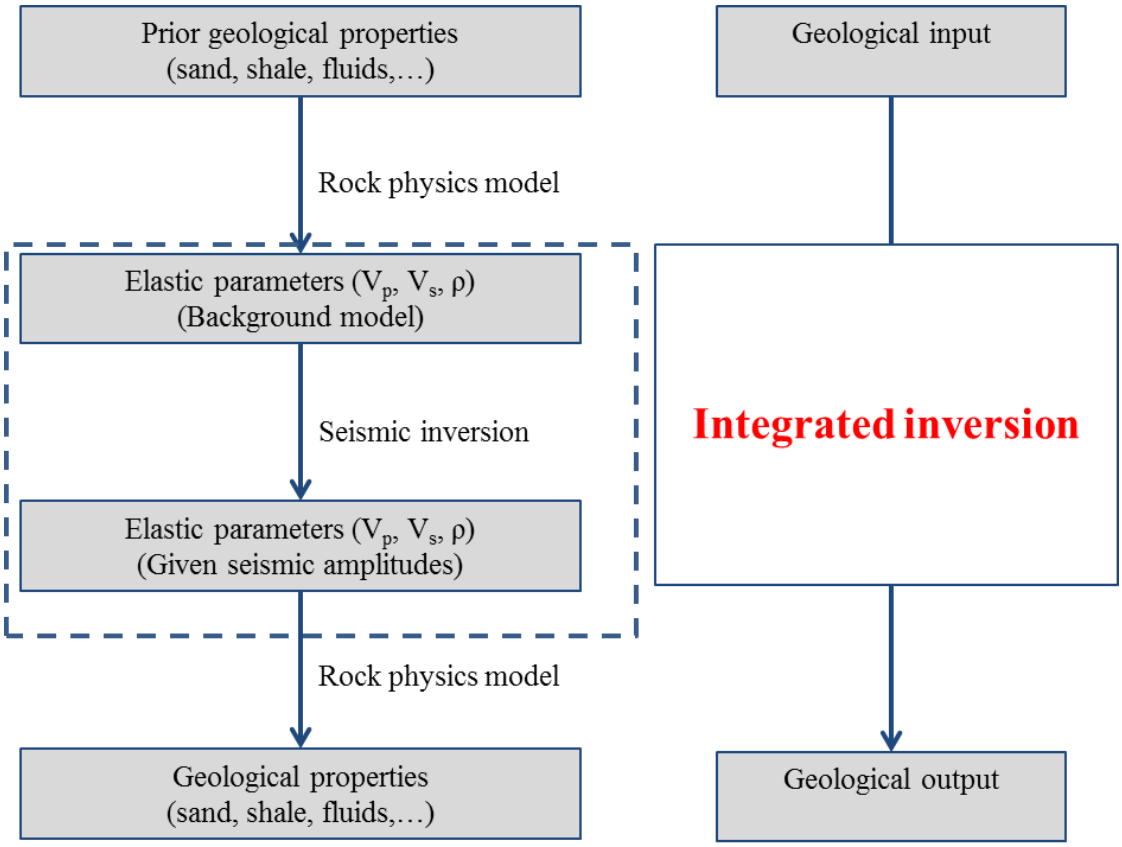

Figure 6.1 Summary of LFP methodology

At first, the well data is used to define the relevant lithology and fluid classes (LFC) in the area. Following, the rock physic is built to define the relationship between elastic rock properties, such as compressional wave velocity, shear wave velocity and density, for each LFC. The rock physics model is important to link from rock properties for each facies to effective elastic properties (Avseth *et al*., 2005). The probability distribution function (PDFs) of the rock properties can be estimated as multidimensional histograms from the well-log data or the simulated data. In exploration settings, the well-log information is often sparse, and the use of rock models might be required. The seismic modelling is performed based on the seismic forward model defined by Buland & Omre (2003). Finally, a stochastic model combines the rock physic model and the seismic inversion to compute the posterior probability of LFCs. With this approach, it is able to efficiently and consistently combine the stochastic rock physics relations with a fast seismic simultaneous inversion (Buland *et al*., 2008)

At a glance, the LFP process given by fast Bayesian seismic simultaneous inversion (Buland *et al*., 2008) is executed by following steps (Figure 6.2):

1. Define categorical facies classes.
2. Specify the rock properties p(m|f) for each facies.
3. Specify spatial prior probabilities p(f) for the facies.
4. Derive the prior model p(m) for the elastic parameters.
5. Estimate the seismic wavelet and the noise covariance.
6. Calculate the solution of the Bayesian AVO inversion
7. Calculate the posterior facies probabilities

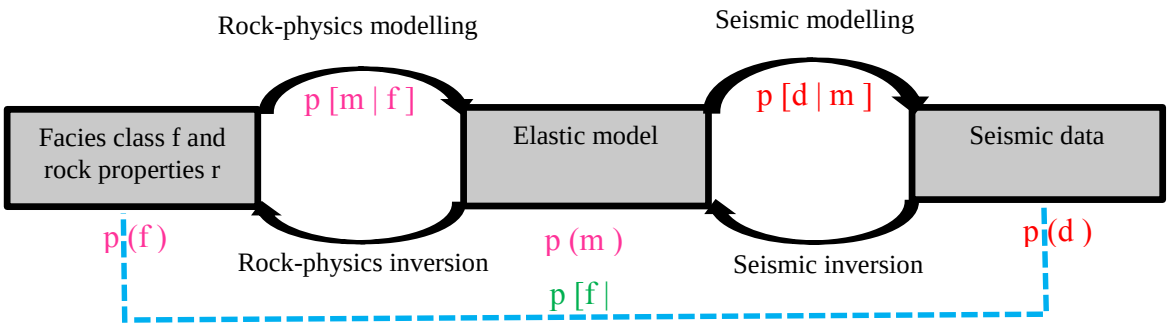

Figure 6.2 The relationship between lithology and fluid classes (facies **f**), elastic model (**m**), and seismic data (**d**)

(Buland *et at*., 2008)

6.2 LFP workflow and interpretation in the Mikkel Field

In the previous sections, structural interpretation and fluid effect study have been done in the Mikkel Field. Prior knowledge of the study area has been accumulated and updated throughout the performed studies. Hence, it is a natural choice to continue with LFP so that we can produce probability of different facies distribution in the Mikkel Field and update structural interpretation if necessary.

As previous discussed, the Garn reservoir remains highly uncertain in interpretation in segment 7 and in the southern part where a complex fault pattern distorted the seismic response. The Garn reservoir was deposited in syn-rift period which leads to its reservoir thickness vary in each fault block. Hence, defining top Garn by shifting Top Spekk is not recommended in this area. In this workflow, it is suggested to firstly perform a blind test without horizons constraint and prior knowledge from wells data. Once the first LFP completes, horizons will be updated accordingly. Afterward, the second LFP will re-run with updated horizons and prior knowledge of the LFCs from well data. Summary of the proposed workflow can be found in Figure 6.3

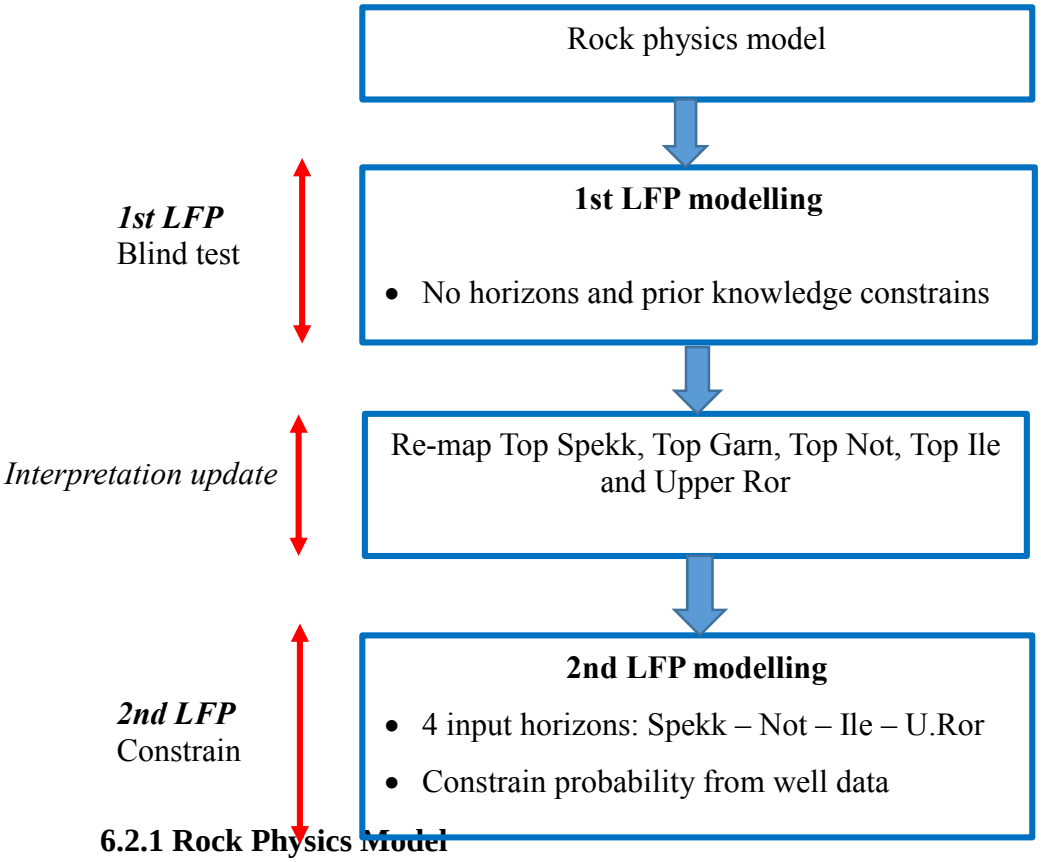

Figure 6.3 Proposed workflow of LFP in the Mikkel Field

6.2.1 Rock Physics Model

It is necessary to build a rock phyisics model prior to performing LFP. A total of four wells which have elastic log of the interval from Top Spekk to Upper Ror were used to generate the rock physics model. They are 6407/6-3, 6407/6-4, 6407/6-5 and 6407/6-A-1H. Elastic logs such as Vp, Vs and density from those wells were displayed on cross-plot of AI versus Vp/Vs and AI versus GI; and coloured by facies in Figure 6.4. The cross-plot in Figure 6.4 shows the cluster of gas sand (red) is deviated from other facies though it shares a similar AI range (X axis) to upper part of the shale cluster (green). However, they are well separated on Vp/Vs range (Y axis). Moreover, the shale seems to have two different characteristics having higher and lower Vp/Vs ratio. According to lithology description of the Spekk Formation (NPD website), its formation contains high amount of organic matters which explains the high Vp/Vs ratio as a typical hot shale character. Hence, the shale is separated into normal (hard) shale which is main lithology of the Not Formation and hot shale representing the organic shale in the Spekk Formation. In addition, calcite, fine sand and cemented sand appear as a scatter points on both cross plots. In well log data, calcite, fine sand and cemented sand are thin inter-bedded layers that their thickness varies between 0.5 m to 2.5 meter. Those facies are mainly found within the Ile reservoir and they are the main factor reducing permeability in the reservoir. Since this study attempts to define the porosity trend in the Mikkel Field, rock physics model tries to capture them though they are challenging in the seismic resolution. Calcite, fine sand and cemented sand are later merged into one cemented sand class in rock physics model

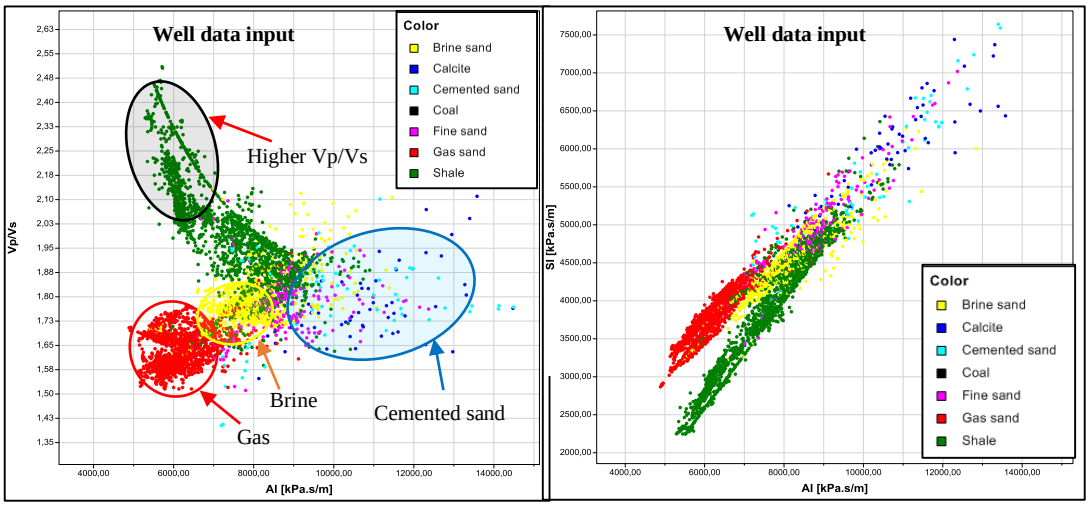

Figure 6.4 Cross plot AI versus Vp/Vs (left) and AI versus SI (right) coloured by facies in Z axis of four wells data

Lastly, the rock physics model was bı hard shale and cemen

final cross plot is shown in Figure 6.5. Gaussian distribution was chosen for each LFC. The distribution for each LFC along AI and Vp/Vs are as shown in Figure 6.6

LFC	**Classification**
Hot Shale	Vsh > 0.5 1.9 < Vp/Vs < 2.45 AI < 7000
Gas sand	Vsh > 0.5 PhiT > 0.2 SWT < 0.5
Brine sand	Vsh > 0.5 Phie > 0.2 SWT > 0.5 1.69 < Vp/Vs < 1.83 AI > 7300
Hard shale	Vsh > 0.5 1.85 < Vp/Vs < 2 AI > 7000
Cemented sand	PhiT < 0.12 1.7< Vp/Vs < 1.9 AI > 10000

Table 6.1 Classification of five LFC built in rock Physics model

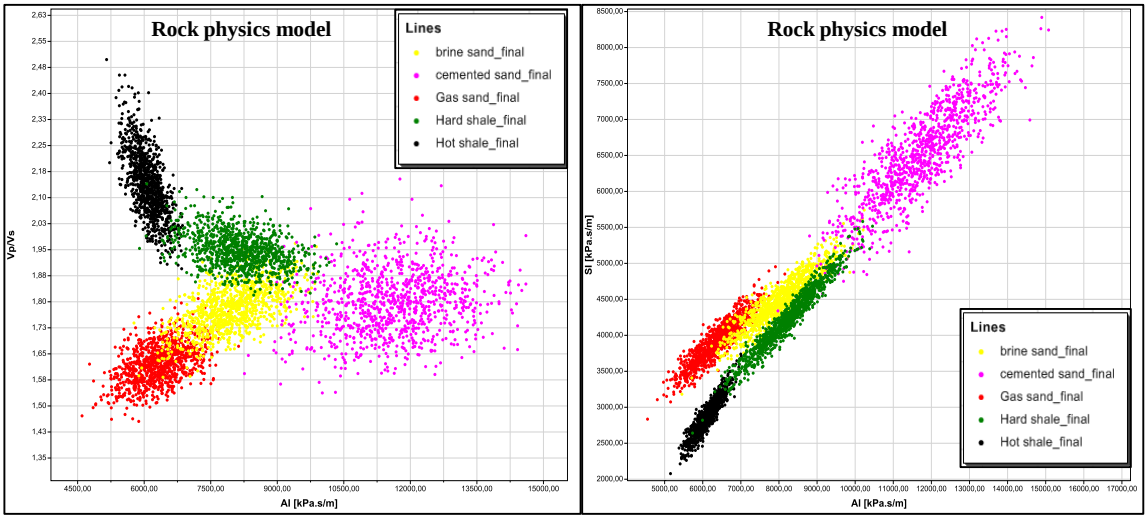

Figure 6.5 Cross-plot AI- Vp/Vs (left) and AI-SI (right) of 5 LFC in rock physics model

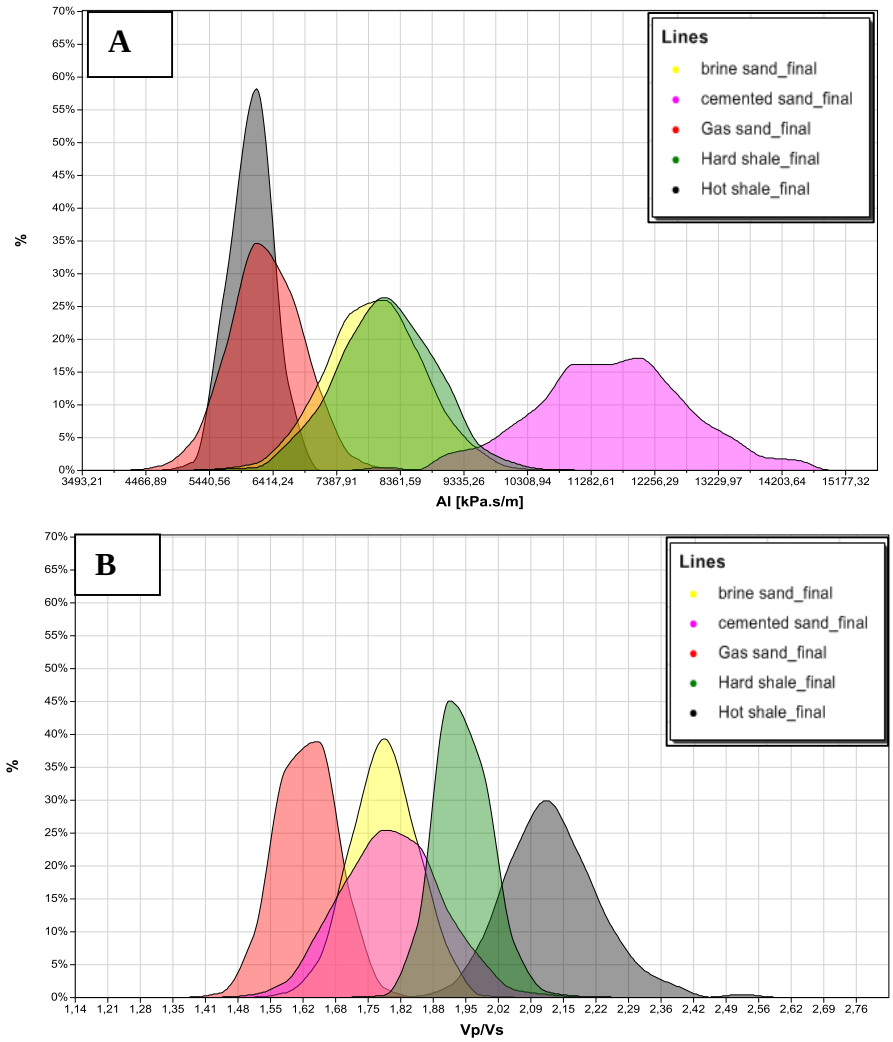

Figure 6.6 Gaussian distribution of five LFCs (A) AI distribution of each LFC and (B) Vp/Vs distribution of each LFC

6.2.2 Pcube without horizons constraining

In addition to the rock physic model, Pcube also requires angle stack seismic, signal to noise ratio and scaled wavelet. Those inputs are necessary to perform Bayesian AVO inversion. Four angle stacks after data conditioning in section 3.2 were used in the inversion. The target wavelet and the scale factor which were fine-tuned in the synthetic well tie and AVO modelling in section 4.1 continued to the inversion. Seismic signal to noise ratio was set at 1.5 in Pcube.

First Pcube was run without horizons constraints. The inversion window was specified by two horizons which were Top Spekk and Upper Ror. The constant probability was designed for five LFCs such as probability of hot shale is 20%, probability gas sand is 25%, probability of brine sand is 25%, probability of hard shale is 20% and probability of cemented sand is 10%. The uncertainty of each input horizon was also given into LFP and it was based on mapping experiment. For detail, Top Spekk and Upper Ror uncertainty were set at 10 ms and 40 ms respectively. Figure 6.7 shows the summary of the first Pcube background model.

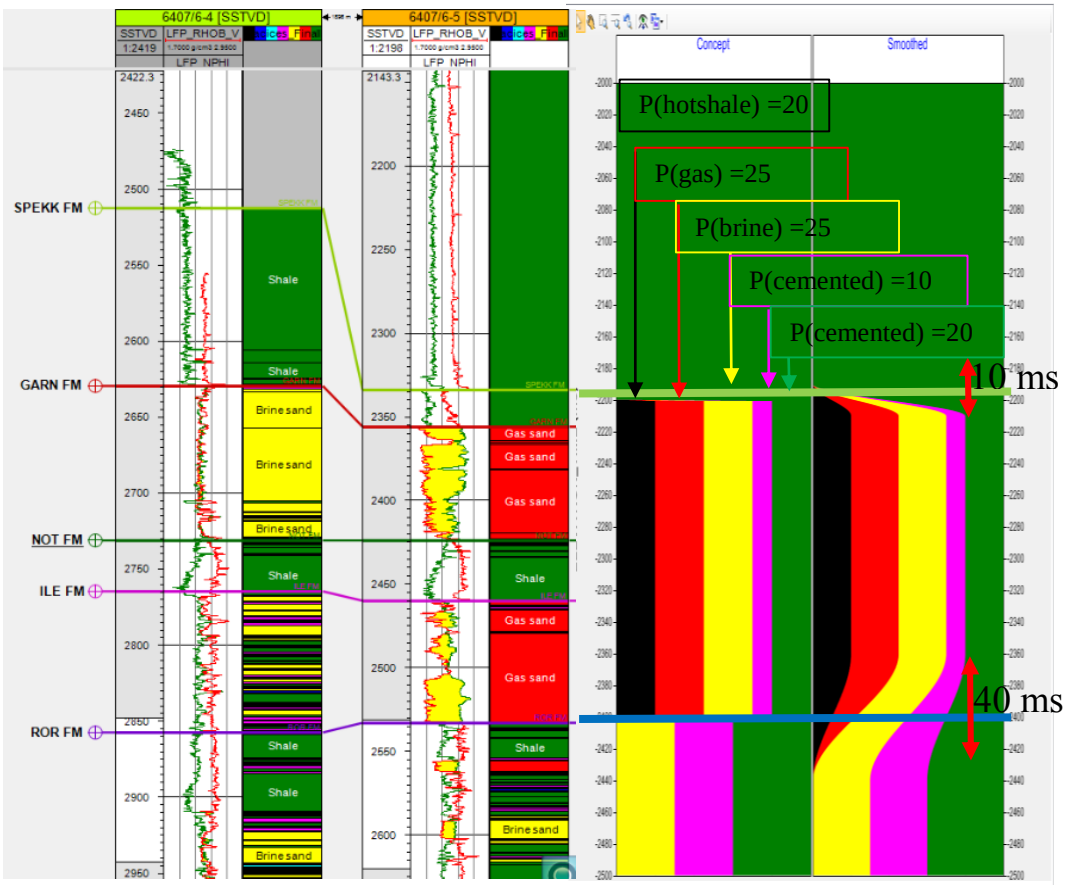

Figure 6.7 Background model of the first Pcube

The Pcube result produces a set of probability cubes for each LFC. In total, five probability cubes for the five LFCs were computed such as hot shale, gas sand, brine sand, hard shale and cemented sand. There is also an absolute cube which is classified as the most probable LFC among the others has been selected at one location and always sums at 1.

Figure 6.8 and Figure 6.9 show the results from the first Pcube at the northern part of the Mikkel Field. They gave a good response for defining hot shale, gas sand and hard sand although first LFP didn't have neither prior knowledge nor reservoir horizons to constrain. The probability of hot shale in the Speek Formation is stronger at the flank of structure and lower or even zero at the crest where erosion could affect. Gas sand probability is highlighted as two separated bodies represented for the Garn reservoir and the Ile reservoir. Especially, the hard shale in the Not formation is well defined with a doubling of its probability from initial input model 20% to final result 40% and its continuity is consistent with horizons map.

Furthermore, Figure 6.10 shows the probabilities of the five LFCs at IL 5374 crossing through segment 7. The probability of hot shale is moderate high and the result seems like hot shale in the Speek Formation deposited as a thick package from Top Spekk to Top Not in segment 7. The hard shale of the Not Formation is still recognized and its layer follows the dipping angle as seen in the seismic data. However, the gas sand probability of the Garn Formation and the Ile Formation is very low or almost zero in segment 7. Previous studies in AVO and EEI indicated that there was not any bright up event in far and ultra-far cube to indicate hydrocarbons. The first Pcube result is consistent with those observations. Probability of brine sand in the Garn reservoir are higher in this area which lead to convince that segment 7 would have no gas presence.

Finally, maximum attributes of five LFC cubes were generated. Figure 6.11 is a result of maximum probability extract of hot shale at time window of 50 ms below Top Spekk, probability of gas sand at time window of 25 ms below Top Garn and probability of gas sand at time window of 25 ms below Top Ile. In general, probability of hot shale has increased from 20% to 40%-50%. Probabilities of gas sand in the Garn Formation and the Ile Formation in northern part crease from 25% to 35% - 45% in the high structure while segment 7 has very low value and almost zero probability of gas sand.

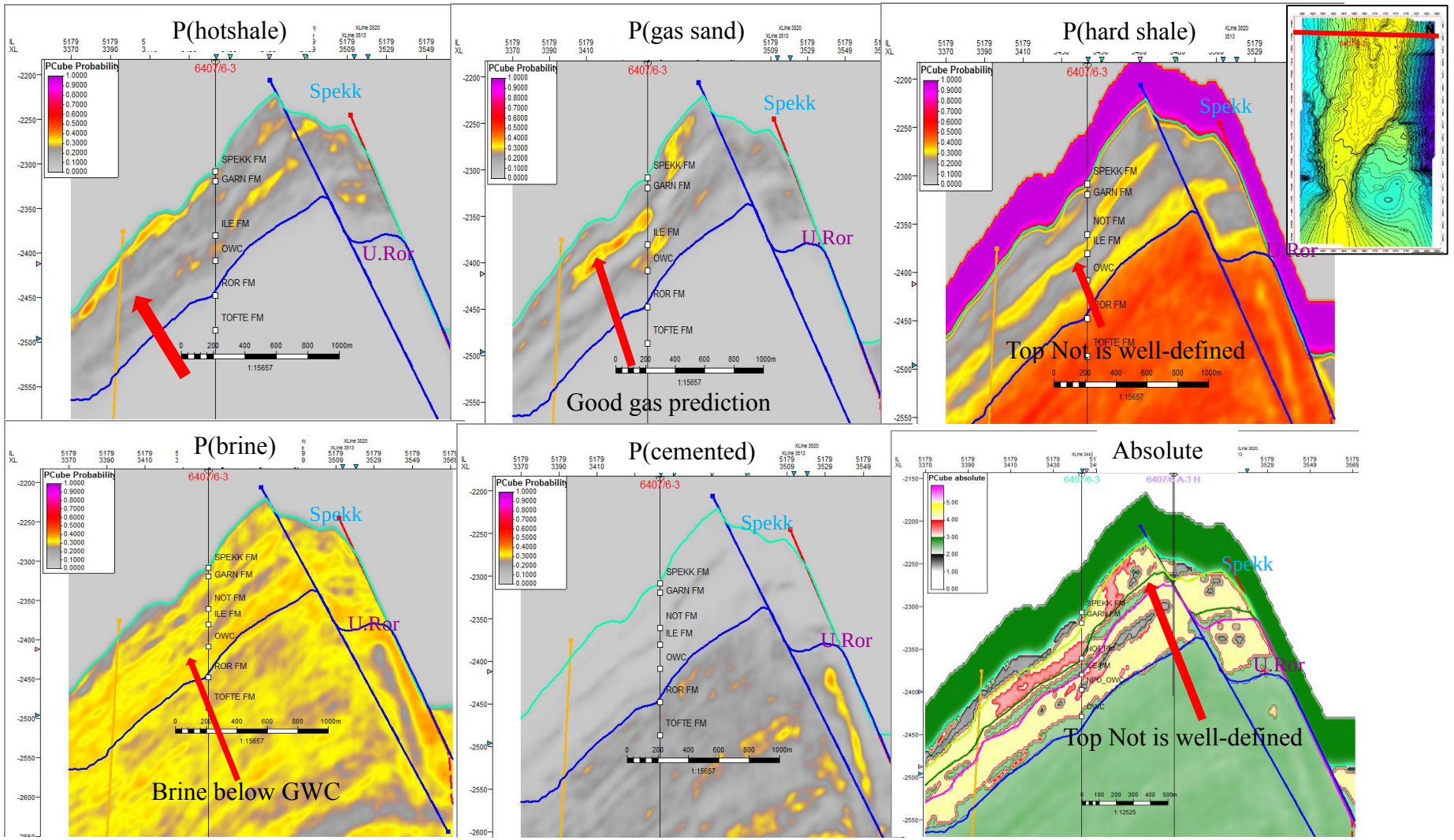

Figure 6.8 Probability of each LFC of the first Pcube at IL 5374

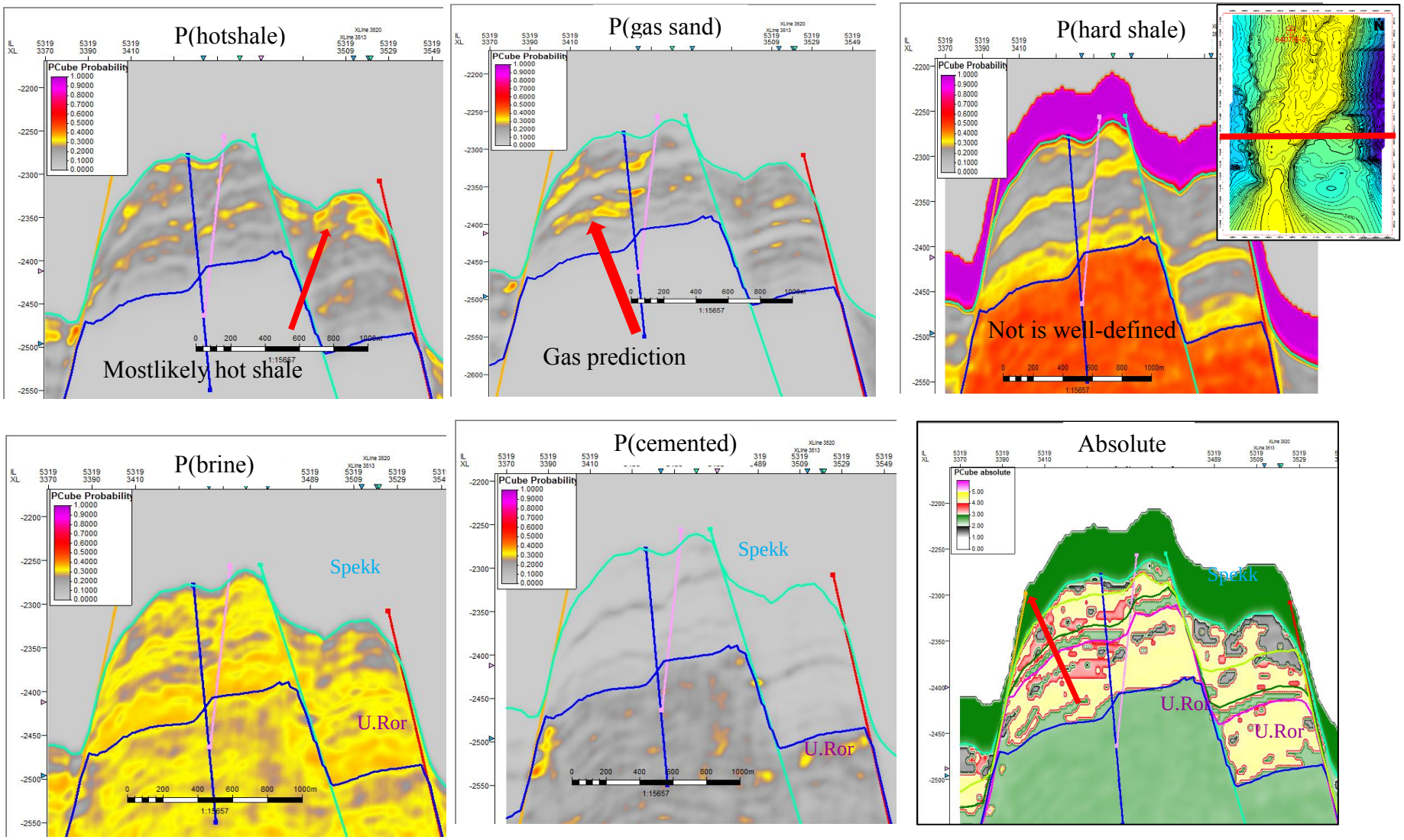

Figure 6.9 Probability of each LFC of the first Pcube at IL 5319

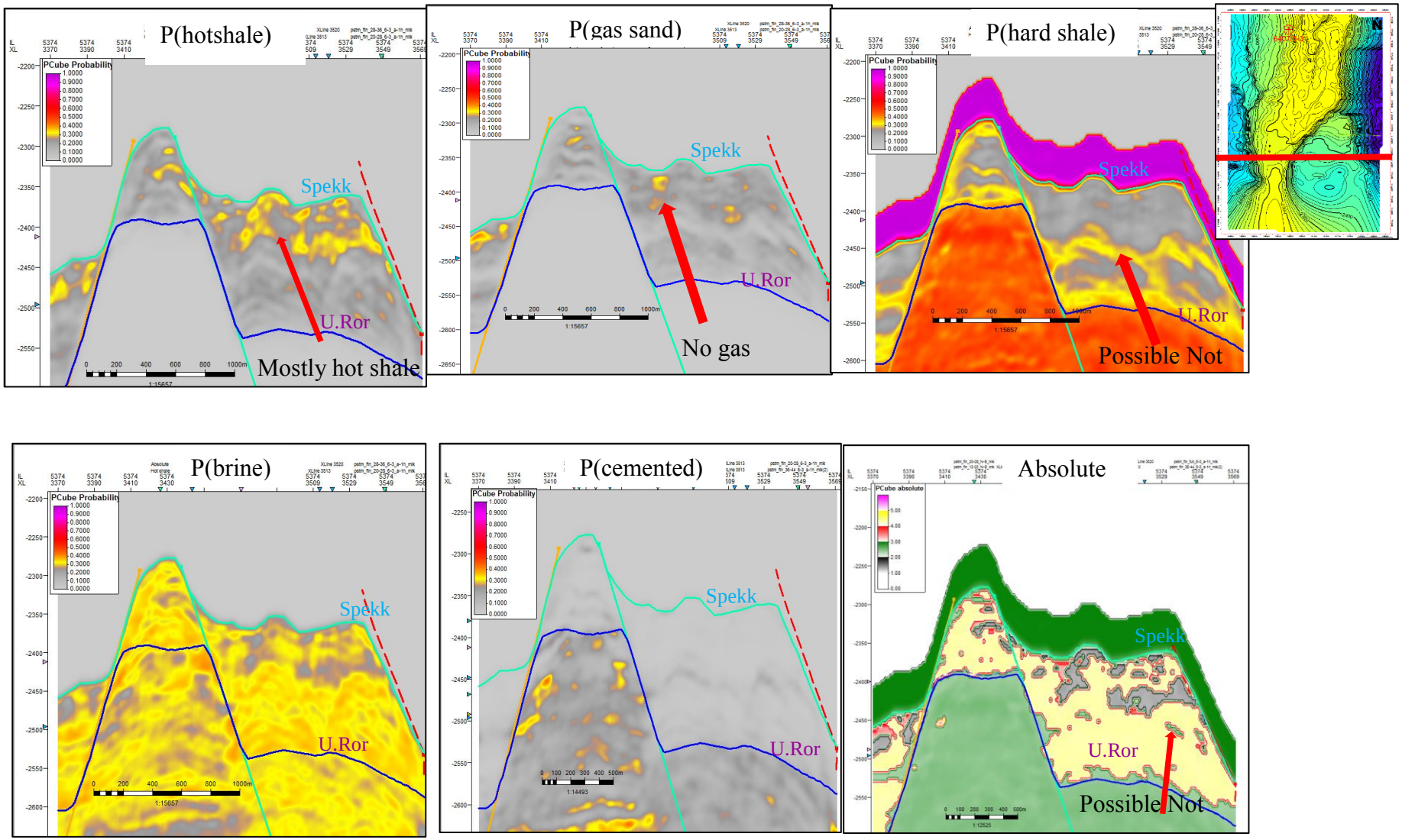

Figure 6.10 Probability of each LFC of the first Pcube at IL 5374

Maximum probability of hot shale of Top Spekk	Maximum probability of gas sand of Top Garn	Maximum probability of gas sand of Top Ile

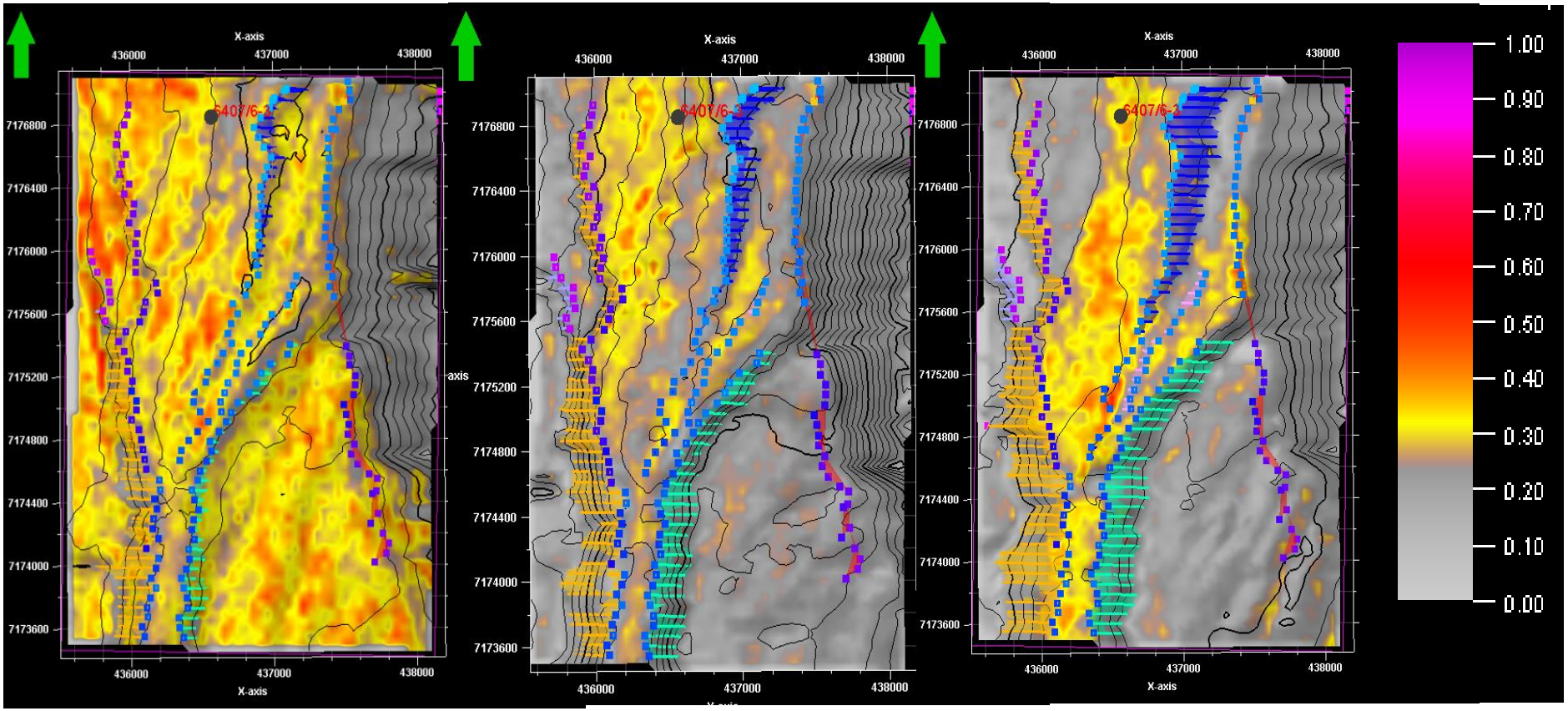

Figure 6.11 Map view of the Mikkel Field, showing maximum probability of hot shale in time window of 50ms below Top Spekk (left), probability of gas sand in time window of 25ms below Top Garn (middle), probability of gas sand in time window of 25ms below Top Ile (right) of the first Pcube.

6.2.3 Pcube constrained by horizons

After the first Pcube, horizons are updated and revised to introduce to the second Pcube. The Garn reservoir still remains uncertain in segment 7. Therefore, the second Pcube excluded Top Garn horizon and contained four main horizons which are Top Spekk, Top Not, Top Ile and Upper Ror. The Spekk Formation and the Garn Formation will be merged into one interval in the second Pcube.

The prior probabilities of each LFC are analyzed from the well log data and the knowledge from the geological conceptual model. As an example, the probability of brine sand in the Ile reservoir would be higher than the Garn reservoir as GWC from the well log was found in the Ile reservoir. The detail of input prior probability of LFCs in each interval is described in table 6.2

Since the horizons are updated from the first Pcube, their uncertainties are reduced in the second LFP as such the upper Ror horizon is reduced to 25ms uncertainty. The final background model for the second LFP is as shown in Figure 6.12.

Interval	P(hot shale)	P (gas sand)	P(brine sand)	P(hard shale)	P(cemented)
Spekk - Not	40	40	20	0	0
Not - Ile	0	0	0	100	0
Ile- U. Ror	0	40	35	15	10

Table 6.2 Summary of input prior probability of LFCs in the second Pcube

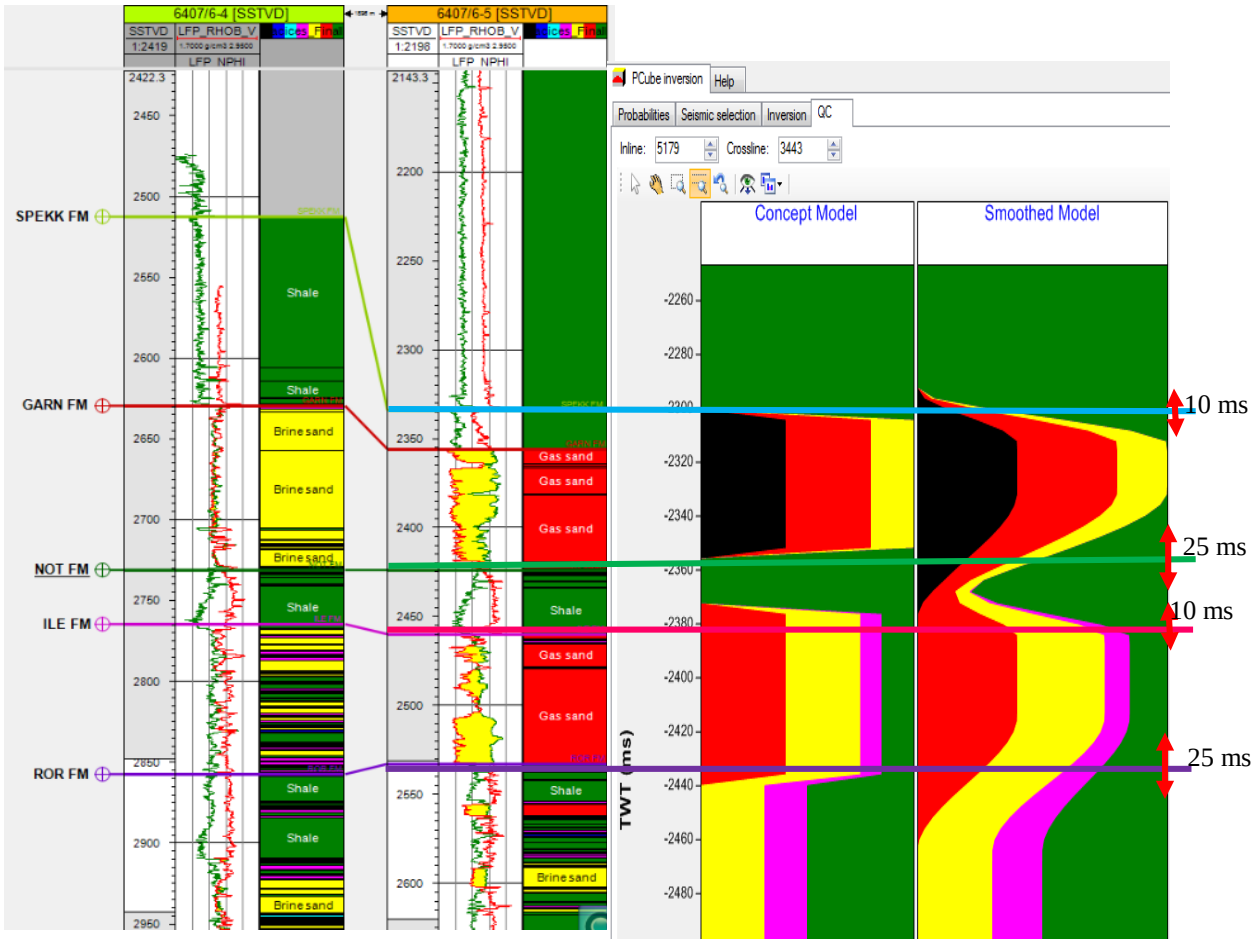

Figure 6.12 Background model of the second Pcube

The results of the second Pcube are presented in Figure 6.13 to 6.16. Figure 6.13 and 6.14 show the similar observation of the first Pcube, the probabilities of LFCs are consistent with the structural mapping and the fluid effect observation in the previous sections. Probabilities of gas sand in the Garn reservoir and the Ile reservoir increase from 40% to 60% to 70% in the northern part of the Mikkel Field. Hot shale in the Spekk Formation has high probability in down-thrown block and erosion in some part at structure high. Brine sand mostly appears in the lower Ile reservoir. Hard shale in the Not Formation is consistent with its horizons though some minor fluctuation of structural interpretation in some traces. Probability of cemented sand is very low and remains unchanged from prior input. It is due to seismic vertical resolution is not able to detect thin beds. In general, the results of LFCs are as expected and consistent with the analysis from AVO and EEI which grows confidence in this study.

Figure 6.15 and 6.16 mainly focus in the southern part and segment 7. The result shows high probability of hot shale from Top Spekk to Top Not. Probabilities of gas sand in the Garn and

the Ile reservoir reduce from 40% to around 30% in segment 7 while increase to 50-70% in the higher structure located on western side of segment 7. Brine sand probability is very high in the Ile reservoir at the flank of structure. It could be explained that Top Ile is lower than the GWC. A random line cross from the northern part where well 6407-6/3 through segment 7 was created as shown in Figure 6.16. It is clearly shown that structure is higher in north and lower in south. Hot shale and brine sand probabilities increase significantly in the south while gas sand has the opposite trend.

Finally, a maximum probability of five LFC extracted in the time window of the main horizons was generated from Figure 6.17 to 6.19. Figure 6.17 is a result of maximum probability extract of hot shale in the time window of 50 ms below Top Spekk and hard shale in the time window of 25ms below Top Not. The probabilities of hot shale and hard shale are high in all of the study area. Figure 6.18 shows the maximum probability extract of gas sand in the time window of 25ms below Top Garn and brine sand in the time window of 5ms below Top Garn. The probability of gas sand in Top Garn increases from 40% to about 40% - 70% in the northern high structure where well 6407/6-3 is located. The probability of gas sand in Top Garn at the northern high is consistent with AVO, EEI observation of gas effect in far/ultra-far stack. It is necessary to emphasis that both probabilities of gas sand and brine sand in the Garn Formation are low in segment 7. They seem absent in segment 7, instead hot shale lithology of the Speek Formation is dominated as a thick package from Top Spekk to Top Not. A concern would arise if segment 7 would be a shaley deposited sediment or erosion would happen in the Garn Formation leading to an absence of sand reservoir. The result of Pcube agrees with the AVO modelling and EEI fluid cube that the interval between Top Spekk to Top Not is dimming in Far/ultra-Far as AVO behavior of hot shale in segment 7.

Following, Figure 6.19 is maximum probability extract of gas sand in the time window of 25ms below Top Ile and brine sand in the time window of 5ms below Top Ile. Gas sand in the Ile Formation is mainly concentrated in northern high structure and its probability has increased from 40% to 55%-75%. In opposite, probability of brine sand is low in the northern high structure and increases from 40% to 60%-70% in the eastern downthrown fault block. Based on attribute map, there is a shift between gas sand and brine sand in the Ile reservoir which occurs at -2400ms to -2420 ms, which coincidently matches with GWC observation in wireline data.

In general, probability of LFCs has changed compared to the first LFP as the prior knowledge and horizons were introduced into the second LFP. In detail, probability of hot shale has increased from 40% to 60%-75% and distributed most of the Mikkel Field. Probability of gas sand in the Garn and the Ile increased from 40% to 55% - 70% in the Northern high structure and reduces to 20-30% at segment 7.

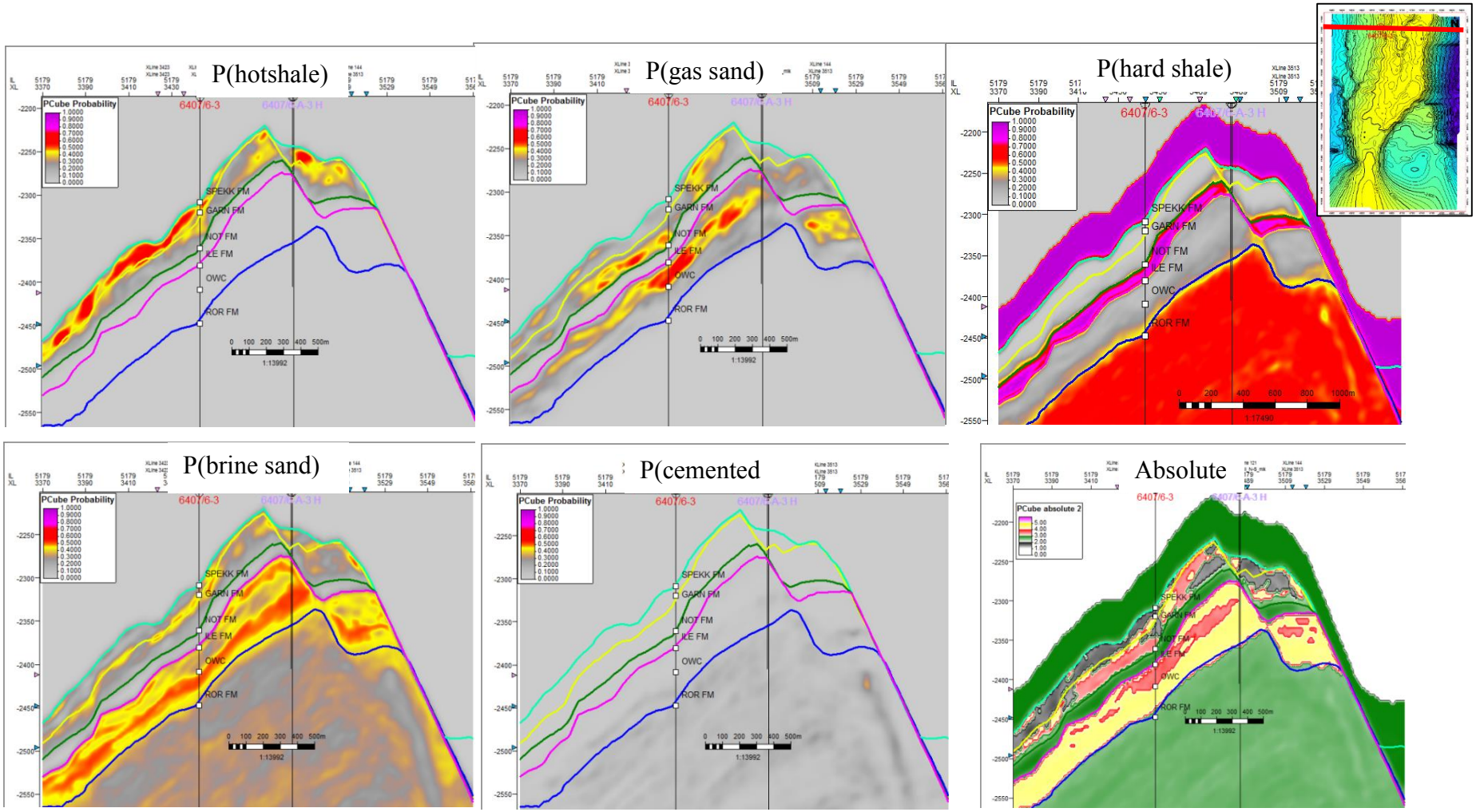

Figure 6.13 Probability of each LFC of the second Pcube at IL 5179

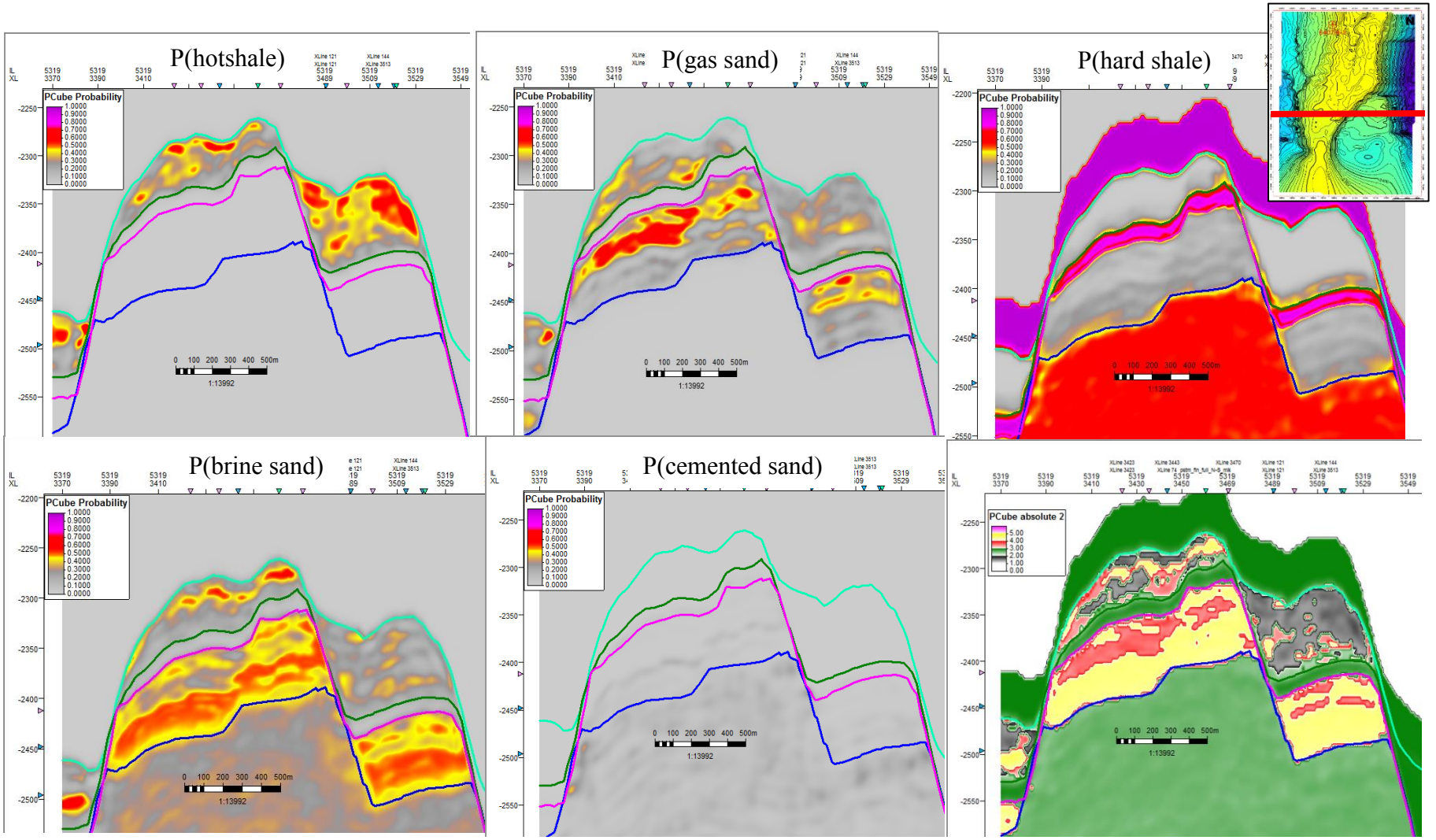

Figure 6.14 Probability of each LFC of the second Pcube at IL 5319

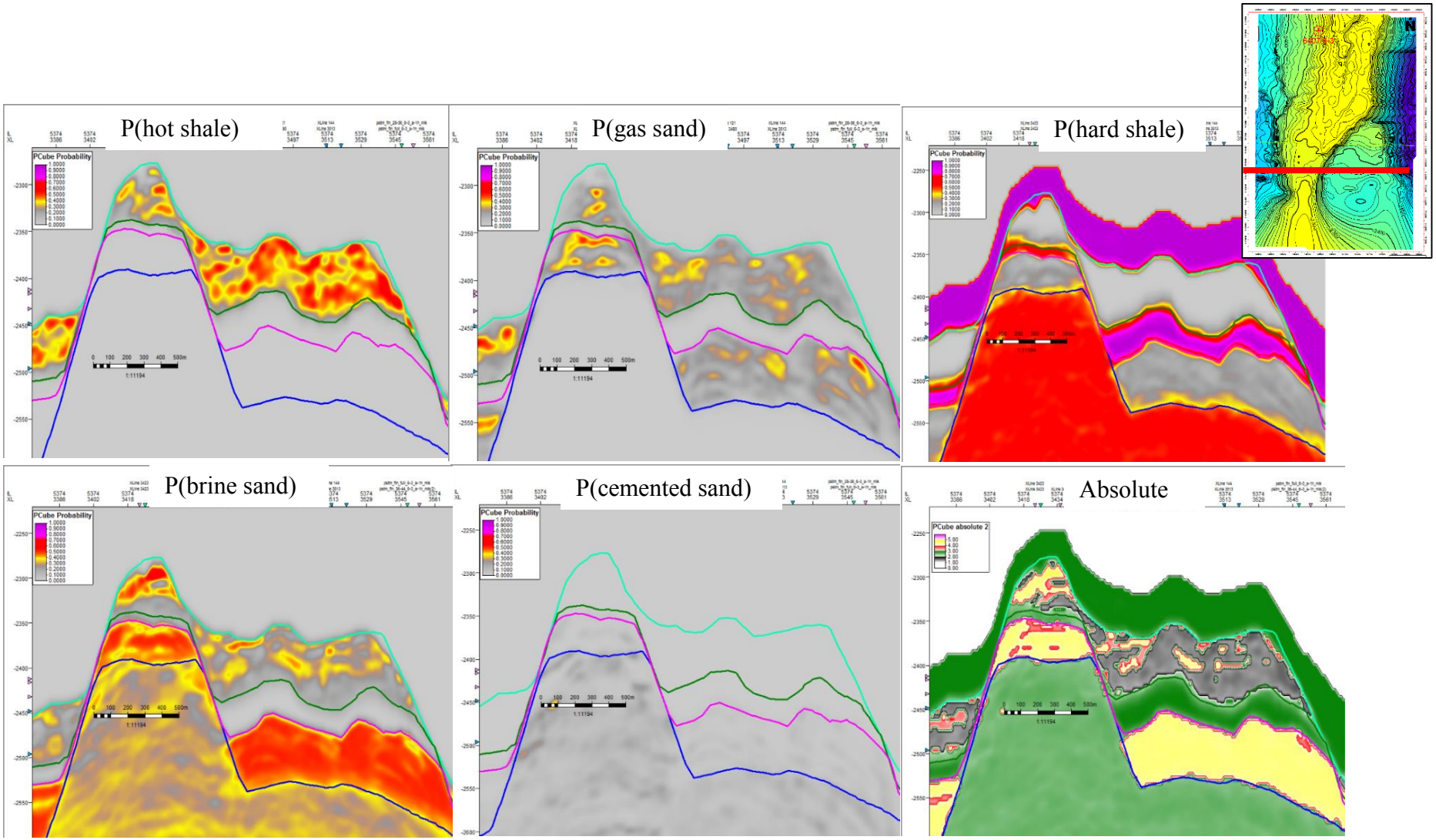

Figure 6.15 Probability of each LFC of the second Pcube at IL 5414

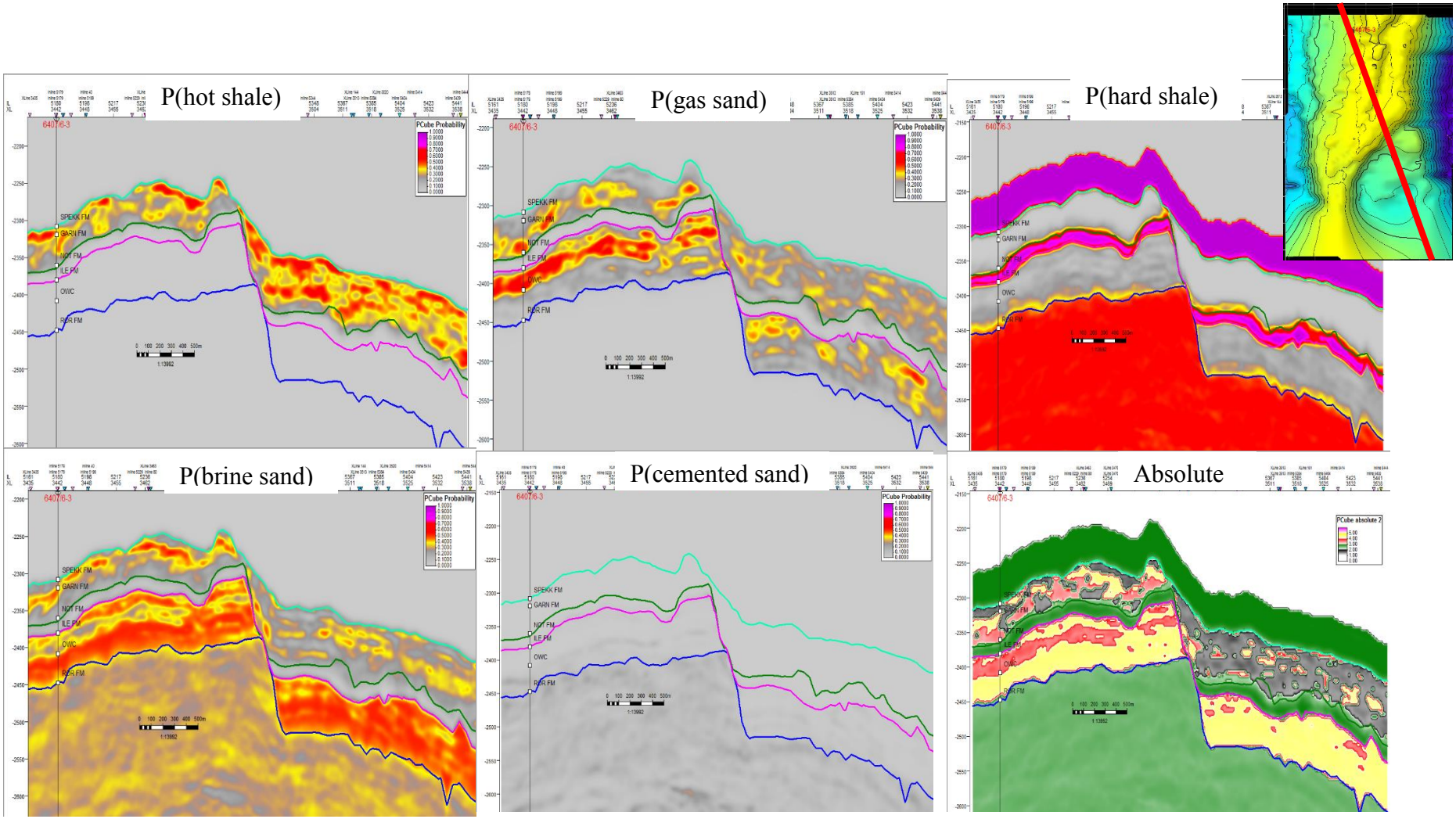

Figure 6.16 Probability of each LFC of the second Pcube at a random line

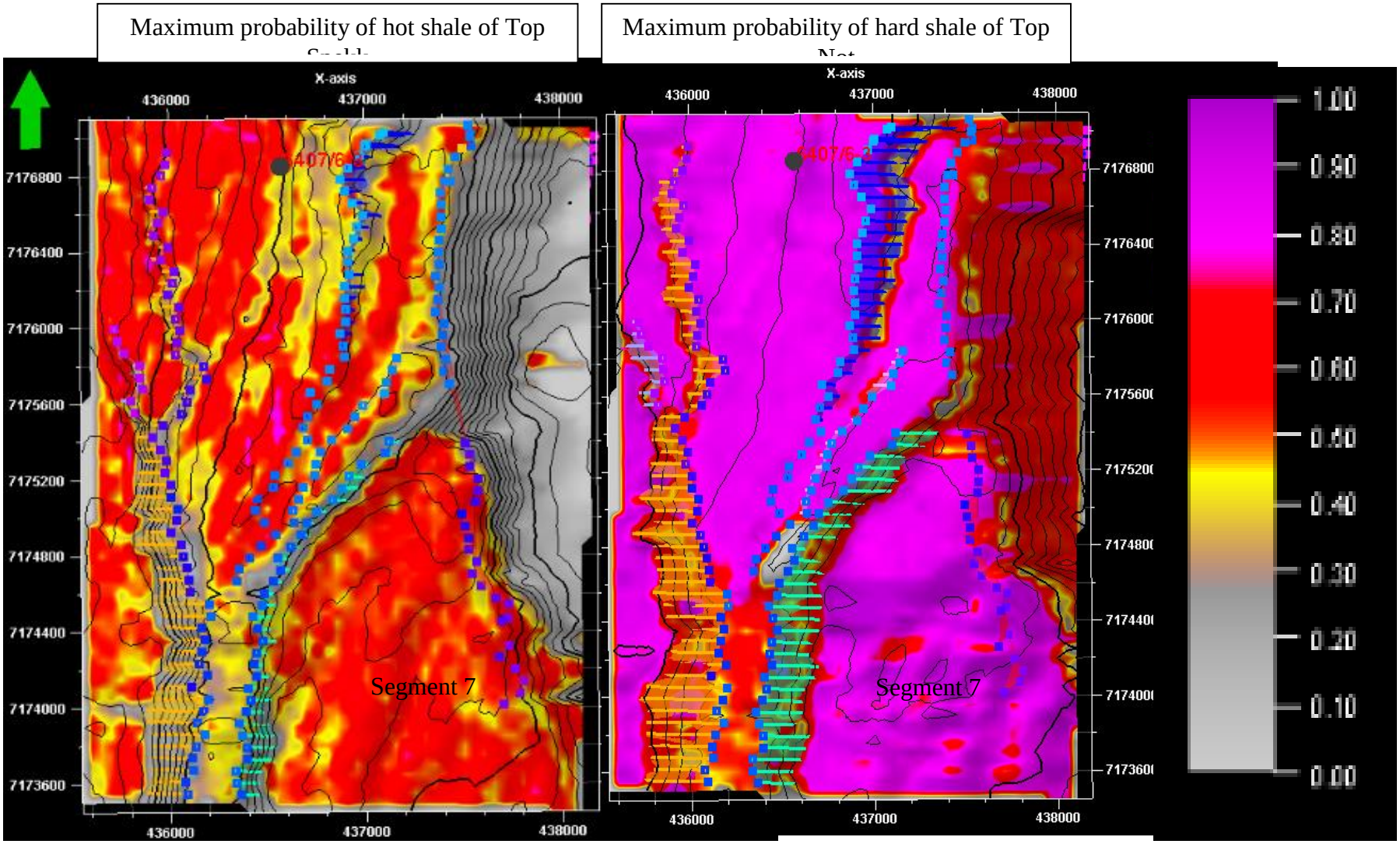

Figure 6.17 Map view of the Mikkel Field, showing maximum probability of hot shale in time window of 50 ms below Top Spekk (left), probability of hard shale in time window of 25 ms below Top Not (right) of the second Pcube

Maximum probability of gas sand of Top Garn

Maximum probability of brine sand of Top Garn

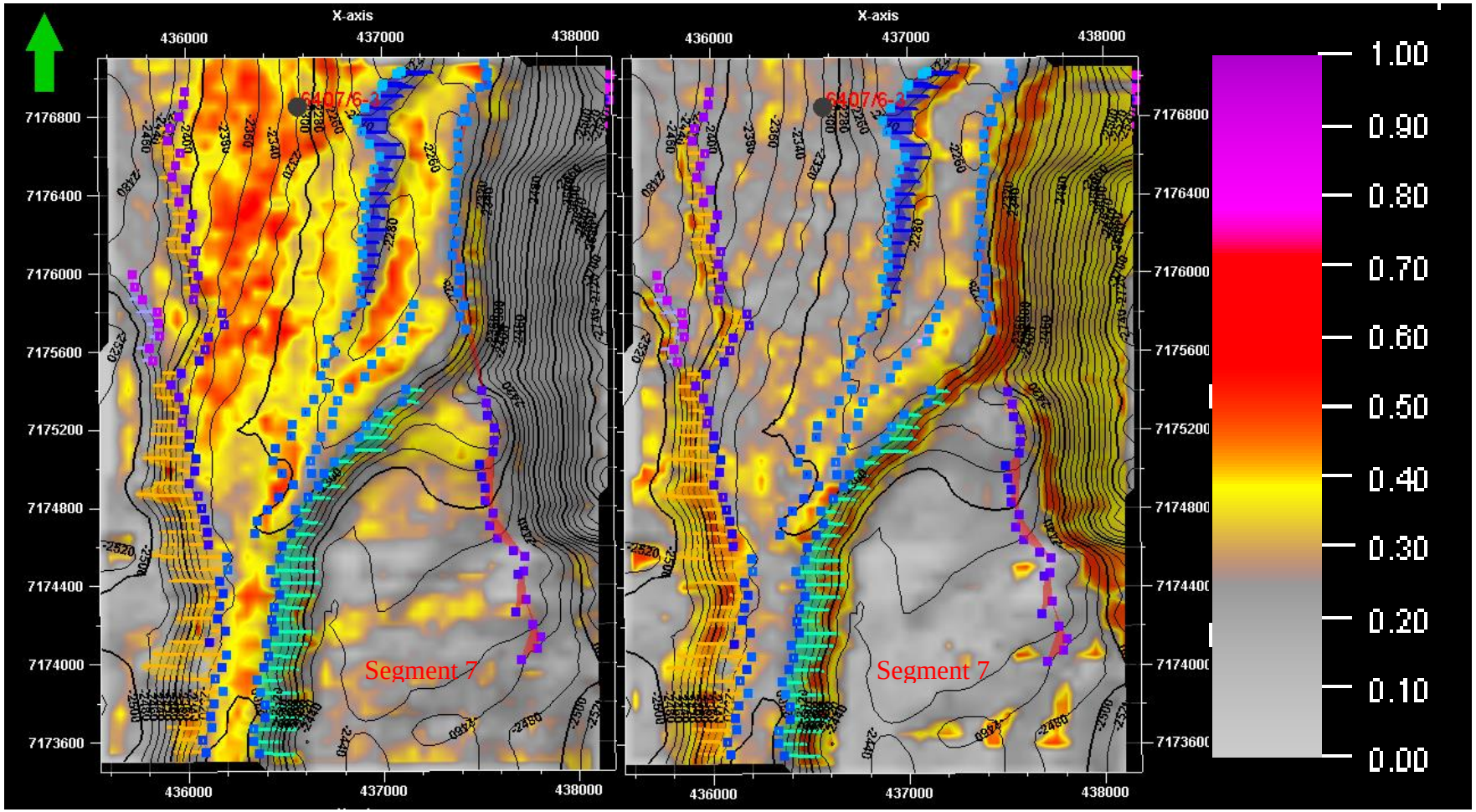

Figure 6.18 Map view of the Mikkel Field, showing maximum probability of gas sand in time window of 25 ms below Top Garn (left), probability of brine sand in time window of 5ms below Top Garn (right) of the second LFP.

Probability of gas sand of Top Ile

Probability of brine sand of Top Ile

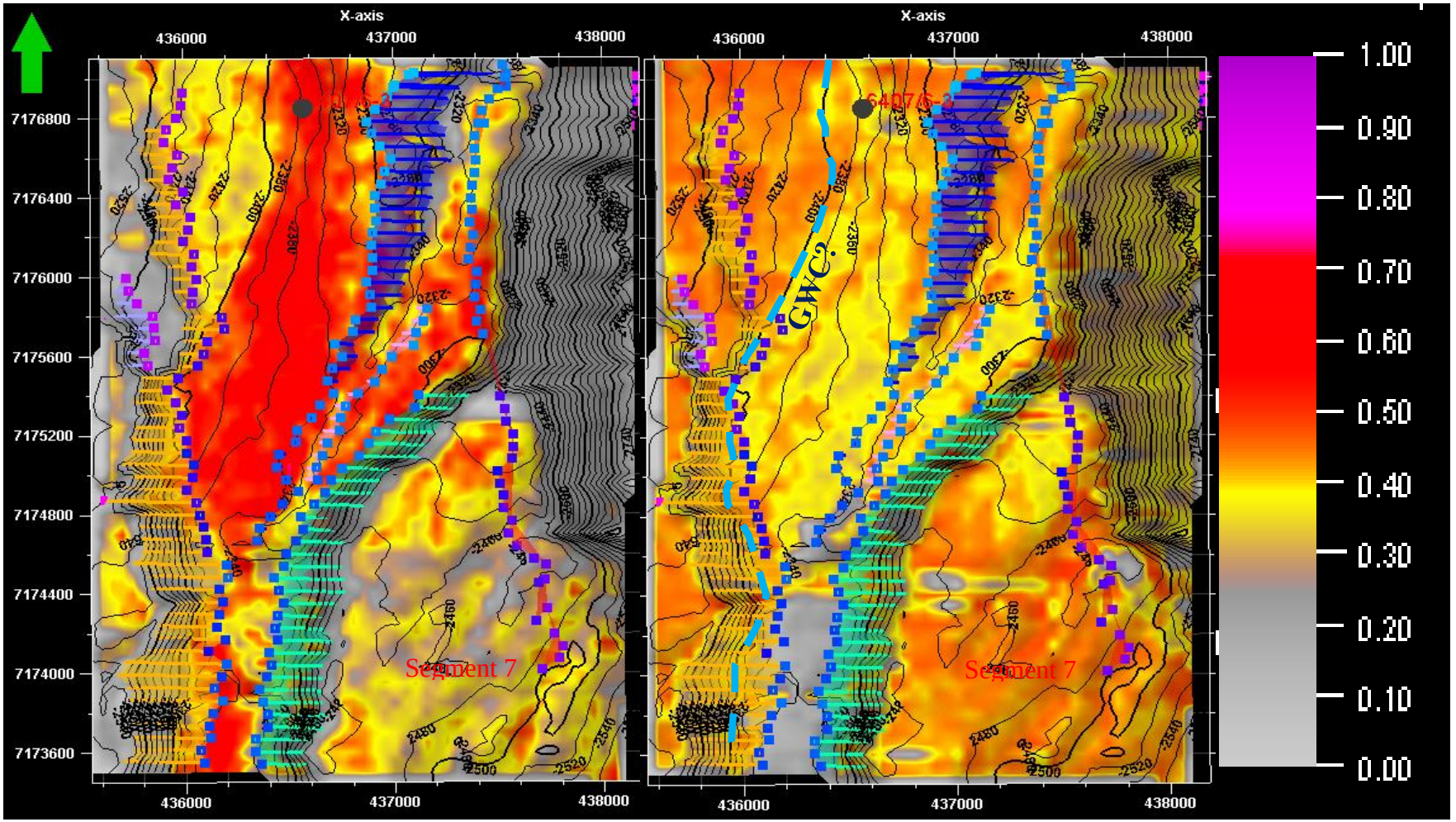

Figure 6.19 Map view of the Mikkel Field, showing maximum probability of gas sand in a time window of 25 ms below Top Ile (left), brine sand in a time window of 5ms below Top Ile (right) of the second LFP

7. Discussion and Conclusion

In this chapter, the discussion section is mainly focused on Pcube results and the remaining issues in the Mikkel Field. The conclusion will summarize the methodology and application of Bayesian Lithology and Fluid inversion from prestack seismic data.

7.1 Discussion

The segment 7 was concluded that it has not contributed to production of the Mikkel Field from the dynamic reservoir model of Statoil AS. Therefore, there was an attempt to study the Mikkel Field, specifically segment 7 in the new 2014 angle stacks seismic. There are two main objectives in this study: (1) analyze remaining hydrocarbons in the Mikkel Field to reduce risk in the decision of in-filled well location in a future development plan and (2) an attempt to define the porosity trend in the Ile reservoir.

The four main key horizons such as Top Spekk, Top Garn, Top Not and Top Ile were interpreted to delineate their structures in the study area. Top Garn was the most difficult horizon as its amplitude is always weak and varying, dependent on the cap rock thickness. Statoil recommended to interpret Top Garn by shifting Top Spekk using isochoric map. It is a common strategy if the horizon is difficult to recognize. However, it is risky to shift horizon in the syn-rift pattern as thickness and reservoir properties vary in each fault block. Hence, it was challenging to map each horizon prior to performing LFP. To support structural mapping, AVO, coloured inversion and EEI were carried out to analyze each formation behavior and its fluid effect on angle stacks. This helps to not only increase confidence in mapping but also explain the result of Pcube in the Mikkel Field.

The final Pcube result suggested that the Ile reservoir has low probability of gas sand presence in segment 7, slightly reduce to 30%-40% from prior input 40% while the northern high structure has increased probability of gas sand to 70%. The Top Ile structure in segment 7 is possibly lower than the GWC so that the brine sand presence is expected to be high in segment 7. The Garn reservoir in segment 7 has low probability of both gas sand and brine sand, instead the probability of hot shale is very high in interval between Top Spekk to Top Not. This phenomenon was observed in AVO, SCI and EEI analysis when Top Garn in segment 7 is dim in far/ultra-far, which is a typical AVO behavior of hot shale in the Spekk Formation. That would lead to two hypotheses: (1) the Garn Formation may not consist sand in deep area as experienced in drilled wells or (2) its formation would have eroded as

happened in well 6407/5-B-H-3. For any scenario, the result from Pcube seems support the query from the dynamic model in Statoil that segment 7 has not shown any contribution to production in the Mikkel Field in terms of water and gas. As every model has its limitation, the LFP result is dependent on angle stack seismic quality. Fault shadow effects could significantly reduce signal to noise ratio in the Mikkel Field. In segment 7, it has been observed a dipping strata from the Ile reservoir to the Garn reservoir as shown in Figure 7.1 and 7.2. The strata changed from planar to sub-planar in the western structure high to dipping in segment 7. There was not any clear fault throw to support the interpretation. However, the strata from the Ile Formation to Top Not seemed to experience rotation as typical titled fault blocks. In addition, segment 7 is downthrown of the main north-south fault. Deposited sediment in segment 7 would have been re-worked from western structure high. If this is the case, sediment in the syn-rift period would be different to the observation from the drilled wells and the current rock physics model may not capture this phenomenon. Since segment 7 has a complex fault pattern and re-worked sediments, seismic quality would be affected and signal to noise ratio would be reduced. That leads to some degree of uncertainty in the LFP result in segment 7. Figure 7.3 is a variance amplitude map at -2467 ms showing discontinuity of the seismic amplitude in near angle stack. In the left of Figure 7.3, there was clear trend of main bounding faults and those were mapped as shown. In the right of Figure 7.3, some of small faults were marked in segment 7 though the variance map doesn't show a clear discontinuity. It is recommended to analyze structural fault interpretation and its influence on sediment deposit in the Mikkel Field for the future to predict sediment in un-drilled area and improve rock physics model.

The second attempt was defining the porosity trend in the Ile formation. Although this is not suitable with the applied LFP method. There was an effort to define cemented sand distribution as a main factor reducing reservoir permeability. However, cemented sand appeared as thin bedded layer with thickness varying between 0.5 m to 2.5 m which is below seismic resolution. LFP could not predict its presence from seismic data. Perhaps, a depositional environment study could help to define the trend of calcite cemented sand in the Mikel Field and a geological model will solve this objective.

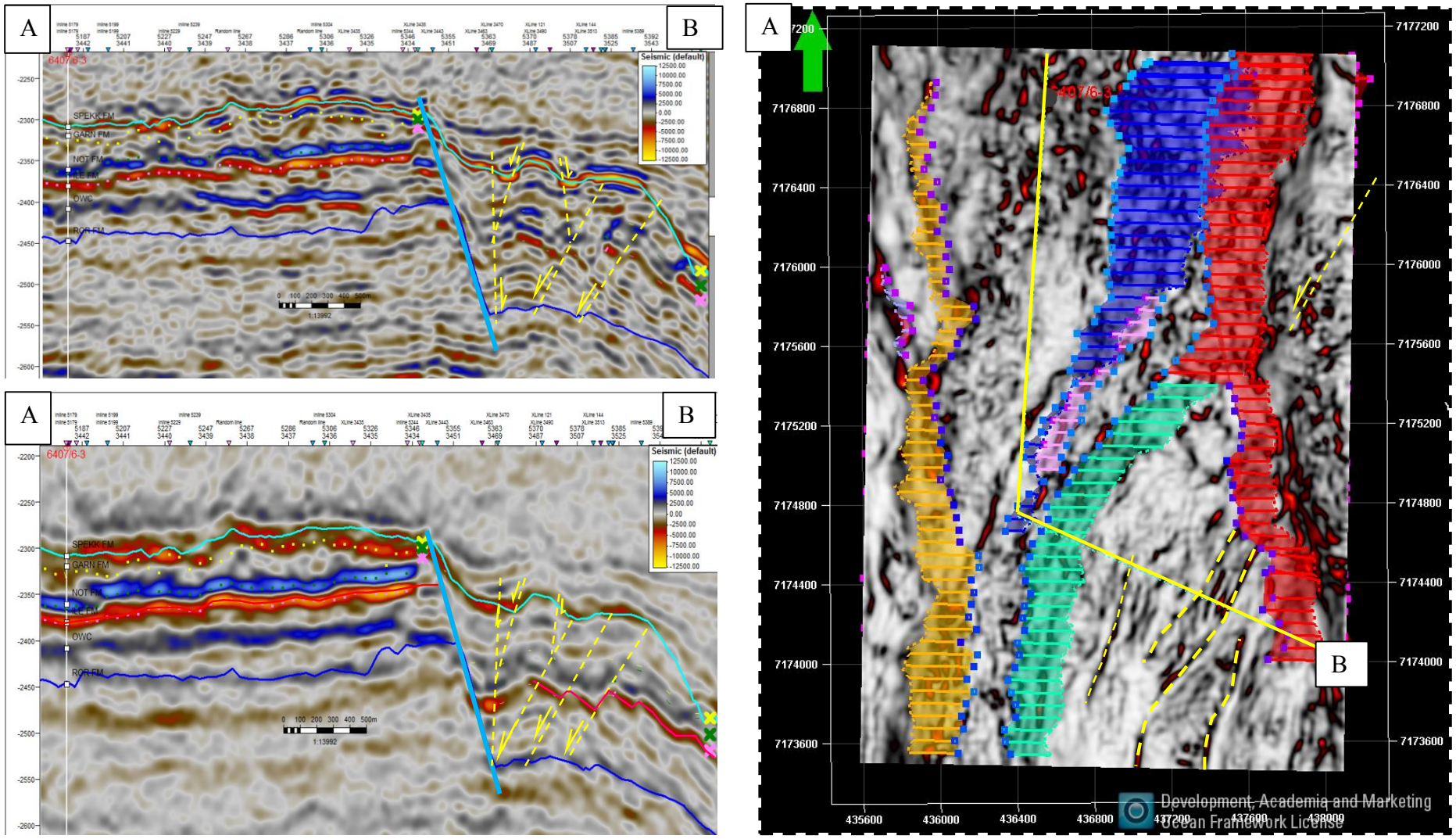

Figure 7.1 Near angle stack versus far angle stack (left upper- left lower) and variance attribute at -2460 ms of arbitrary line (right)

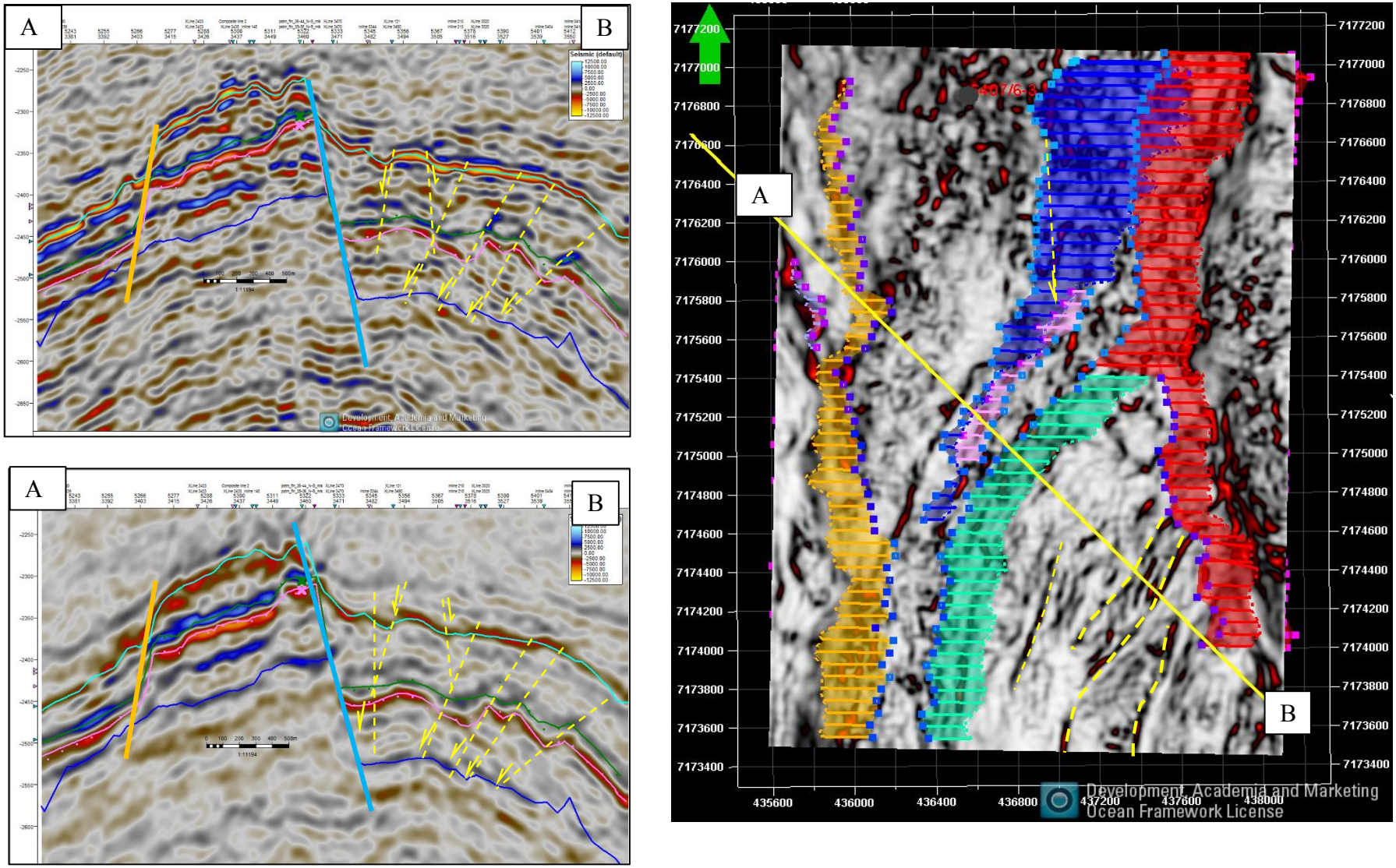

Figure 7.2 Near angle stack versus far angle stack (lef upper- left lower) and variance attribute at -2460 ms of random line (right)

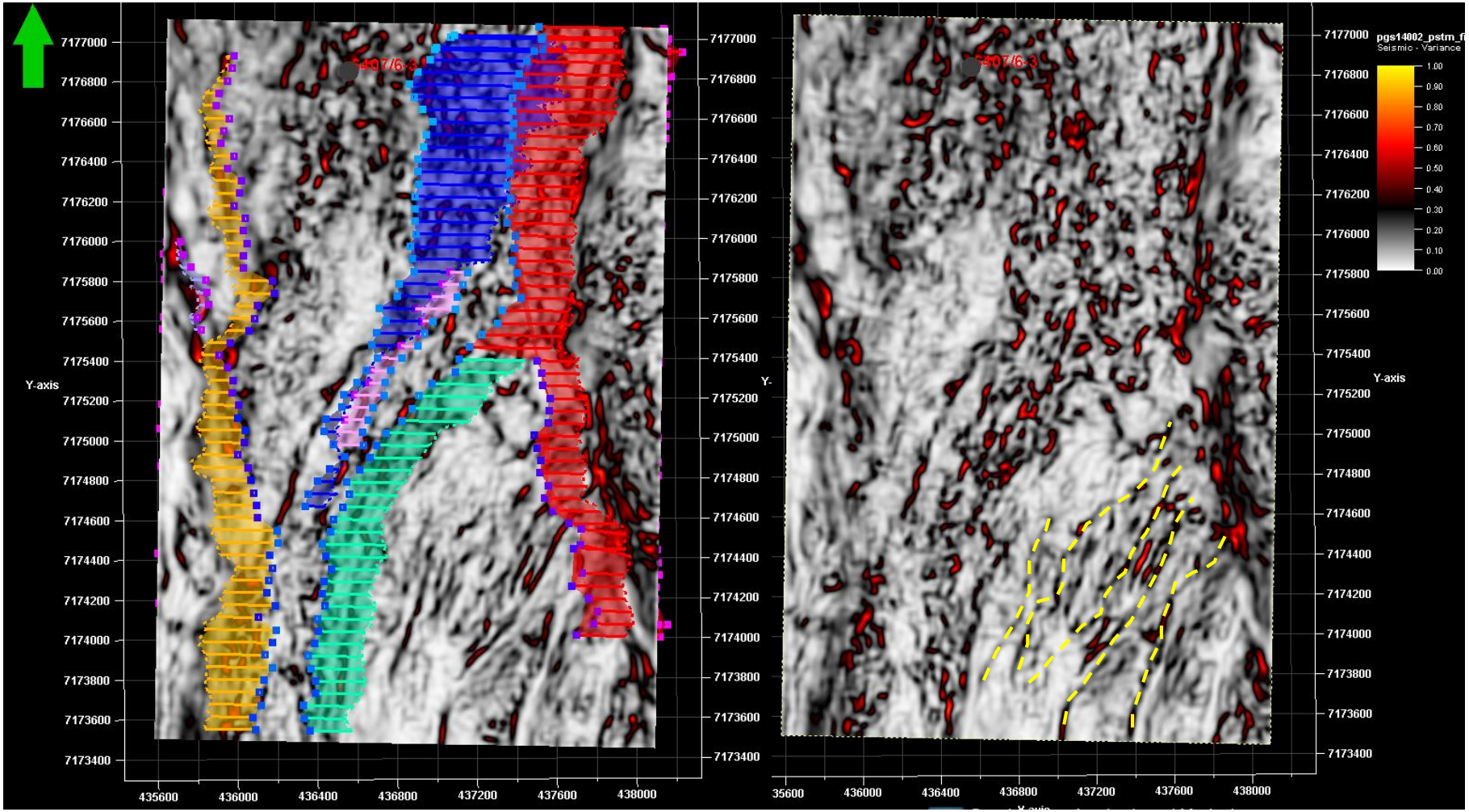

Figure 7.3 Variance attribute at -2460 ms (left) and -2467 ms (right)

7.2 Conclusion

Seismic inversion is a standard workflow in exploration and development to predict the lithology and fluid. In the exploration setting, the prior knowledge is often sparse and comes from regional geology or neighbouring wells. In contrast, development fields always possess a great amount of prior knowledge of the reservoirs that constrains LFP results more accurately and with more stability.

In the lithology and fluid prediction from prestack seismic data, the rock physics model is essential. It is important to define all existing facies in rock physics model that represents lithology in the study area. Often, the production fields can be benefits with substantial information of lithology and reservoir properties from drilled wells. The relationship between facies and elastic properties can defined from well log data directly in development fields. That would reduce uncertainty for the rock physics model. In the exploration setting, the well log may be sparse and the rock model might be required.

The seismic inversion for LFP has shown a great benefit in this case study of the Mikkel Field. The result of LFP supported structural mapping, especially the areas with presence of AVO class II/IIp are always highly uncertain in interpretation. The inversion also helped to predict the lithology and fluid classes in the un-drilled area to reduce the risk in decision making for future development plan. However, the uncertainty from seismic inversion is often high and rarely assessed. By using the additional techniques of AVO and EEI, the interpreter can analyze the fluid effect and lithology change to improve the prior knowledges and explain the results of LFP.

Reference

Avseth, P., T. Mukerji, and G. Mavko. (2005). Quantitative seismic interpretation: Cambridge University Press

Brekke, H., Sjulstad, H.I., Magnus, C. and Williams, R.W. (2001). Sedimentary environments offshore Norway — an overview. In: Sedimentary Environments Offshore Norway – Palaeozoic to Recent (Eds O.J. Martinsen and T. Dreyer), Norw. Petrol. Soc. (NPF) Spec. Publ., 10, 7–37.

Bukovics, C., Cartier, E.G., Shaw, N.D. and Ziegler, P.A. (1984). Structure and development of the mid-Norway continental margin. In: Petroleum Geology of the North European Margin (Ed. A.M. Spencer), pp 407–423. Graham and Trotman, London.

Buland, A., & Omre, H. (2003a). Bayesian linearized AVO inversion. *Geophysics*, *68*, 185-198

———. (2003b). Bayesian wavelet estimation from seismic and well data: Geophysics, 68, 2000-2009.

———. (2003c). JointAVO inversion, wavelet estimation and noise level estimation using a spatially coupled hierarchical Bayesian model: Geophysical Prospecting, 51, 531–550

Buland, A., Kolbjørnsen, O., Hauge, R., Skjæveland, Ø., & Duffaut, K. (2008). Bayesian lithology and fluid prediction from seismic pre-stack data. *Geophysics*, *73*(3), C13-C21

Corfield, S. and Sharp, I.R. (2000). Structural style and stratigraphic architecture of fault propagation folding in extensional settings: a seismic example from the Smørbukk area, Halten Terrace, Mid-Norway. Basin Res., 12, 329–341.

Corfield, S., Sharp, I.R., Håger, K.-O., Dreyer, T. and Underhill, J. (2001). An integrated study of the Garn and Melke formations (Middle to Upper Jurassic) of the Smørbukk area, Halten Terrace, mid-Norway. In: Sedimentary Environments Offshore Norway – Palaeozoic to Recent (Eds O.J. Martinsen and T. Dreyer), Norw.

Dalland, A., Worsley, D. and Ofstad, K. (1988). A lithostratigraphic scheme for the Mesozoic and Cenozoic succession offshore mid- and northern Norway. Norw. Petrol. Direct. Bull., 4, 1–65.

Doré, A.G. (1992). Synoptic palaeogeography of the Northeast Atlantic Seaway: late Permian to Cretaceous. In: Basins on the Atlantic Seaboard: Petroleum Geology, Sedimentology and Basin Evolution (Ed. J. Parnell), Geol. Soc. London Spec. Publ., 62, 421–446.

Doré, A.G., Lundin, E.R., Jensen, L.N., Birkeland, Ø., Eliassen, RE. and Fichler, C. (1999). Principal tectonic events in the evolution of the northwest European Atlantic margin. In: Petroleum Geology of Northwest Europe — Proceedings of the 5th Conference (Eds A.J. Fleet and S.A.R. Boldy), 41‑61. Geol. Soc. London

Duijndam, A. J.W. (1988a). Bayesian estimation in seismic inversion part I: Principles: Geophysical Prospecting, 36, 878–898.

———. (1988b). Bayesian estimation in seismic inversion part II: Uncertainty analysis: Geophysical Prospecting, 36, 899–918.

Ehrenberg, S.N., Gjerstad, H.M. and Hadler-Jacobsen, E. (1992). Smørbukk Field: a gas condensate trap in the Haltenbanken province, offshore mid-Norway. In: *Giant Oil and Gas Fields of the Decade 1978–1988* (Ed. M.T. Halbouty), *AAPG Mem*., 54, 323–348

Eidsvik, J., P. Avseth, H. Omre, T. Mukerji, and G. Mavko. (2004). Stochastic reservoir characterization using prestack seismic data: Geophysics, 69, 978–993.

Gjelberg, J., Dreyer, T., Høie, A., Tjelland, T. and Lilleng, T. (1987). Late Triassic to Mid-Jurassic development on the Barents and Mid-Norwegian shelf. In: Petroleum Geology of North West Europe (Eds J. Brooks and K. Glennie), pp 1105–1129. Graham and Trotman, London.

Gunning, J., and M. Glinsky. (2004). Delivery: An open-source model-based Bayesian seismic inversion program: Computers and Geosciences, 30, 619–636.

Hallam, A., Crame, J.A., Mancenido, M. O., Francis, J. and Parrish, J.T. (1994). Jurassic climates as inferred from the sedimentary and fossil record. In: *Palaeoclimates and Their Modelling; With Special Reference to the Mesozoic Era* (Eds J.R.L. Allen, B.J. Hoskins, B.W. Sellwood, R.A. Spicer and P.J. Valdes), pp 79–88. Chapman & Hall, London.

Helland-Hansen, W., Ashton, M., Lømo, L. and Steel, R.J. (1992). Advance and retreat of the Brent Delta: recent contributions to the depositional model. In: *Geology of the Brent Group* (Eds A.C. Morton, R.S. Haszeldine, M.R. Giles and S. Brown), *Geol. Soc. London Spec. Publ*., 61, 109–127.

Houck, R. T. (2002). Quantifying the uncertainty in an AVO interpretation: Geophysics, 67, 117–125.

Jackson, J.S. and Hastings, D.S. (1986). The role of salt patterns and hydrocarbon play generation movements in the Tectonic history of Halten banken and Traena banken and its relationship to structural styles. In: Habitat of Hydrocarbons on the Norwegian Continental Shelf (Ed. A.M. Spencer), pp 241–257. Graham and Trotman, London.

Kemper, M., & Huntbatch, N. (2012). From Inversion Results to Reservoir Properties. Adapted from oral presentation at AAPG International Conference and Exhibition, Milan; Italy.

Koch, J.-O. and Heum, O.R. (1995). Exploration trends of the Halten Terrace. In: Petroleum Exploration and Exploitation in Norway (Ed. S. Hanslien), Norw. Petrol. Soc. (NPF) Spec. Publ., 4, 235–251.

Lancaster, S., & Whitcombe, D. (2000). Fast-track "coloured" inversion. Paper presented at the SEG Expanded Abstracts.

Marsh, N., Imber, J., Holdsworth, R.E., Brockbank, P. and Ringrose, P.S. (2010). The structural evolution of the Halten Terrace, offshore Mid-Norway: extensional fault growth and strain localisation in a multi-layer brittle– ductile system. Basin Res., 22, 195–214.

Messina, C., Nemec, W., Martinus, A.W. and Elfenbein, C. (2014). The Garn Formation (Bajocian-Bathonian) in the Kristin Field, Halten Terrace: its origin, facies architecture and primary heterogeneity model. In: From Depositional Systems to Sedimentary Successions on the Norwegian Continental Margin, First Edition. Edited by A. W. Martinius, R. Ravnås, J. A. Howell, R. J. Steel, and J. P. Wonham, *Int. Assoc. Sedimentol. Spec. Publ.* (2014) 46, 513–550

NPD. (2016). Retrieved from Norwegian Petroleum Directorate: http://www.npd.no/en/

Pascoe, R., Hooper, R., Storhaug, K. and Harper, H. (1999). Evolution of extensional styles at the southern termination of the Nordland Ridge, Mid-Norway: a response to variations in coupling above Triassic salt. In: Petroleum Geology of Northwest Europe — Proceedings of the 5th Conference (Eds A.J. Fleet and S.A.R. Boldy), pp 83–90. Geol. Soc. London.

Rob Simm and Mike Bacon. (2014). Seismic Amplitude: An interpreter's Handbook. Cambridge University Press, Cambridge, 38pp.

Russel, Brian., Hampson, Dan., Bankhead, Bradley. (2006). An inversion primer. CSEG recorder, 31(2), 96-103

Scales, J. A., and L. Tenorio. (2001). Prior information and uncertainty in inverse problems: Geophysics, 66, 389–397.

Skar, T., Van Balen, R.T., Arnesen, L. and Cloetingh, S**.** (1999) Origin of overpressures on the Halten Terrace, offshore mid-Norway: the potential role of mechanical compaction, pressure transfer and stress. In: *Muds and Mudstone: Physical and Fluid-Flow Properties* (Eds A.C. Aplin, A.J. Fleet and J.H.S. Macquaker), *Geol. Soc. London Spec. Publ.*, **158**, 137‑156.

Smith, A.G., Smith, D.G. and Funnel, B.M. (1994). Atlas of Mesozoic and Cenozoic Coastlines. Cambridge University Press, Cambridge, 112 pp.

Spencer, A.M., Birkeland, Ø. and Koch, J.-O. (1993). Petroleum geology of the proven hydrocarbon basins, offshore Norway. First Break, 11, 161–176.

Tarantola, A., 1987, Inverse problem theory: Elsevier Science Publ Co., Inc.

Ulrych, T. J., M. D. Sacchi, and A.Woodbury. (2001). ABayes tour of inversion: Atutorial: Geophysics, 66, 55–69.

Whitcombe, D. N., Connolly, P. A., Reagan, R. L., & Redshaw, T. C. (2002). Extended elastic impedance for fluid and lithology prediction. *Geophysics, 67*(1), 63-67.

Withjack, M.O., Meisling, K.E. and Russell, L.R. (1989). Forced folding and basement-detached normal faulting in the Halten banken area, offshore Norway. In: Extensional

Tectonics and Stratigraphy of the North Atlantic Margin (Eds A.J. Tankard and H.R. Balkwill), AAPG Mem., 46, 567–575.